

Speckles in Laser Doppler Perfusion Imaging

Vinayakrishnan Rajan

The work described was carried out at the Biophysical Engineering Group, Faculty of Science and Technology, Institute for Biomedical Technology (BMTI), University of Twente, P. O. Box 217, 7500 AE, Enschede, The Netherlands

The research presented in this thesis was financially supported by the Dutch Technology Foundation STW under grant No. TTF 5840



Speckles in laser Doppler perfusion imaging

By Vinayakrishnan Rajan

Ph.D Thesis, University of Twente, Enschede, The Netherlands, 2007
With references – With summary in English and Dutch

Copyright © Vinayakrishnan Rajan, 2007
All rights reserved.

Front cover illustration: Picturisation of Zernike van Cittert theorem by which the back-scattered spatial intensity distribution of light on the tissue surface can be considered as a Fourier transform pair of the intensity correlation function on a distant speckle pattern. f_1 and f_0 represent Doppler shifted and non-Doppler shifted light fractions respectively.

Printed by Print Partners Ipskamp, P.O. Box 333, 7500 AH, Enschede, The Netherlands.

ISBN 978-90-365-2580-0

**SPECKLES IN
LASER DOPPLER PERFUSION IMAGING**

DISSERTATION

to obtain
the doctor's degree at the University of Twente,
on the authority of the rector magnificus,
prof.dr. W.H.M. Zijm,
on account of the decision of the graduation committee,
to be publicly defended
on Thursday, 11 October 2007 at 15:00 hrs.

by

Vinayakrishnan Rajan

born on 8 October 1979
in Anthinadu, India

This dissertation has been approved by:

Promotor : prof. dr. A. G. J. M. van Leeuwen

Assistant promotor : dr. Wiendelt Steenbergen

To my Parents...

Table of contents

Chapter 1	Introduction	1
Chapter 2	Review of methodological developments in laser Doppler flowmetry	5
Chapter 3	Speckles in laser Doppler perfusion imaging	37
Chapter 4	Quantification of spatial intensity correlations and photodetector intensity fluctuations of coherent light reflected from turbid particle suspensions	47
Chapter 5	Effect of speckles on the depth sensitivity of laser Doppler perfusion imaging	59
Chapter 6	Influence of tissue optical properties on laser Doppler perfusion imaging, accounting for photon penetration depth and the laser speckle phenomenon	73
Chapter 7	Speckle size and decorrelation time; space-time correlation analysis of coherent light dynamically scattered from turbid media	95
Chapter 8	The relationship between local scalp skin temperature and cutaneous perfusion during scalp cooling	107
Chapter 9	Summary and outlook	123
Samenvatting		133
Acknowledgements		139
Publications		141
Curriculum Vitae		145

Chapter 1

Introduction

1. General introduction

Non invasive diagnosis of skin microcirculation is of increasing importance for a wide range of clinical applications. The microcirculation of the skin, being the largest organ in the human body with a regulatory and sensory role, can provide essential information about serious diseases which cause vascular disorders. Also skin blood flow assessment is used as a diagnostic tool for drug tests, wound healing and curing rate after plastic and reconstructive surgery in dermatology.

Many methods are available for skin blood flow measurements, such as the ^{133}Xe wash out technique [1], capillary microscopy [2], thermography [3], Doppler ultrasound [4] and laser Doppler flowmetry [5]. Each has its own advantages and disadvantages. Laser Doppler flowmetry (LDF) is a method to measure microcirculatory blood flow in tissue, and has become the focus of numerous studies in research as well as clinical settings. The major advantage of laser Doppler techniques in general is their non invasiveness and the ability to measure the micro circulation of the tissue and fast changes of perfusion during provocations. Under certain conditions, the technique can measure perfusion quantitatively (although relative) in real time. Since the commercialization of the technique, LDF has a modest but stable and steadily growing market.

Laser Doppler flow meters are available as laser Doppler perfusion monitoring (LDPM) and laser Doppler perfusion imaging (LDPI) instruments. LDPM is a one point measurement method which records the integrated perfusion in a sampling volume in real time. LDPI instruments [6, 7] map the perfusion on a larger area by scanning the laser beam over the area of interest.

1.1. Scope of this thesis

In most of the optical biomedical diagnostic techniques the unknown and heterogeneous tissue optical properties make it a difficult task to probe the structure or function of the tissue. In scanning laser Doppler perfusion imaging, the changes in time and space of tissue optical properties result in a change in the perfusion signal due to the influence of photon statistics (mainly: optical path lengths) and the speckle phenomenon. Both aspects influence the response of the system in terms of the flux or perfusion level signal. These effects will result in an erroneous estimation of the perfusion in a region where the optical properties are either spatially heterogeneous or change in time. For example during a vasodilatory stimulus the tissue optical properties change, which can be observed by the skin color varying in time. In the case of burn diagnosis the heterogeneous nature of the burnt tissue and the presence of inflammation can influence the perfusion signal independent of perfusion. So in order to have a quantitative estimation of the perfusion in these complex situations these effects have to be addressed and special care has to be taken to arrive at a conclusion regarding a perfusion change.

In this thesis we address the influence of tissue optical properties on laser Doppler perfusion imaging through the speckle phenomenon. For this a quantitative experimental validation of the influence of speckles on the signal response with changes in tissue optical properties has to be performed. It is important also to develop a method for the quantitative estimation of the size and number of speckles involved in the detection process. Prior knowledge of the modulation depth and depth sensitivity variation with tissue optical properties will benefit in a better understanding and interpretation of perfusion maps.

1.2 Overview of this thesis

A review of methodological developments in laser Doppler perfusion monitoring and imaging techniques is given in **chapter 2**. In this chapter the working principle of LDF and the theoretical background are discussed. The more recent methodological developments of the technique are reviewed in detail. The limitations of the methods are discussed and the research done so far to overcome these limitations is critically assessed.

The importance of speckles in laser Doppler perfusion imaging is experimentally proved in **chapter 3**. The influence of speckles on the signal amplitude and the Doppler spectrum is demonstrated experimentally on particle suspensions with different scattering levels and varying beam width. It is shown that the type of tissue affects the instrumental response through the effect of

lateral light diffusion on the number of speckles involved in the detection process.

In **chapter 4**, a model is presented for predicting the spatial intensity correlation function of dynamic speckle patterns formed by light backscattered from turbid suspensions. An experimental validation of these predictions is given for particle suspensions with various degrees of scattering anisotropies and scattering levels, illuminated by broad and narrow beams. The model presented in chapter 4 is extended to combined static-dynamic media as given in **chapter 5**. In this chapter the changes in the modulation depth of the photocurrent fluctuations is predicted in a free beam laser Doppler experiment for motion at different depths within static tissue media, taking into account the speckle phenomenon.

In **chapter 6**, the influence of tissue optical properties on the signal response as mediated by the speckle effect was analyzed in real tissue by comparing the signal from normal skin and port wine stained skin for various beam diameters. The validated method to predict the modulation depth of the signal is used to quantify the overall sensitivity and the depth resolved response of LDPI due to the combined effect of photon penetration depth statistics and the speckle phenomenon. A range of tissue optical properties and scattering depths are used.

The space-time behavior of dynamic speckles is discussed in **chapter 7**. The dependence of the decorrelation time on the spatial intensity correlation of speckles is studied. A high speed CMOS camera is used to capture the dynamic speckle patterns generated by light back-scattered from polystyrene particles undergoing Brownian motion. The temporal autocorrelation of speckle intensity fluctuations is studied for different beam diameters and scattering levels. The space-time correlation of the speckles is also analyzed to get information about the influence of spatial correlation on the decorrelation time of speckles. The results of this space-time analysis provide an explanation of the observations in chapter 3 about an increase in average Doppler shift in the power spectra of photodetector current fluctuations with an increase in the diameter of the illuminating beam.

A somewhat different topic where laser Doppler flowmetry is involved is described in **chapter 8**, where the relationship between local scalp temperature and cutaneous perfusion during scalp cooling is analyzed. Cooling the scalp during administration of chemotherapy can prevent hair loss [8]. It reduces both skin blood flow and hair follicle temperature, thus affecting drug supply and drug effect in the hair follicle [9]. The extent to which these mechanisms contribute to the hair preservative effect of scalp cooling remains unknown. The purpose of this study was to establish a relationship between local skin temperature and cutaneous blood flow in a setting that is relevant for clinical practice of scalp cooling in chemotherapy treatment. For this, the scalp was cooled using a commercially available scalp cooling device, and

temperature and perfusion were measured using thermocouples and laser Doppler perfusion probes, respectively.

Finally a summary and outlook of the research described in this thesis is given as **chapter 9**.

References

1. O. A Larsen, N. A. Lassen and F. Quaade, "Blood flow through human adipose tissue determined with radioactive xenon," *Acta Physiol.Scand.* **66**, 337-345 (1996).
2. A. Bollinger, P. Butti, J. P. Banas, H. Trachsler and W. Seigenthaler, "Red cell velocity in nailfold capillaries in man measured by a television microscope technique," *Microvasc. Res.* **7**, 61-72 (1974).
3. C. M. Black, R. P. Clark, K. Darton, M. R. Goff, T. D. Norman, H. A. Spikes, "A pyroelectric thermal imaging system for use in medical diagnosis," *J Biomed Eng* **12**, 281-286 (1990).
4. P. A. Payne, R. Y. Faddoul and S. M. Jawad, "A single channel pulsed Doppler ultrasound instrument for measurement of skin blood flow," *Practical Aspects of skin Blood Now Measurement* (London: Biological Engineering Society, 1985).
5. A. P. Shepherd, and P.Å Öberg (Eds) 1990 *Laser Doppler blood flowmetry* Kluwer Academic Publishers, Boston.
6. T. J. H Essex and P. O. Byrne, "A laser Doppler scanner for imaging blood flow in skin," *J.Biomed. Eng.* **13**, 189-193 (1991).
7. K. Wårdell, A. Jakobsson and G. E. Nilsson, "Laser Doppler perfusion imaging by dynamic light scattering," *IEEE Trans. Biomed. Eng.* **40**, 309-316 (1993).
8. C. Protière, K. Evans, J. Camerlo, M. P. d'Ingrado, G. Macquart-Moulin, P. Viens, D. Maraninchi and D. Genre, "Efficacy and tolerance of a scalp-cooling system for prevention of hair loss and the experience of breast cancer patients treated by adjuvant chemotherapy," *Support. Care Cancer* **10**, 529-537 (2002).
9. E. G. Grevelman and W. P. M. Breed, "Prevention of chemotherapy-induced hair loss by scalp cooling," *Ann. Oncol.* **16**, 352-358 (2005).

Chapter 2

Review of methodological developments in laser Doppler flowmetry*

Laser Doppler flowmetry is a non invasive method to measure microcirculatory blood flow in tissue. In this review the technique is discussed in detail. The theoretical and experimental developments to improve the technique are reviewed. The limitations of the method are elaborated and the research done so far to overcome these limitations is critically assessed.

* V. Rajan, B. Varghese, T. G. van Leeuwen, and W. Steenbergen, "Review of methodological developments in laser Doppler flowmetry," in press, *Lasers in Medical Science*.

1. Introduction

Laser Doppler Flowmetry (LDF) is a noninvasive diagnostic method to measure blood flow in tissue. The technique is based on measuring the Doppler shift [1] induced by moving red blood cells to the illuminating coherent light. A laser Doppler instrument output often gives flux, velocity and concentration of the moving blood cells. These parameters are extracted from the power spectrum of the photocurrent fluctuations produced by reflected light illuminating a photodetector. There are two types of perfusion measurements in practice, laser Doppler perfusion monitoring (LDPM) and laser Doppler perfusion imaging (LDPI).

Since the commercialization of the technique in the early 80s, LDF has a modest but stable and steadily growing commercial market. Figure 1 illustrates the growth of the use of LDF in research by the number of peer reviewed articles published each year[#] in which laser Doppler flowmetry techniques have been used (LDPM and LDPI).

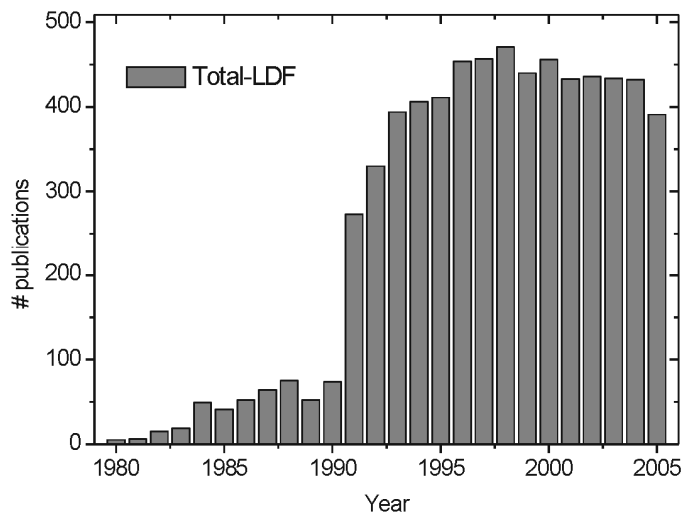


Fig. 1 Publications using LDF techniques from 1980 till 2006

[#] Web of Science (ISI Web of Knowledge), search terms ((laser AND Doppler) OR (laser-Doppler)) AND (perfusion OR microcirculation OR flowmetry)

Other techniques which were used for blood flow measurements before the evolution of the laser Doppler technique were the Xenon washout technique [2] and the radioactively labeled micro sphere technique [3, 4]. These techniques require an injection of a radio active substance into the blood stream.

Doppler ultrasound methods to measure blood flow are non-invasive but are incapable of measuring the microcirculation. In table 1 various techniques to measure skin blood flow are compared.

The major advantage of the laser Doppler techniques in general is their non invasiveness and the ability to measure the microcirculatory flux of the tissue and fast changes of perfusion during provocations. The technique can measure perfusion quantitatively (although relative) in real time

There are some limitations of the technique. The major limitations are the influence of tissue optical properties on the perfusion signal, the motion artifact noise, lack of quantitative units for perfusion, lack of knowledge of the depth of measurement and the biological zero signal (perfusion measured at no flow condition). These limitations motivate ongoing research in both the instrumentation and theoretical aspects of the technique.

Laser Doppler flowmetry techniques for measuring blood flow were reviewed by many authors considering different aspects of the technique. Early developments in laser Doppler flowmetry and its clinical applications were reviewed by Shepherd and Oberg [10]. Obeid et al. [12] reviewed the limitations of the technique. In a later review Vongsavan and Matthews [13] compared the performance of two instruments which were then widely used in clinics: Periflux model PF3 (Perimed, Stockholm, Sweden) and Moor blood flow monitor model MBF3D/42 (Moor instruments, Axminster, Devon, UK). Leahy et al. [14] reviewed the principles and use of laser Doppler instruments discussing different aspects of the method. In a recent review Briers [9] compared laser Doppler techniques with speckle techniques which progressed in parallel. A review of whole-field blood velocity measurement techniques can be found in Vennemann et al. [15]. This article reviews laser Doppler velocimetry, laser speckle methods, magnetic resonance and ultrasound particle image velocimetry techniques used for perfusion monitoring and velocity mapping.

In this article we review the developments in laser Doppler perfusion monitoring and imaging with emphasis to more recent advances. The methodological progress of the technique is followed in detail and a special emphasis is given to the limitations of techniques and the research in this regard. This review will not cover imaging methods based on Laser Speckle Contrast Analysis (LASCA).

Table 1. Methods to measure skin blood flow				
Technique	Noninvasive	Principle	Measured quantity	Disadvantages
Fluorescent tracers [5]	No	A fluorescent dye is injected in to the blood stream. Tissue fluorescence is taken as an indication of blood flow.	Blood flow distribution	No quantitative measurement. Cannot study fast changes in blood flow.
Radioactive microsphere technique [3]	No	Radioactive microspheres are injected in to the blood stream, mean blood flow is estimated from the recovered isotope count from excised tissue	Mean blood flow	Tissue needs to be excised for the measurement, no real time measurement possible
^{133}Xe wash out technique [2]	No	^{133}Xe is injected subdermally. The rate of clearance is a measure of blood flow	Absolute blood flow	Point measurement. Does not give information about regional blood flow
Capillary microscopy [6]	Yes	The distance traveled by erythrocytes in successive frames gives a measure of blood velocity	Capillary distribution and blood velocity	Measures only one or few capillaries. Capillary perpendicular to the skin surface cannot be visualized
Thermography [7]	Yes	Skin temperature radiation is imaged and is related to the blood flow	Temperature map of the skin	Skin temperature and blood flow are not directly related
Doppler ultrasound [8]	Yes	Based on the Doppler shift imparted by moving blood cells to the probing sound waves	Spatially resolved velocity	Resolution insufficient for smallest vessels, only sensitive to one velocity component
Speckle techniques [9]	Yes	Speckles generated by back scattered photons from the tissue analyzed in spatial and temporal domain to estimate blood flow.	Decorrelation time and speckle contrast, related to blood flow.	No spectral information, quantitative measurement is not possible.
Laser Doppler flowmetry [10]	Yes	Based on the Doppler shift imparted by the moving red blood cells to the probing light.	Relative concentration and velocity of moving red blood cells	No absolute measurement, no depth information
Doppler OCT [11]	Yes	Combination of Doppler velocimetry with low-coherence optical interferometry	Spatially resolved velocity of moving red blood cells	Limited probing depth 1-2mm, only sensitive to one velocity component

1.1 Working principle of LDF techniques

1.1.1 Light scattering in tissue

When a beam of laser light illuminates a small area of tissue photons will be scattered by static and dynamic particles. The moving red blood cells will impart a Doppler shift to the photon which depends on the scattering angle, the wavelength and velocity vector of the scatterer. If a wave with frequency is ω scattered from a moving particle with a velocity v (Fig 2) the Doppler shift can be written as: $\Delta\omega = |v||k_i - k_s| \cos \beta$ Where k_i is the incident wave vector, k_s is wave vector of the scattered wave and β is the angle between the velocity vector and the scattering vector which is defined as $(k_i - k_s)$. With α the scattering angle and λ the wavelength of the light in the medium, the Doppler shift can be written as $\Delta\omega = 2(2\pi/\lambda)|v| \sin(\alpha/2) \cos \beta$. In a tissue with a large number of moving particles and for sufficiently long photon path lengths, photons will undergo more than one Doppler shift, which will result in a range of Doppler shifted frequencies. Moreover, the random orientation of microcirculatory blood vessels and randomization of the photons with different scattering events give rise to a range of Doppler shifts, even when all particles would move at the same speed.

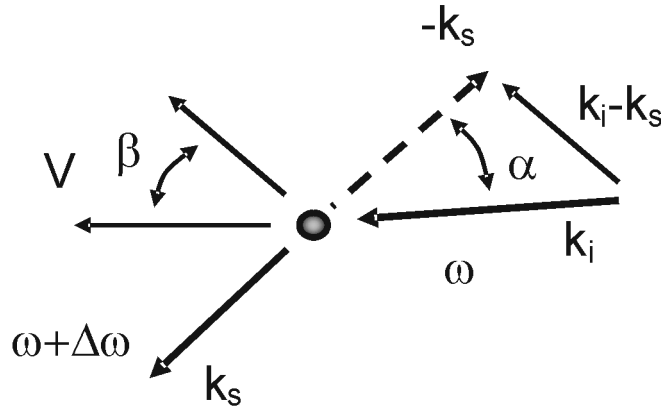


Fig. 2 Scattering of a photon with a wave vector k_i and frequency ω by a moving RBC with velocity V .

1.1.2 Extraction of laser Doppler signal

In laser Doppler flowmetry the interference of Doppler-shifted light with non-Doppler shifted light on the photodetector generates a dynamic speckle pattern. As result of the dynamic speckle patterns the detector current signal will fluctuate. If the signal generated by the photodetector is from only Doppler

shifted light it is called a homodyne signal in the laser Doppler terminology. The scattering from a tissue matrix with a sufficiently small volume of blood (dynamic scatterers) will result in a signal produced mainly by interference of Doppler shifted light with non-Doppler shifted light, a situation called heterodyne. It can be derived [16] that the AC signal generated by a fluctuating speckle pattern, normalized by the DC², is equal to

$$\frac{\langle i_{AC}^2 \rangle}{\langle i_{DC} \rangle^2} = \frac{1}{N} f_D (2 - f_D) \quad (1)$$

with $\langle i_{AC}^2 \rangle$ the mean square of the photocurrent fluctuations, $\langle i_{DC} \rangle$ the mean photocurrent, N the number of speckles on the detector and f_D the Doppler shifted fraction of all detected photons. In this, it is assumed that the photodetector surface is, on average, homogeneously illuminated. Figure 3 illustrates the intensity fluctuations of the photodetector signal generated by dynamic speckle patterns.

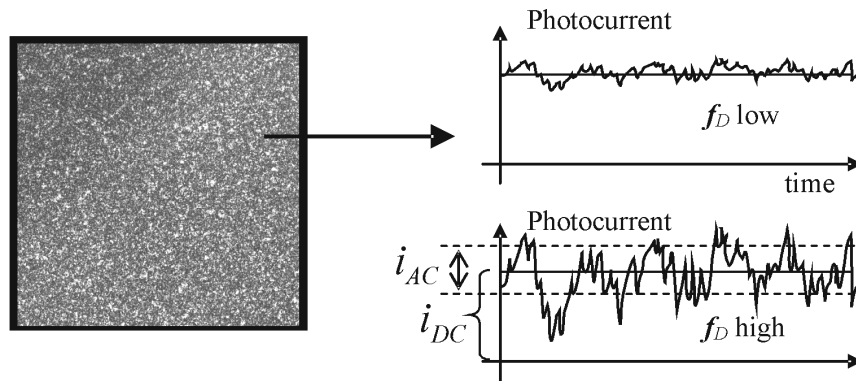


Fig. 3 Speckles generated by light backscattered from a particle suspension. On the right; an illustration of the photodetector intensity fluctuations resulting from the dynamic speckle pattern. f_D is the Doppler shifted fraction of all detected photons.

In order to extract the flux and concentration of the moving blood cells a power spectrum of detector current fluctuations is measured. Fig. 4 shows a power spectrum of detector current fluctuations (averaged over 500 spectra) obtained from laser light back scattered from right cheek of a human subject. The moment of order i of the power spectrum is defined as

$$M_i = \int_0^{\infty} \omega^i P(\omega) d\omega \quad (2)$$

Bonner and Nossal [17] showed that the first moment $i = 1$ in Eq. (2) is linearly proportional to the root mean square (rms) velocity of moving red blood cells and its concentration provided the blood concentration is small (negligible multiple scattering). The first moment was defined as the perfusion signal which is the average concentration times the average rms velocity of moving red blood cells (RBC). The zero order moment (M_0) is equal to the modulation depth of the photocurrent as defined by Eq. (1), and is proportional to the concentration of moving red blood cells and hence the weighted first moment (M_1/M_0) gives the average Doppler shift (proportional to the average velocity) imparted by the moving blood cells. Since the laser Doppler instrument cannot present blood flow in absolute values perfusion is expressed in terms of arbitrary perfusion units (PU).

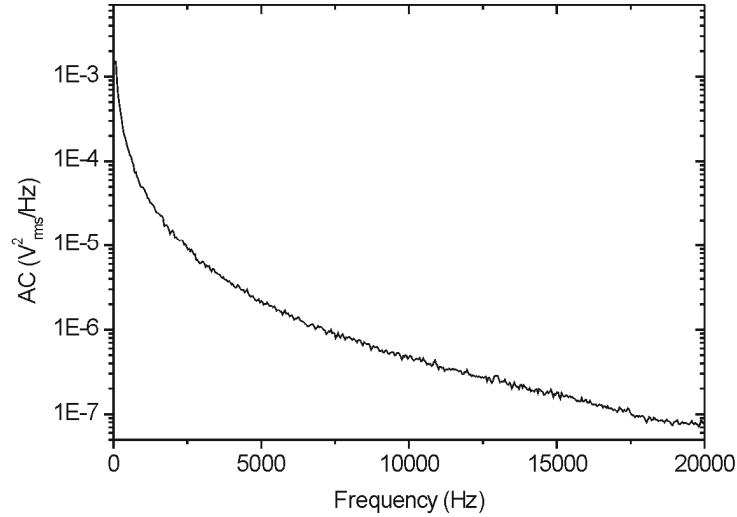


Fig. 4 Power spectrum of laser Doppler signal measured from human skin in vivo.

In arriving at the expression relating blood flow and moments of the power spectra Bonner and Nossal [17] used the following assumptions. 1) light is randomized in direction in all tissues independent of blood flow and blood volume; 2) Doppler shift due to blood flow principally arise from the scattering of diffuse light from moving red blood cells; 3) the mean number of RBCs by which a typical detected photon is Doppler shifted increases linearly with the number density of RBC's flowing within the microcirculation; 4) the Doppler broadening is increased by multiple scattering from more than one moving red blood cell. Moreover the linear relationship depicted by the model between first moment and the concentration of RBC is valid only for small fractions of red blood cells (negligible multiple scattering).

1.1.3 Laser Doppler perfusion monitor

A laser Doppler perfusion monitor uses a fiber optic probe with one multimode fiber to deliver the laser light, often from a semiconductor laser diode, to the tissue and another multimode fiber to detect the back scattered photons (Fig. 5(a)). It is a one point measurement method which records the integrated perfusion in a sampling volume in real time. The measurement depth and sampling volume depend on the wavelength and the fiber separation used. In normal skin and using laser Doppler instruments with a probe with standard fiber separation (0.25 mm) and 780 nm wavelength, the measuring depth is one half to one millimeter and the measurement volume is about 1mm³. In LDPM often the perfusion signal is normalized with DC² to make readings independent of the actual laser power.

The main manufacturers of laser Doppler instruments are Perimed AB, Moor Instruments Ltd, Transonic Systems Inc, Oxford Optronix Ltd and LEA Medizintechnik. The wavelengths used most often by these systems are 630, 780 and 830nm with typical fiber-to-fiber distances of 0.25, 0.5 and 0.78mm (except for the instruments by LEA, see section 3.1.1).

1.1.4 Laser Doppler perfusion imager

A laser Doppler perfusion imaging instrument maps the perfusion from a larger area by scanning the laser beam over the area of interest. Figure 5(b) illustrates the schematic of a scanning laser Doppler perfusion imager. The advantage of this instrument over the monitor is that it is non contact in nature, so it can be used in clinical situations where contact with the tissue may be undesirable. Also it gives a perfusion map of a larger area which gives average perfusion in a heterogeneous tissue in a single measurement. In LDPI we often find DC normalization, probably because that gives better results for heterogeneous tissue surfaces.

The main manufacturers of laser Doppler perfusion imagers are Perimed AB and Moor Instruments Ltd. The latest imager model PIM3 of Perimed AB uses a stepwise scanning of laser beam (670-690 nm, beam

diameter 1mm). A complete scanning of an area of 5x5cm (up to 50x50cm is possible) with a resolution of 256x256 pixels takes 4-5 minutes, for a 25cm distance of scanning head from the imaging surface. The spatial resolution of the image is 1mm, and is limited by the beam diameter.

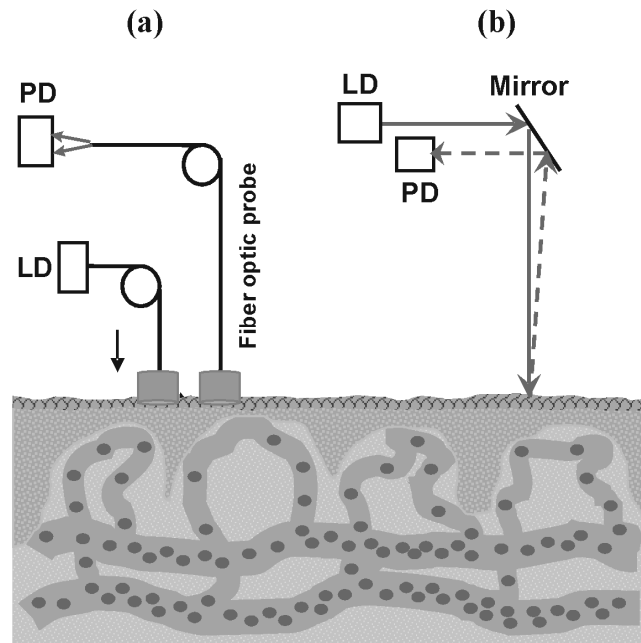


Fig. 5 An illustration of (a) LDPM and (b) LDPI geometries on a tissue model. LD-Laser Diode, PD-Photo Detector.

Moor instruments Ltd. use a continuously scanning beam, and includes different lasers in their imaging systems (633, 785 and 830nm), also a dual wavelength system is available. The spatial resolution of the image is typically 1mm, and a high resolution version is also available (0.1mm). The scanning time is about 6 minutes for a 50cm x 50cm image at 256 x 256 pixel resolution, at a speed of 4ms/pixel and 100cm distance.

2. Recent theoretical developments

2.1 Attempts towards velocity resolved laser Doppler perfusion measurements

For a proper physiological interpretation of laser Doppler measurements, it would be useful to extract the velocity distribution of red blood cells from the power spectrum. As explained in the theory in order to get an absolute velocity

measurement one needs to know the scattering angle (α), the angle between the velocity vector and the scattering wave vector (β), and the number of Doppler shifts in the case of multiple scattering. Dorschel and Muller et al. [18] tried to solve the problem of the angle β (angle φ in their manuscript) with the assumption of an isotropically distributed angle between the velocity and the scattering vector and calculated a corrected frequency spectrum as if all vectors were parallel. The spectrum was corrected for various directions of velocity and reference vector by multiplying the Doppler shift by the differential coefficient of the spectrum which ultimately will lead to a velocity resolved flow measurement. Even though the approach is theoretically valid only for a fixed relation between the scattering vector and the direction of the moving scatterer remarkable results were obtained from the phantom measurements. The problem of non constant scattering angle and influence of multiple Doppler shifts are a limitation of their approach.

Larsson et al. [19] proposed a method to extract concentration measures of RBC associated with a certain absolute velocity. The concentration was estimated by fitting Monte Carlo derived Doppler spectra arising from known velocities to the measured Doppler power spectrum. It was assumed that if multiple Doppler shifts are negligible the power spectrum formed by a laser Doppler instrument can be considered to be from a number of single velocity spectra,

$$H_{tot}(\omega') = \sum_i c_{v_i} H_{v_i}(\omega') \quad (3)$$

where H_{tot} is the multiple velocity Doppler histogram, c_{v_i} is the concentration of the scatterers that move with a velocity v_i and H_{v_i} is the normalized single velocity Doppler histogram produced by the velocity v_i . In principle, by fitting the simulated single velocity Doppler spectra to the measured spectra the concentration of scatterers with that velocity can be extracted. Experiments were done with both RBC and microsphere suspensions. For Monte Carlo simulation of RBC Doppler spectra a two parameter Gegenbaur kernel phase function was used to describe the light scattering process. The results showed a nice match between simulated and measured spectra. Experiments with single and double-tube flow phantoms confirmed the validity of their model to extract concentrations associated with related absolute velocities.

There are some limitations in the model. The presented model only works with single Doppler scattering and very low concentration suspensions. Also an isotropic distribution of the light fluence was assumed for the simulation which is valid only for photons traveled at least one reduced mean free path length mfp' . So the validity of the assumption is questionable considering the very low scattering levels used for the experiments. Also the influence of the heterogeneity of the optical properties, multiple Doppler shifts

and distribution of velocity components has to be addressed in considering the applicability of their model in real tissue.

Liebert et al. [20] also considered the decomposition of a spectrum into individual velocity components similar to Larsson et al. [19]. Single scattering Doppler shifted power spectra were assumed and the concentration of a particular velocity component was calculated either by solving a model equation in which the power spectrum is defined by a set of linear equations composing of different frequency components. The calculated average concentration was used to find the distribution of concentration of different velocity components by

$$c(V) = \sum_{j=1}^M a_v h_v(\Delta f_j) \quad (4)$$

where a_v is a weighting factor which they derive from their model. Here the Doppler shifted probability distribution $h_v(\Delta f_j)$ is summed over the frequency which gives the distribution of probability of Doppler scattering events as a function of speed. The proposed model could extract the distribution of adjacent velocities from power spectra but it is valid only for single Doppler shifts and is not yet validated experimentally.

2.2 Modeling of deep perfusion measurements

In order to interpret deep perfusion signals measured with a large source detector spacing one needs to address the problem of multiple Doppler shifts where the classical approach fails. Binzoni et al. [21] proposed an algorithm to model the power spectrum of the laser Doppler signal which can be fitted to the experimental spectra to calculate the rms velocity of the moving particles and the mean number of scattering events. Three unknown model parameters were defined as \bar{m} , v and β which are the average number of collisions which a detected photon makes with a moving particle, the velocity of the particle and a factor that depends on the optical coherence of the signal at the detector surface respectively. These parameters were found by fitting the model function describing the power spectrum on the measured data. It was proved that the model works even at large inter optode spacing (1.5cm) and \bar{m} values greater than one (multiple scattering) where the classical Bonner and Nossal model fails. Another interesting result was that the model could calculate the mean velocity without the influence of concentration changes and the number of scattering events. This showed the advantage of the proposed method over the classical approach. There are few limitations in this model which prevent it from measuring the absolute flow. One of the model functions β (the coherence factor) is showing large variations. Also it was known [17] that β depends on the optical properties of the tissue. So in order to have reliable information the variation of β should be studied further. The window of the spectrum chosen

seems to be rather small (8 kHz) compared with the source-detector distance used. At larger detector distances and measuring volumes considered in the study, a higher bandwidth of frequencies can be expected. Since the model considers large detector distances and multiple Doppler shifts the proposed model is a good stepping stone for measuring the absolute rms velocity from laser Doppler perfusion data.

One of the limitations of the Bonner and Nossal model [17] is that it assumes a random/Brownian motion to the red blood cells. The actual speed distributions of red blood cells in tissue consist of a Brownian and a translational component. The translational component is particularly important while measuring the deep flow where the contribution from larger arterioles is significant. Binzoni et al. [22] took into account the Brownian component and the translational component in the tissue perfusion. They proposed a theoretical model to calculate different moments in laser Doppler spectra which contains the Brownian velocity and translational velocity. The proposed method is a rather complicated power series of the average number of photon collisions \bar{m} and the translational velocity V_{trans} . The model also deals with the biological zero problem in laser Doppler flowmetry which is the observation of a nonzero perfusion with a complete arterial occlusion. It was claimed that during arterial occlusion $V_{trans}=0$ which makes only the Brownian motion to contribute in their equation. Even though the validity of the assumptions were not calculated experimentally this approach could show the limitation of the classical approach in dealing with the translational motion of the scatterers when multiple Doppler scattering is considered.

Lohwasser and Soelkner [23] suggested an LDF algorithm to calculate the average blood cell velocity in deep perfusion measurements with a penetration depth ranging from 10 to 30mm. They matched measured spectra with analytical diffusion theory models and Monte Carlo simulations. The spectra predicted with the diffusion model match well with the measured spectra in the case of large fiber separations. An analytical fit was defined based on a simple equation

$$\log[s(f)] = c + \beta f \quad (5)$$

where $s(f)$ is the measured power spectrum and c and β are constants. $1/\beta$ is proportional to the average velocity which is found from the measured spectra by an analytical fitting. Here a frequency window was defined for fitting based on a quality function neglecting low frequency spectra (3 kHz in their experiments). Based on the results it was claimed that the perfusion in deep tissues can be measured without the influence of perfusion in superficial layers. This is particularly suitable for perfusion measurements in brain cortex avoiding the influence of scalp perfusion. But issues like the influence of absorption and scattering on the model independent of perfusion were not discussed. Also the selection of the frequency window will be very critical when the perfusion of

the superficial layer is very high which will cause unwanted higher frequency components to appear in the selected window.

3. Technical innovations and introduction of new methods based on laser Doppler flowmetry

After the first publication of the potential of the Doppler effect induced by blood cells to measure blood flow by Stern [24] it took several steps for laser Doppler flowmetry to evolve as a clinically applicable tool. The major steps in this regard started with Watkins and Holloway [25] who followed by Stern [24] developed a processor for clinical applications. Later on Bonner and Nossal [17] developed a signal processor with a well defined theoretical base. This processor was further modified [26, 27] and was widely accepted by researchers and manufacturers.

A detailed review of early technical innovations (till 1990) in laser Doppler flowmetry can be found in Ref. [10]. Laser Doppler perfusion monitoring (LDPM) which is a one point measurement technique was then extended to produce a perfusion map of an area of tissue by stepwise scanning of the laser beam over the tissue surface, called laser Doppler perfusion imaging (LDPI). Essex and Byrne [28] developed a laser Doppler scanner which can produce an image of $500 \times 700 \text{ mm}^2$ in 6 minutes with a spatial resolution of 3mm. A scanning mirror was used to steer the beam which moves continuously over the measurement region. The back scattered photons were collected with a lens system with a photodetector in focus. Followed by this Wardell et al. [29], reported on a scanning laser Doppler system without using a lens in front of the detector. The system used a stepper motor to steer the beam in a stepwise manner over the measurement region. A correction factor was used based on the distance of the source to the tissue surface. A flow simulator was used for the validation of the instrument. In this part of the review we will discuss the recent technical developments in perfusion monitoring and imaging.

3.1 Technical innovations in laser Doppler perfusion monitoring

3.1.1 Signal processing in laser Doppler flowmetry

In order to estimate the perfusion from the Doppler broadened photodetector signal, several frequency weighted signal processing algorithms were developed [10]. Koelink et al. [30] developed a digital signal processing method and compared this with the performance of analogue signal processing methods. The digital method used a time domain approach based on the time derivatives of the photocurrent fluctuations. It was found that the digital signal processor was more accurate and had a large dynamic range. The automatic optimization of the amplification of the input signal in the digital processor was found to be very user friendly compared to the analogous method. The bandwidth selection

in signal processing is very critical [12] and should be sufficient for the coverage of major frequency range of the signal avoiding the white noise. Chen et al. [31] developed an adaptive processing bandwidth adjustment in which the Doppler spectra was first fitted to with a Lorentzian function and the bandwidth at the half the maximum of the Lorentzian function was used as an indicator of the major frequency range of the signal. The processing bandwidth was then tuned according to the calculated bandwidth values.

3.1.2 Depth sensitivity in LDF

To achieve some degree of depth resolved perfusion monitoring, the concepts of using either different wavelengths [32, 33] or changing the source to detector distance [34] have been considered. Since the optical absorption by blood and to a smaller extent the scattering level of the tissue differs significantly for green, red and infrared light this may be utilized to measure the blood flow in tissue volumes of different size in depth. Figure 6 depicts the calculated wavelength dependence of penetration depth of light into oxygenated blood, deoxygenated blood and tissue. The light penetration depth ($1/\mu_{eff}$) into oxygenated and deoxygenated blood was calculated based on the optical properties of whole blood reported by Faber et al [35]. The penetration depth of light into tissue (water content: 80%, wavelength dependence $\mu'_s: \lambda^{-0.37}$) was calculated assuming a blood volume: 5%(oxygenation: 80%) [36]. Green light (543nm) has a smaller penetration depth (0.33mm) into tissue compared to red light (633nm) which has 3.14mm penetration depth and infrared light (800nm) having 4.3mm penetration depth.

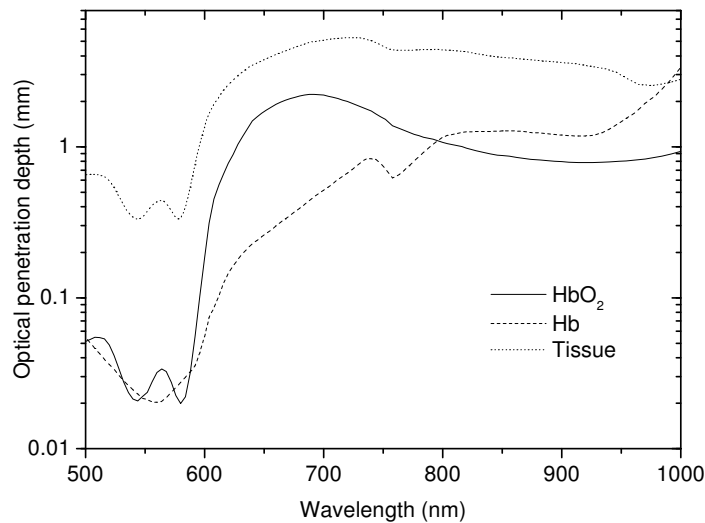


Fig. 6 The calculated wavelength dependent penetration depth of light into oxygenated blood, deoxygenated blood and tissue (blood volume: 5%, oxygenation: 80%, water content: 80%, reduced scattering coefficient (μ'_s) at 800nm: 0.75mm^{-1}) over the wavelength range from 500 to 1000nm.

Gush and King [37] used a red (632.8nm) and green (543.5nm) He-Ne laser to determine the dependence of flow response measurement on wavelength. They measured on forearm and finger pulp and found that flow response differs according to the laser wavelength used, with the green LDF more sensitive to a change in blood flow. It was observed that since the penetration depth of green light is smaller than red light (Fig. 6) the laser Doppler signal obtained with red light shows more high frequency components than the green light signal. Moreover a heat provocation test showed that green light is more sensitive to the changes of blood flow during vasodilatation, and showed an increase in the high frequency component in the power spectrum where as it falls in the case of red light. This observation was explained based on the results of Einav et al. [38] which showed that when vessel diameter increases, the more or less parabolic blood velocity profile becomes more flat-topped and shows an increase in velocity close to the vessel wall compared to the velocity at the axis which remains in the same range. So green light which probes the periphery of the larger microvessels only, due to a much larger absorption than red and near infrared light (Fig. 6, optical penetration depth of

oxygenated and deoxygenated blood), shows a larger increase in higher Doppler frequency components compared to red light which will multiply scatter throughout the vessel, and would also encounter blood with slightly reduced velocity. Figure 7 illustrates the situation.

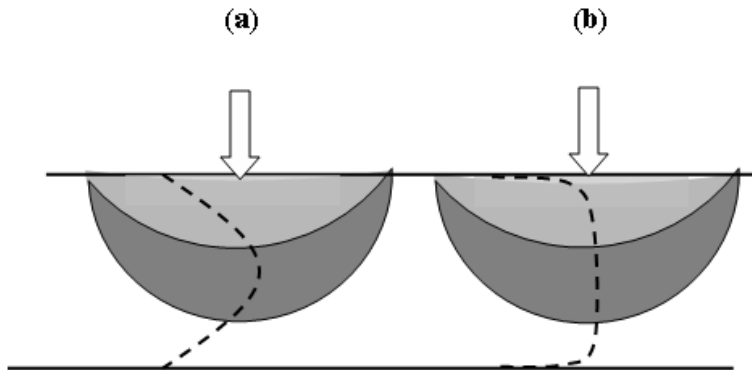


Fig. 7 Effect of vasodilation on the velocity response of green light and red light (dark shade); (a) before vasodilation blood flow shows a parabolic velocity profile (dotted line), green light probes only the periphery of the vessel where the velocity is low (b) Vasodilation produces a flat topped velocity profile [38] where the green light probes mainly the wall region where the velocity has increased to a larger extent than in the centre. In both situations red light probes a larger volume covering large part of the velocity profile which makes the red light less sensitive to flow change compared to the green light.

In a more sophisticated study Koelink et al. [39] used a dual wavelength laser Doppler flowmeter with wavelength 633nm and 800nm in combination with Monte Carlo simulation to show depth dependent flow measurement using different wavelengths. Measurements on healthy volunteers showed that two laser systems respond in different ways to an occlusion. Monte Carlo simulations in a three layer system showed a significant difference in Doppler shifted photons and number of Doppler scattering events probed in two wavelengths in deeper layers: an 800 nm laser probes deeper and shows a higher spectral band width compared to 633 nm.

Another aspect which was studied was changing the source to detector separation which showed the feasibility of depth dependent laser Doppler perfusion monitoring [34, 40]. Liebert et al. [41] developed a multi channel probe with seven parallel fibers of 200 micrometer fixed close to each other, which gives an emitter to detector distance of 0.2 to 1.2mm. Measurements with a flow model showed that a large separation between source and detector

increases sensitivity to deeper flows whereas a small detector separation measures more superficially.

3.1.3 Deep perfusion measurement techniques

In order to measure deep tissue perfusion, for example in muscle or brain, a new type of near-infrared laser Doppler monitors was developed. This employed a high source power (or a modulated source) in combination with a large source to detector separation (20-60mm). Lohwasser and Soelkner [23] used a 120 mW laser and showed that they could measure flow up to a depth of 30mm. Binzoni et al. [21] used a source to detector separation of 1.5 to 2.5 cm to measure the muscle rms velocity. To measure deeply without exceeding the laser safety limit pulsed light sources have been considered. Kolinko et al. [42] developed nano and picosecond laser source based laser Doppler flowmeters which can potentially measure deep perfusion, and can be used for time resolved perfusion measurements. Kolkman et al. [43] reported on a pulsed laser Doppler flowmeter based on a 15 kHz repetition rate pulsed laser diode of 20mW peak power, which will give an average power of 4.7mW. They sampled each peak signal of back scattered laser pulses to construct a power spectrum. Results showed a significant increase in signal to noise ratio compared to the signal obtained from a cw laser source of the same average power. Even though the depth probed by cw and pulsed LDF were not compared, this method has the potential to measure deep without exceeding the safety limits.

In a novel laser Doppler flowmetry and remission spectroscopy system (Oxygen-To-See (O2C), LEA Medizintechnik, Giessen, Germany) a wavelength of 820 nm (30 mW) was used in the laser Doppler part of the instrument. Using probes with a detection fiber up to a distance of 15mm from the source fiber it was claimed that the instrument offers a sampling depth of up to 15mm.

3.1.4 Integrated systems

The idea of miniaturizing the laser Doppler flowmeter and avoiding fiber movement artifacts has led to the concept of an integrated probe for laser Doppler perfusion monitoring [44]. De Mul et al. [44] developed a probe (\varnothing 16mm and 13mm long) in which a solid state diode laser source (AlGaAs, 5mW, 840nm) and detectors were integrated. This avoided the use of optical fibers and related motion artifacts. This probe has been commercially available as the Diodopp (Applied Laser Technologies, The Netherlands). Higurashi et al. [45] reported on a lighter and smaller integrated probe (1.5mm thick \times 2mm wide \times 3mm long) in which they used a more compact InGaAsP-InP distributed feed back laser diode (1310nm). Due to the edge-emitting behavior of the latter, a micromachined concave mirror was required for beam deflection. Recently Serov et al. [46] reported on an integrated optoelectronic probe with a vertical cavity surface emitting laser diode (VCSEL). In such a laser, the vertically

emitted beam avoids the use of deflection optics. The laser diode and custom made integrated circuit with detectors, amplifiers and other electronics were integrated in the probe. The probe had a size of $\varnothing 6 \times 6 \text{ mm}^3$ with a custom chip of $1.2 \times 0.8 \text{ mm}$ size, containing a photodetector pair (PIN photodiodes) and all necessary electronics. A comparative study of the system with a commercial fiber optic laser Doppler instrument was performed. Results obtained on a subject during physical exercise showed that the signal measured with the integrated probe was not influenced by motion artifacts whereas the fiber optic instrument showed a significant influence of motion artifacts. However the SNR of the integrated probe instrument was less compared to the commercial device because of the small coherence length of the multimode VCSEL (0.6mm) compared to the edge-emitting single mode diode lasers used in conventional systems (6mm).

3.1.5 Path-length-resolved laser Doppler flowmetry

A totally different refinement introduced in laser Doppler flowmetry was the path length resolved interferometer based LDF. A laser Doppler based instrument to measure path length resolved flow was introduced by Petoukhova et al. [47]. A Mach-Zehnder interferometer with multimode graded index fibers and a low coherent light source was used. By tuning the path length in the reference arm, photons which traveled a specific optical path length in the sampled medium can be selected. It was shown [48], that in this way, Doppler shifts of multiply scattered light can be obtained which are independent of the absorption properties of the surrounding medium. Varghese et al. [49] developed a phase-modulated Mach-Zehnder interferometer which can measure the optical path length distribution from a mixture of static and dynamic scatterers with increased signal to noise ratio. This method allows measuring the optical path length distribution of back scattered photons from a tissue matrix and can resolve the contribution of photons (static and dynamic) with specific path lengths to the Doppler power spectra. The advantage is that one can compensate for the changes in optical properties which cause intra- and interindividual variation in perfusion measured with conventional laser Doppler flowmeters.

3.2 Laser Doppler perfusion imaging

After the introduction of scanning laser Doppler [28, 29], the perfusion imaging technique has undergone a dramatic progress with the development of technology. Commercial scanning systems became available which can make color maps of perfusion on an area of tissue [52, 53]. Wardell and Nilsson [52] introduced duplex laser Doppler perfusion imaging which allows studies of temporal blood flow changes by frequently updated single or multipoint recordings. Linden et al. [53] developed enhanced high resolution LDPI with a focused laser beam of FWHM less than 40 micrometer. A lateral resolution of

40 micrometer was achieved using this beam diameter. For a review of a range of clinical applications of LDPI, see Briers et al. [9]. Harrison et al. [54] and Kernick and Shore [55] provided a critical assessment on the performance of the imaging systems with a flow model.

The measurement speed of the scanning laser Doppler imagers is limited by the requirement of scanning a beam through the area of investigation. A scanning with a step size of 1mm takes a few minutes to scan a 128*128 points area. Some applications of perfusion imaging like drug test and burn wound diagnosis demand a much faster measurement. With evolution of CMOS technology a new full field laser Doppler perfusion imaging system was introduced [56, 57] which can make a 2D map of perfusion relatively faster. In this system a diverging laser beam illuminates an area of tissue and a CMOS sensor captures the back scattered photons with a lens. A number of frames (typically 1024) are captured with a sampling rate of several kilohertz (depending on the selected region of interest on the image array). A 2D perfusion map can be plotted by processing the signal captured by each pixel in time. The advantage of this system is that it can make perfusion maps much faster than the conventional scanning beam systems. Also since there is no scanning part in the system movement artifacts can be avoided. The speed and the sampling rate of this system are improving very fast with the development of CMOS technology.

Another full-field approach for laser Doppler imaging was reported [58, 59] based on a frequency shifting off axis holography. The set up consists of a heterodyne measurement of the scattered field, two Bragg cells were used for frequency shifting of the reference beam. A CCD sensor was used to record the interference pattern and the Doppler line width was calculated by a time domain FFT of the pixels of the image. The technique has the advantage that it requires only a much slower camera compared to one proposed by Serov et al. [56, 57]. Also the number of frames required (32 images) to process the signal is much less compared to the earlier report (1024 images) for about 50 Hz spectral resolution. But the measurement speed is limited by the frequency scanning by the Bragg cell. Also only the $\frac{1}{4}$ of the pixels of each frame can be used to describe the image, reducing the area of investigation.

4. Calibration standards

Since the laser Doppler perfusion signal is a relative measure of flux, standardization is required in comparing the level of perfusion in different measurements and from different instruments. A calibration system for this requirement was a topic of research since the early days of LDF, with various purposes: 1) to check the instrument stability, 2) to establish the linearity of the instrument response to blood flow, 3) to establish relations between different

instruments, and 4) to relate the reading of the instrument to real perfusion, if possible.

There is no golden standard yet available to calibrate the Laser Doppler instrument for perfusion measurements. Since the distribution of blood vessels in tissue and optical properties is heterogeneous it is difficult to calibrate an instrument to measure absolute blood flow per unit volume of tissue. Often a comparison between laser Doppler flowmetry and an alternative method is complicated because of the difference in techniques and probed volume [60-63]. Another approach which was tested for an absolute flow measurement was either measuring on a well defined tissue preparation [64] or on flow models [26, 65]. But these methods cannot be considered as calibration methods on a day to day basis for clinical use. Therefore a simple method has been in use for frequent and easy calibration of laser Doppler instrumentation. This is a simple aqueous suspension of polystyrene microspheres in Brownian motion called Motility Standard. The Doppler shift generated by the particles in Brownian motion is used to calibrate the system's overall integrity for a comparison of measurements in different time intervals. But this method has some major shortcoming as mentioned by Liebert et al. [66]. Due to its completely dynamic properties, such suspensions induce Doppler shifts leading to a pure homodyne measurement, whereas in real tissue the majority of photons are un-shifted which produces totally different heterodyne spectra.

Several studies were carried out to develop a calibration device for absolute flow measurement. Most of the devices are based on flow models. Nilsson et al. [27] used a mechanical fluid model based on polyacetal disk with polythene tubing to simulate tissue blood flow. Obeid et al. [65] used a similar flow model to check the linearity of the velocity response of different signal processing algorithms. Another approach was using solid-based systems in which a layer is rotated or translated in between a sandwich of stationary layers [67]. De Mul et al. [68] and Steenbergen and De Mul [69] reported on a standard consisting of a set of layers containing scattering and absorbing particles, either at rest or moving with respect to each other. The advantage of this approach is the absolute predictability of the results with Monte Carlo simulations. Larsson et al. [70] used this system to assess the influence of tissue optical properties on the depth sensitivity and mean sampling depth of a laser Doppler perfusion monitor. All the above mentioned models are more useful as a research tool rather than a calibration device for simple day-to-day use with the laser Doppler instrument.

Liebert et al. [66] developed a simple phantom made of a solution of latex spheres embedded in porous polyethylene material (Vyon). This mixture of static and dynamic scattering phantom produces a more realistic spectrum similar to that obtained in tissue. An ideal calibration system taking into consideration the flow, red blood cell size and tissue optical properties is yet to be developed and seem rather difficult to realize.

A completely different approach was the so-called optoelectronic calibration of laser Doppler devices [71]. In this method, light from an intensity modulated light emitting diode is offered to the detection channel of the device. Varying the modulation frequency and amplitude simulates the effect of varying red blood cell speed and concentration. Such a methodology only tests the detection and signal processing module of laser Doppler flowmetry devices.

5. Biological zero problem

It was found that there is a residual signal in laser Doppler perfusion measurements from the tissue called Biological Zero (BZ), which is present even when there is no flow [72]. Measurements on excised tissue [72] and cadaver skin [73] suggested that the BZ signal primarily originates from Brownian motion and movement of red blood cells. Normally in laser Doppler perfusion measurements it was suggested that this BZ signal should be subtracted from the normal perfusion value to get a better understanding of the perfusion especially in the case of very low perfusion measurements [74-76]. Fagrell and Nilsson [77] suggested that the BZ is due to the residual movement of entrapped blood cells and other moving constituents of living tissue such as vessel wall activity, hair follicles and sweat gland production.

Kernick et al. [78] did a detailed study on BZ based flow model, in-vitro and in-vivo measurements. Their results show that BZ varies linearly with temperature in vivo and in vitro measurements, which is a characteristic of Brownian motion. Also in a flow model with increasing temperature, the BZ output of skin tissue surrounding the flow model increased contributing to the LDF output, but the flow characteristics remained linear. Based on their observations they strongly suggest that the BZ signal in skin is from the Brownian motion of tissue structures and macromolecules in the interstitial space. Before a quantitative comparison of the BZ based on Kernick et al. [78] one should note that they used 0.8mm fibers with 1.2mm center to center fiber separation in combination with a He-Ne laser for their measurements. Earlier Liebert et al. [41] showed that the optical arrangement of the probe has a significant influence on BZ.

Even though Kernick et al. [78] shows that BZ is caused by Brownian motion the question that remains unanswered is whether the Brownian motion contributing to the normal perfusion is quantitatively the same as the Brownian motion during an occlusion. We strongly believe that unless the behavior of this Brownian motion is not fully understood in these two situations it is difficult to reach to a conclusion on the matter of subtracting biological zero from the normal perfusion value.

Zhong et al. [79] proposed an elegant method for solving the Biological Zero problem. They considered the decomposition of the red blood cells speed in to random fluctuation (Brownian motion) and a constant translational

velocity. Based on their model they suggested that a mere subtraction of Biological Zero will lead to an underestimation of the perfusion. As an extension of their model Binzoni et al. [22] developed an analytical solution for different moments of the power spectrum for the Brownian motion for larger inter-optode distances. But since Kernick et al. [78] showed that temperature influences the BZ the validity of these models in real situation can be questioned.

6. Motion Artifacts

One of the inherent limitations of laser Doppler perfusion measurements is the influence of the movement artifacts associated with the perfusion signal. This can be either by tissue motion or by fiber movements in a fiber optic probe. Newson et al. [80] investigated the influence of fiber movements on the perfusion signal by controlled movement of the fiber attached to a shaker. It was found that fiber movements significantly contribute to the low frequency part of the beat frequency spectra from which the blood flow signal is extracted. Gush and King [81] suggested a modification of fiber optic probes to reduce movement artifacts. They suggested that the use of small aperture fibers with fewer modes and keeping the fiber close to the skin reduces the movement artifacts to some extent. Commercial laser Doppler systems use a high-pass filter (often 20 Hz) to filter out the low frequency part of spectra to deal with motion artifacts. The problem of fiber-based movement artifact noise can be solved by using an integrated probe [44-46] where light delivery and detection are on the same probe.

The influence of tissue motion on the blood flow signal was addressed by Oberg [82]. He studied the contribution of tissue motion generated by respiratory and circulatory systems of the human body on the perfusion signal. The measurements with a shaking system mimicking a linear tissue motion in combination with a flow model showed that the flow signal increases linearly with the increase of vibration movements (0-350 micrometer/second) with a constant flow velocity.

Tissue motion and the physical movements of the subjects produce more artifacts in a non-contact measurement technique like laser Doppler perfusion imaging than with monitoring using the probe fixed on the skin [83]. In a scanning LDPI which normally takes a few minutes to finish one complete scan, the motion artifact is of great concern. Karlsson et al. [84] used linearly polarized laser light in combination with a polarization filter in front of the detectors in a cross polarization state to filter out the specularly reflected light. This will also filter out the reflected light which is Doppler shifted because of the motion of the structure and allows only randomly polarized multiply scattered photons to reach the detector. However the polarization filter will also filter out some photons which were Doppler shifted by superficial perfusion,

which reduces the SNR and makes the interpretation of the signal difficult. The emerging full field techniques (section 3.2) which can make a perfusion map very fast compared to the scanning techniques will definitely benefit from a reduced influence of movement artifacts.

7. Multiple Doppler shifts; a theoretical limitation

The theoretical model developed by Bonner and Nossal [17] is the basis of all the conventional laser Doppler perfusion monitors and imagers. One of the assumptions in this model in calculation of the blood flow is that the single Doppler shifted photons are dominant. But in reality this assumption is not valid in case of highly perfused tissue, where a large number of photons interact with more than one moving red blood cell. Nilsson [27] developed a signal processor to correct for the effect of multiple Doppler shifting. He designed a processor in which flux is linearized based on CMBC signal. Evaluation of the processor by Nilsson [27] and also by Ahn et al. [64] showed that this correction method works well till a volume fraction of around 1%. But in a later study by Barnett et al. [85] showed that at higher perfusion rates this processor under estimates the flow. Petoukhova et al. [86] did a comparative study of the output flow signal of two instruments, one with a linearizer and one without. They measured on the cortex of pig kidneys with a range of size and weight, and used an ultrasonic flow meter as a reference. A strong correlation was found between the output signals of the two instruments for a variety of flow values. This suggests that the linearization algorithm is not influencing the perfusion signal for a range physiologically relevant flow values. The fact that the concentration signal is getting saturated at higher flow values [86] and that the response of the power spectral density algorithm is extremely poor above concentrations of 0.2% volume fraction of RBC [85], questions the usefulness of using the linearization algorithm under these conditions.

8. Influence of tissue optical properties

The scattering and absorption of tissue affects the sensitivity of the laser Doppler perfusion signal as well as the depth of probing of the instrument. Larsson et al. [70] studied the influence of optical properties on the laser Doppler perfusion signal. They used a rotating phantom [69] with a stack of static scattering layers made of a mixture of polyvinyl alcohol and hollow polystyrene microspheres with well defined optical properties. The results showed that the perfusion signal is significantly influenced by optical properties for a homogenous flow distribution independent of the source-to-detector fiber separation. The change in optical properties changes the path length traveled by the photons and influences the perfusion signal irrespective of the velocity of

the moving scatterers [17, 88, 89]. A path length resolved laser Doppler as suggested by Petoukhova et al. [47] and Varghese et al. [48] will give a perfusion signal with knowledge of the optical path length the photons traveled, which can compensate for the influence of optical properties. However these are interferometric approaches which cannot be simply added to the existing laser Doppler monitors. Larsson et al. [90] presented an analytical approach for path length compensation [88] predicting the average path length with different source-detector separations. They used diffuse reflectance measurements and Monte Carlo simulations to predict the path length for different fiber separations. A path length compensated perfusion signal independent of optical properties was shown with a simulation model of a single layer system. But in order to validate in vivo results the simulation model has to be further expanded for heterogeneous optical properties with multiple layers.

In a laser Doppler imager where the detector is in the far field the change of tissue optical properties will be reflected by a change in spot size and in turn the number of coherence areas (speckles) on the detector. Since the modulation depth of the signal depends on the number of speckles involved in the detection process, as explained in section 1.1.2, the perfusion signal is influenced by the optical properties of the tissue. The number and size of speckles on the far field detector of the imager depends on tissue optical properties, the distance between the scattering medium and the detector and between detector and lens geometry. Wardell et al. [29] compensated for the variation of the number of coherence areas with distance between the medium and the detector by using a slightly diverging beam. They took the number of coherence areas as an instrumental constant which varies with changes in source to detector distance. Using a diverging beam only gave a partly compensation, since it only corrects for variation of the distance between the tissue and the detector, and not for the variation of tissue optical properties. The concept that the number of coherence areas is an instrumental constant is true in the case of a fiber optic geometry where the number of speckles is determined by the distance of the detector fibers end facet to the detector [16]. But tissue optical properties have an important role in the number of coherence areas generated on the photodetector in an LDPI instrument. Rajan et al. [91] showed that the scattering level of the tissue strongly affects a laser Doppler imager signal due to the consequence of the number of speckles involved in the detection process. They used a range of beam diameters to illuminate an optical phantom to study the influence of speckle size on the perfusion signal. It was observed that with a typical beam diameter of 0.5mm the perfusion signal varies by a factor of 4 when the reduced scattering level varied from 0.5mm^{-1} to 4.0mm^{-1} . This variation drops to a factor of 1.5 when the beam diameter is increased to 4.0mm. This shows the influence of the scattering level on the speckle size which in turn influences the response of the laser Doppler system to the same perfusion level under different optical surroundings.

Recently Rajan et al. [92] reported that the spatial correlations of the intensity of far field dynamic speckle patterns generated by mixed static and dynamic turbid media illuminated by coherent light can be predicted. Based on a theoretical/computational frame work the variance of photocurrent fluctuations was modeled for a far-field detector collecting back-scattered photons on the basis of Monte Carlo derived photon statistics, taking in to account the speckle phenomenon. The speckle size variations were estimated for different scattering levels and anisotropies. The experimental validation of the theoretical model in a configuration similar to laser Doppler perfusion imager showed the potential of the method in predicting the effect of tissue optical properties on the modulation depth of the laser Doppler perfusion imager signal through the speckle phenomenon.

9. Conclusions

The laser Doppler perfusion measurement technique has undergone large progress since its introduction. The improvements in laser technology and fiber optics, and in signal processing, have made LDF into a reliable and user friendly technology. The introduction of the imaging technique opened up clinical research applications where a non contact measurement is a necessity and where perfusion information within an area of tissue is required. The limitations of the technique were thoroughly addressed by the researchers enabling a lot of improvements. But some of the more fundamental limitations given in this review article still demand a revisit, and measuring perfusion in absolute units remains a scientific challenge. The problem of multiple Doppler shifts remains unresolved. The velocity resolved perfusion measurements cited by a few authors need much more research to be applied to real tissue. Also the problem of tissue optical properties should be addressed in case of scanning field laser Doppler perfusion imager. The emerging full field laser Doppler imaging technique has a lot of potential to overcome the motion artifacts and the slow scanning speed of conventional scanning imagers. Here the influence of optical properties on the number of coherence areas will be less because of the use of a full field beam. Regardless of all these limitations laser Doppler methods remains as the most sought after technique for microcirculatory blood flow measurements.

References

1. L. Drain, *The Laser Doppler Technique* (John WileyPress, USA, 1980).
2. O. A. Larsen, N. A. Lassen and F. Quaade, "Blood flow through human adipose tissue determined with radioactive xenon," *Acta. Physiol. Scand.* **66**, 337-345 (1966).

3. A. M. Rudolph, and M. A. Heymann, "The circulation of the fetus in utero Methods for studying distribution of blood flow, cardiac output and organ blood flow," *Circ. Res.* **21**, 163-184 (1967).
4. M. A. Heymann, B. D. Payne, J. I. Hoffman, and A. M. Rudolph, "Blood flow measurements with radionuclide-labeled particles," *Prog. Cardiovasc. Dis.* **20**, 55-79 (1977).
5. D. G. Silverman, F. A. Cedrone, W. E. Hurford, T. G. Bering, and D. D LaRossa, "Monitoring tissue elimination of fluorescein with the perfusion fluorometer: A new method to assess capillary blood flow. *Surgery* **90**, 409 (1981).
6. A. Bollinger, P. Butti, J. P. Banas, H. Trachsler and W. Seigenthaler, "Red cell velocity in nailfold capillaries in man measured by a television microscope technique," *Microvasc. Res.* **7**, 61-72 (1974).
7. C. M. Black, R. P. Clark, K. Darton, M. R. Goff, T. D. Norman, H. A. Spikes, "A pyroelectric thermal imaging system for use in medical diagnosis," *J. Biomed. Eng.* **12**, 281-286 (1990).
8. P. A. Payne, R. Y. Faddoul, and S. M. Jawad (1985) "A single channel pulsed Doppler ultrasound instrument for measurement of skin blood flow," *Practical Aspects of skin Blood Now Measurement* (London: Biological Engineering Society)
9. J. D. Briers, "Laser Doppler, speckle and related techniques for blood perfusion mapping and imaging," *Physiol. Meas.* **22**, 35-66 (2001).
10. A. P. Shepherd, and P. Å Öberg (ed) *Laser-Doppler Blood Flowmetry* (Boston: Kluwer Academic Publishers, 1990).
11. Y. Zhao, Z. Chen, C. Saxer, S. Xiang S, J. F. de Boer, and J. S. Nelson, "Phase-resolved optical coherence tomography and optical Doppler tomography for imaging blood flow in human skin with fast scanning speed and high velocity sensitivity," *Opt. Lett.* **25**, 114-116 (2000).
12. A. N. Obeid, N. J. Barnett, G. Dougherty, and G. Ward, "A critical review of laser Doppler flowmetry," *J. Med. Eng. Technol.* **14**, 178-181 (1990).
13. N. Vongsavan, and B. Matthews, "Some aspects of the use of laser Doppler flow meters for recording tissue blood flow," *Exp. Physiol.* **78**, 1-14 (1993).
14. M. J. Leahy, F. F. M. de Mul, G. E. Nilsson, and R. Maniewski R, "Principles and practice of the laser-Doppler perfusion technique," *Technol. Health Care* **7**, 143-162 (1999).
15. P. Vennemann, R. Lindken, J. Westerweel, "In vivo whole-field blood velocity measurement techniques," *Exp. Fluids* **42**, 495-511 (2007).
16. A. Serov, W. Steenbergen, and F. F. M. de Mul, "Prediction of the photodetector signal generated by Doppler-induced speckle fluctuations: theory and some validations *J. Opt. Soc. Am. A* **18**, 622-630 (2001).

17. R. F. Bonner, and R. Nossal, "Model for laser Doppler measurements of blood flow in tissue," *Appl. Opt.* **20**, 2097-2107 (1981).
18. K. Dörschel, and G. Müller, "Velocity resolved laser Doppler blood flow measurements in skin," *Flow. Meas. Instrum.* **7**, 257-264 (1996).
19. M. Larsson, and T. Strömberg, "Toward a velocity-resolved microvascular blood flow measure by decomposition of the laser Doppler spectrum," *J. Biomed. Opt.* **11**, 014024 (1-9) (2006).
20. A. Liebert, N. Zolek, and R. Maniewski, "Decomposition of a laser-Doppler spectrum for estimation of speed distribution of particles moving in an optically turbid medium: Monte Carlo validation study," *Phys. Med. Biol.* **51**, 5737-5751 (2006).
21. T. Binzoni, T. S. Leung, D. Boggett, and D. T. Delpy, "Non-invasive laser Doppler perfusion measurements of large tissue volumes and human skeletal muscle blood RMS velocity," *Phys. Med. Biol.* **48**, 2527-49 (2003).
22. T. Binzoni, T. S. Leung, M. L. Seghier and D. T. Delpy, "Translational and brownian motion in laser-Doppler flowmetry of large tissue volumes," *Phys. Med. Biol.* **49**, 5445-5458 (2004).
23. R. Lohwasser, and G. Soelkner, "Experimental and theoretical laser-Doppler frequency spectra of a tissue like model of a human head with capillaries," *Appl. Opt.* **38**, 2128-2137 (1999).
24. M. D. Stern, "In vivo evaluation of microcirculation by coherent light scattering," *Nature* **254**, 56-58 (1975).
25. D. Watkins, and G. A. Jr. Holloway, "An instrument to measure cutaneous blood flow using the Doppler shift of laser light," *IEEE Trans. Biomed. Eng.* **BME-25**, 28-33 (1978).
26. G. E. Nilsson, T. Tenland, P. A. Oberg, "Evaluation of a laser Doppler flowmeter for measurement of tissue blood flow," *IEEE Trans. Biomed. Eng.* **BME-27**, 597-604 (1980).
27. G. E. Nilsson, "Signal processor for laser Doppler tissue flowmeters," *Med. Biol. Eng. Comput.* **22**, 343-348 (1984).
28. T. J. H. Essex, and P. O. Byrne, "A laser Doppler scanner for imaging blood flow in skin," *J. Biomed. Eng.* **13**, 189-193 (1991).
29. K. Wårdell, A. Jakobsson and G. E. Nilsson, "Laser Doppler perfusion imaging by dynamic light scattering," *IEEE Trans. Biomed. Eng.* **40**, 309-316 (1993).
30. M. H. Koelink, and F. F. M. de Mul, B. J. M. Leerkotte, J. Greve, H. W. Jentink, R. Graaff, A. C. M. Dassel, and J. G. Aarnoudse, "Signal processing for a laser-Doppler blood perfusion meter," *Signal process.* **38**, 239-252 (1994).
31. Y. Y. Chen, Y. H. Lin, I. C. Jan, R. S. Liu, N. K. Chou and G. J. Jan, "Adaptive processing bandwidth adjustment for laser Doppler flowmetry," *Med. Bio Eng. comput.* **42**, 277-281 (2004).

32. L. Duteil, J. Bernengo, and W. Schalla, "A double wavelength laser Doppler system to investigate skin microcirculation," *IEEE Trans. Biomed. En.* **BME-32**, 439-447 (1985).
33. A. N. Obeid, D. Bogget, N. J. Barnett, G. Dougherty, and P. Rolfe P, "Depth discrimination in laser Doppler skin blood flow measurement using different lasers," *Med. Biol. Eng. Comput.* **26**, 415-419 (1988).
34. H. W. Jentink, F. F. M. de Mul, R. G. A. M. Hermsen, R. Graaff, and J. Greve, "Monte Carlo simulations of laser Doppler blood flow measurements in tissue," *Appl. Opt.* **29**, 2371-2381 (1990).
35. D. J. Faber, M. C. G. Aalders, E. G. Mik, B. A. Hooper, M. J. C. van Gemert and T. G. van Leeuwen van, "Oxygen saturation-dependent absorption and scattering of blood," *Phys. Rev. Lett.* **93**, 028102-1-028102-4 (2004).
36. R. G. M. Kolkman, Photoacoustic & pulsed -laser Doppler monitoring of blood concentration and perfusion in tissue (PhD thesis, University of Twente, 1998).
37. R. J. Gush, and T. A. King, "Discrimination of capillary and arterio-venular blood flow in skin by laser Doppler flowmetry," *Med. Bio. Eng. comput.* **29**, 387-392 (1991).
38. S. Einav, H. J. Berman, R. L. Fuhro, P. R. DiGiovanni, S. Fine, J. D. Fridman, "Measurement of velocity profiles of red blood cells in the microcirculation by laser Doppler anemometry (LDA)," *Biorheology* **12**, 207-210 (1975).
39. M. Koelink, F. F. M. de Mul, J. Greve, R. Graaff, A. C. M. Dassel, and J. G. Aarnoudse, "Laser Doppler blood flowmetry using two wavelengths: Monte-Carlo simulations and measurements," *Appl. Opt.* **33**, 3549-3558 (1994).
40. A. Jakobsson, and G. Nilsson, "Prediction of sampling depth and photon pathlength in laser Doppler flowmetry," *Med. Biol. Eng. Comput.* **31**, 301-307 (1993).
41. A. Liebert, M. Leahy, and R. Maniewski, "Multichannel laser-Doppler probe for blood perfusion measurements with depth discrimination," *Med. Biol. Eng. Comput.* **36**, 740-747 (1998).
42. V. G. Kolinko, F. F. M. de Mul, J. Greve, and A. V. Priezzhev, "Feasibility of picosecond laser-Doppler flowmetry provides basis for time-resolved Doppler tomography of biological tissue," *J. Biomed. Opt.* **3**, 187-190 (1998).
43. R. G. M. Kolkman, E. Hondebrink, R. A. Bolt, W. Steenbergen, and F. F. M. de Mul, "Pulsed-laser Doppler flowmetry provides basis for deep perfusion probing," *Rev. Sci. Instrum.* **72**, 4242-4 (2001).
44. F. F. M. de Mul, J. van Spijker, D. van der Plas, J. Greve, J. G. Aarnoudse, and T. M. Smits, "Mini laser-Doppler (blood) flow monitor

- with diode laser source and detection integrated in the probe,” *Appl. Opt.* **23**, 2970–2973 (1984).
45. H. Higurashi, R. Sawada and T. Ito, “An integrated laser blood flowmeter,” *J. Lightwave Technol.* **21**, 591–595 (2003).
 46. A. N. Serov, J. Nieland, S. Oosterbaan, F. F. M. de Mul, H. van Kranenburg, H. H. P. Th. Bekman and W. Steenbergen, “Integrated Optoelectronic Probe Including a Vertical Cavity Surface Emitting Laser for Laser Doppler Perfusion. Monitoring,” *IEEE Trans. on Bio-Med. Eng.* **53**, 2067-2074 (2006).
 47. A. L. Petoukhova, W. Steenbergen, and F. F. M. de Mul, “Path-length distribution and path-length-resolved Doppler measurements of multiply scattered photons by use of low-coherence interferometry,” *Opt. Lett.* **26**, 1492-1494 (2001).
 48. A. L. Petoukhova, W. Steenbergen, T. G. van Leeuwen, and F. F. M. de Mul, “Effects of absorption on coherence domain path length resolved dynamic light scattering in the diffuse regime,” *Appl. Phys. Lett.* **81**, 595-597 (2002).
 49. B. Varghese, V. Rajan, T. G. van Leeuwen, and W. Steenbergen, “Path-length-resolved measurements of multiple scattered photons in static and dynamic turbid media using phase-modulated low-coherence interferometry,” *J. Biomed. Opt.* **12**, 024020 (1-7) (2007).
 50. X. Huang, L. Lu, R. J. Gush, and D. M. Boggett (1996) A new, fast, high resolution laser Doppler imager for clinical and research use. Proc6th World Congress for Microcirculation (Munich, Germany)
 51. G. Nilsson “Laser Doppler perfusion imaging for assessment of cutaneous microcirculation,” *Phlebologie* **26**, 87-91 (1997).
 52. K. Wardell, G. E. Nilsson, “Duplex laser Doppler perfusion imaging,” *Microvasc. Res.* **52**, 171-82 (1996).
 53. M. Linden, H. Golster, S. Bertuglia, A. Colantuoni, F. Sjöberg, and G. Nilsson, “Evaluation of enhanced high-resolution laser Doppler imaging in an in vitro tube model with the aim of assessing blood flow in separate microvessels,” *Microvasc. Res.* **56**, 261–270 (1996).
 54. D. K. Harrison, N. C. Abbot, J. S. Beck, and P. T. A. McCollum, “Preliminary assessment of laser Doppler perfusion imaging in human skin using the tuberculin reaction as a model,” *Physiol. Meas.* **14**, 241-52 (1993).
 55. D. P. Kernick and A. C. Shore, “Characteristics of laser Doppler perfusion imaging in vitro and in vivo,” *Physiol. Meas.* **21**, 333-340 (2000).
 56. A. Serov, W. Steenbergen, and F. F. M. de Mul, “Laser Doppler perfusion imaging with a complimentary metal oxide semiconductor image sensor,” *Opt. Lett.* **25**, 300-302 (2002).

57. A. Serov, B. Steinacher and T. Lasser, "Full-field laser Doppler perfusion imaging and monitoring with an intelligent CMOS camera," *Opt. Express* **13**, 3681-3689 (2005).
58. M. Atlan, M. Gross, B. C. Forget, T. Vitalis, A. Rancillac, and A. K. Dunn, "Frequency-domain wide-field laser Doppler in vivo imaging," *Opt. Lett.* **31**, 2762-2764 (2006).
59. M. Atlan, and M. Gross, "Laser Doppler imaging revisited. *Rev. Sci. Instrum.* **77**, 1161031 -1161034 (2006).
60. T. Cochrane, T. Fail, and S. B. Sherriff, "Comparison of laser Doppler and Doppler ultrasound in lower limb vascular diagnosis," *Clin. Phys. Physiol. Meas.* **8**, 231-238 (1987).
61. A. M. Seifalian, G. Stansby, A. Jackson, K. Howell, and G. Hamilton, "Comparison of laser Doppler perfusion imaging, laser Doppler flowmetry, and thermographic imaging for assessment of blood flow in human skin," *Eur. J. Vasc. Surg.* **8**, 65-9 (1994).
62. G. Dougherty, N. J. Barnett, and S. J. Pettinger, "A prototype instrument combining laser Doppler flowmetry and reflection pulse oximetry," *Clin. Phys. Physiol. Meas.* **13**, 105-114 (1992).
63. G. A. Holloway, and D. W. Watkins, "Laser Doppler measurement of cutaneous blood flow," *J. Invest. Dermatol.* **69**, 306-309 (1977).
64. H. Ahn, K. Johansson, O. Lundgren, and G. E. Nilsson, "In vivo evaluation of signal processors for laser Doppler tissue flowmeters," *Med. Bio. Eng. comp.* **25**, 207-211 (1987).
65. A. N. Obeid, "In vitro comparison of different signal processing algorithms used in laser Doppler flowmetry," *Med. Biol. Eng. Comput.* **31**, 43-52 (1993).
66. A. Liebert, M. Leahy, and R. Maniewski, "A calibration standard for laser-Doppler perfusion measurements," *Rev. Sci. Instrum.* **66**, 5169-5173 (1995).
67. A. P. Shepherd, G. L. Riedel, J. W. Kiel, D. J. Haumschild, and L. C. Maxwell, "Evaluation of an infrared laser-Doppler blood flowmeter," *Am. J. Physiol. Gastrointest. Liver Physiol.* **252**, G832-G839 (1987).
68. F. F. M. de Mul, M. H. Koelink, M. L. Kok, P. J. Harmsma, J. Greve, R. Graaff, and J. G. Aarnoudse, "Laser-Doppler velocimetry and Monte Carlo simulations on models for blood perfusion in tissue," *Appl. Optics* **34**, 6595-6611 (1995).
69. W. Steenbergen, and F. F. M. de Mul, "New optical tissue phantom and its use for studying laser Doppler blood flowmetry," *Proc. SPIE* **3196**, 12-23 (1998).
70. M. Larsson, W. Steenbergen, and T. Strömberg, "Influence of optical properties and fibre separation on laser Doppler flowmetry," *J. Biomed. Opt.* **7**, 236-243 (2001).

71. A. Liebert, and P. Lukaszewicz, D. Boggett, and R. Maniewski, "Optoelectronic standardization of Laser Doppler perfusion monitors," *Rev. Sci. Instrum.* **70**, 1352-1353 (1999).
72. T. Tenland, E. G. Sælerud, G. E. Nilsson, P. Å. Öberg, "Spatial and temporal variations in human skin blood flow," *Int. J. Microcirc. Clin. Exp.* **2**, 81–90 (1983).
73. L. Caspary, A. Creutzig, K. Alexander, "Biological zero in laser Doppler fluximetry," *Int. J. Microcirc. Clin. Exp.* **7**, 367– 371 (1988).
74. B. Fagrell, Perimed's LDV flowmeter, In: A. P. Shepherd, and Öberg (ed.) *Laser-Doppler Blood Flowmetry*. (Boston: Kluwer Academic Publishers, 1990).
75. G. E. Nilsson, Peripheral vascular diseases, In: A. P. Shepherd and P. Å. Öberg (ed) *Laser-Doppler Blood Flowmetry* (Boston: Kluwer Academic Publishers, 1990).
76. N .C. Abbot, and J. Swanson-Beck, "Biological zero in laser Doppler measurements in normal, ischaemic and inflamed human skin," *Int. J. Microcirc. Clin. Exp.* **2**, 89–98 (1993).
77. S. Fagrell, and G. Nilsson, "Advantages and limitations of one point laser Doppler perfusion monitoring in clinical practice," *Vasc. Med. Rev.* **6**, 97–101 (1995).
78. D. P. Kernick, J. E. Tooke, and A. C. Shore, "The biological zero signal in laser doppler fluximetry –origins and practical implications," *Pflügers Arch – Eur. J. Physiol.* **437**, 624–631 (1999).
79. J. Zhong, A. M. Seifalian, G. E. Sælerud, and G. E. Nilsson, "A mathematical analysis on the biological zero problem in laser Doppler flowmetry. *IEEE Trans. Biomed. Eng.* **45**, 354–364 (1988).
80. T. P. Newson, A. Obeid, R. S. Wolten, D. Boggett, and P. Rolfe, "Laser Doppler velocimetry: the problem of fibre movement artifact," *J. Biomed. Eng.* **9**, 169-172 (1987).
81. R. J. Gush, and T. A. King "Investigation and improved performance of optical fibre probes in laser Doppler blood flow measurement," *Med. Biol. Eng. Comput.* **678**, 29–36 (1987).
82. P. Å Öberg, "Tissue motion – a disturbance in the laser-Doppler blood flow signal?," *Technol. Health Care* **7**: 185–192 (1999).
83. M. G. D. Karlsson, M. Larsson, T. Strömberg, and K. Wårdell, "Influence of tissue movements on laser Doppler perfusion imaging *Proc. SPIE* **4624**, 106–114 (2002).
84. M. G. D. Karlsson, and K. Wårdell, "Polarized laser Doppler perfusion imaging—reduction of movement-induced artifacts. *J. Biomed. Opt.* **10**, 064002(1-9) (2005).
85. N. J. Barnett, G. Dougherty, and S. J. Pettinger, "Comparative study of two laser Doppler blood flowmeters," *J. Med. Eng. Technol.* **14**, 243-249 (1990).

86. A. L. Petoukhova, W. Steenbergen, F. Morales, R. Graaff, E. D. de Jong, J. M. Elstrodt, F. F. de Mul, and G. Rakhorst, "Instrument-independent flux units for laser Doppler perfusion monitoring assessed in a multi-device study on the renal cortex," *Microvasc. Res.* **66**, 83-90 (2003).
87. D. Boggett, A. N. Obeid, J. Blond, and P. Rolf, "Calibration of a laser Doppler skin blood flow meter using a simple fluid model and digital signal processing," In K. Copeland (ed.) *Electronics in Medicine and Biology- Selected Papers (IERE, London)*, 241-247 (1986).
88. H. Nilsson, M. Larsson, G. E. Nilsson, and T. Strömberg, "Photon pathlength determination based on spatially resolved diffuse reflectance," *J. Biomed. Opt.* **7**, 478-485 (2002).
89. R. Nossal, R. F. Bonner, and G. H. Weiss, "Influence of path length on remote optical sensing of properties of biological tissue," *Appl. Opt.* **28**, 2238-2244 (1989).
90. M. Larsson, H. Nilsson, and T. Strömberg, "In vivo determination of local skin optical properties and photon path length by use of spatially resolved diffuse reflectance with applications in laser Doppler flowmetry," *Appl. Opt.* **42**, 124-134 (2003).
91. V. Rajan, B. Varghese, T. G. van Leeuwen, and W. Steenbergen, "Speckles in laser Doppler perfusion imaging," *Opt. Lett.* **31**, 468-470 (2006).
92. V. Rajan, B. Varghese, T. G. van Leeuwen, and W. Steenbergen, "Quantification of spatial intensity correlations and photodetector intensity fluctuations of coherent light reflected from turbid particle suspensions," *Phys. Rev. E* **75**, 060901-4 (2007).

Chapter 3

Speckles in laser Doppler perfusion imaging*

We report on the quantitative influence of speckles in laser Doppler perfusion imaging. The influence of speckles on the signal amplitude and the Doppler spectrum is demonstrated experimentally on particle suspensions with different scattering levels and varying beam width. It was shown that the type of tissue affects the instrumental response through the effect of lateral light diffusion on the number of speckles involved in the detection process. These effects are largest for narrow beams.

* This chapter has been published as: V. Rajan, B. Varghese, T. G. van Leeuwen, and W. Steenbergen, "Speckles in Laser Doppler Perfusion Imaging," *Opt. Lett.* **31**, 468 (2006).

1. Introduction

Laser Doppler perfusion imaging (LDPI) is a non-invasive technique to measure blood flow maps on an area of tissue. The fundamental output quantity of a laser Doppler flowmetry (LDF) instrument is the first moment M_1 of the power spectrum $P(\omega)$ of the photocurrent fluctuations, the i^{th} moment being defined as [1]

$$M_i = \int_0^{\infty} P(\omega) \omega^i d\omega \quad (1)$$

often normalized with DC^2 to cancel out laser power fluctuations. In LDF multiple waves illuminating the detector generate a dynamic speckle pattern which causes fluctuations in the detector signal. Other techniques for measuring perfusion from dynamic speckles are based on calculation of differences between subsequent speckle fields [2] and speckle contrast analysis [3]. Briers [4] compared speckle contrast and laser Doppler techniques and showed the common physical basis of laser Doppler and laser speckle techniques. In this letter we show that speckles have an essential effect on LDPI signals. Quantifying the speckle phenomenon and its spatial properties is essential to account for the system response to different tissue optical properties and beam diameters. The influence of the number of speckles on the LDPI signal as influenced by the beam size was earlier mentioned by Wårdell *et al.* [5]. However the effect of scattering on the number of speckles and the LDPI signal was not reported. Piederrière *et al.* [6] reported the effect of particle size and concentration on the static speckle size as a function of polarization. Other studies mainly concerned the effect of scattering on temporal field fluctuations in situations of constant speckle size. Bonner and Nossal [1] included the coherence in an instrumental response factor β which they determined by calibration. Boas and Yodh [7], following Bonner and Nossal, used a constant, β which depends on the experimental set up. Also Binzoni *et al.* [8] state β to be an instrumental factor that depends upon the optical coherence of the signal at the detector surface. These studies [1, 7, 8] exclude the effects of scattering on the spatial field correlation function and on β . They used fiber optic systems in which the spatial field correlation function is an instrumental constant, which is not the case in a laser Doppler perfusion imager where a free beam geometry is used. In this work we demonstrate the effect of multiple scattering on the spatial field correlation at the tissue surface, when using a free laser beam for illumination and a detector which collects the back-scattered photons propagated through free air.

2. Theoretical background

It can be derived [9] that the AC signal generated by a fluctuating speckle pattern, normalized by the DC², is equal to

$$\frac{\langle i_{AC}^2 \rangle}{\langle i_{DC} \rangle^2} = \frac{1}{N} f_D (2 - f_D) \quad (2)$$

with $\langle i_{AC}^2 \rangle$ the mean square of the photocurrent fluctuations, $\langle i_{DC} \rangle$ the mean photocurrent, N the number of speckles on the detector and f_D the Doppler shifted fraction of all detected photons. In this, it is assumed that the photodetector surface is, on average, homogeneously illuminated.

In LDPI instrumentation, two modes of detection are adopted: 1. illuminating a photodetector without focusing the light by a lens. This is the mode of detection used in the device developed by Wårdell *et al.* [5] 2. focusing the light using a lens, as implemented in the LDPI instrument of Essex and Byrne [10]. Below we will show, that for both modes of detection, the relation between the number of speckles within the detector, and the geometric properties of the tissue spot that emits diffusely reflected light, is identical.

For simplicity, we assume that the diffuse reflection by the tissue happens within a confined circular region with area A_{tis} , which has a uniform irradiation. A photodetector with area A_{det} (not necessarily circular) is placed at distance ℓ_1 from the tissue (Fig 1, dotted line representation). The speckle area on the photodetector, A_{sp} , can be written as [9, 11], $A_{sp} = \lambda^2 / \Omega_1$, with Ω_1 the solid angle subtended by the irradiating tissue spot on the photodetector. For ℓ_1 much larger than the size of the light-emitting spot, this quantity is taken as $\Omega_1 = A_{tis} / \ell_1^2$. Substituting this in equation (2) will give

$$\frac{\langle i_{AC}^2 \rangle}{\langle i_{DC} \rangle^2} = \frac{\lambda^2 \ell_1^2}{A_{det} A_{tis}} f_D (2 - f_D) \quad (3)$$

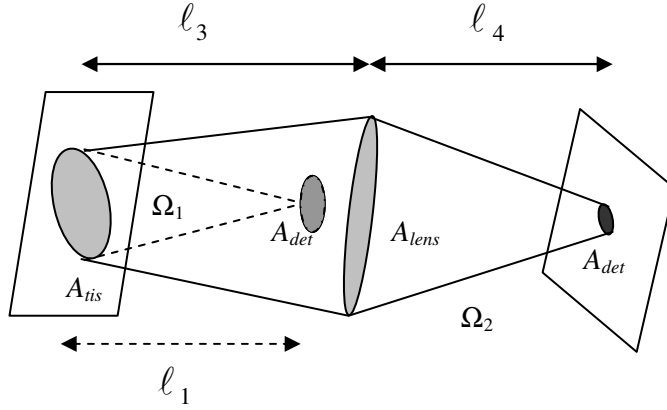


Fig. 1 Schematic of diffusely reflected focused (solid line representation) and unfocused light (dotted lines) illuminating a photo detector.

Now we place a lens with area A_{lens} on a distance ℓ_3 to the tissue. This lens produces an image of the light-emitting tissue spot on the photodetector plane (Fig. 1, solid line representation) which is placed at a distance ℓ_4 from the lens. We assume, that this image is completely within the physical borders of the photodetector. Hence, the effective photodetector area A_{det} that must be taken into account is the area of the image on the detector, which depends on the magnification $M = \ell_4 / \ell_3$ realized by the lens, giving $A_{det} = A_{tis} M^2$. Furthermore, the speckle area now is governed by the solid angle $\Omega_1 = A_{lens} / \ell_4^2$ subtended by the lens, instead of a solid angle subtended by the irradiating spot on the tissue. With this eq. (2) can be written as

$$\frac{\langle i_{AC}^2 \rangle}{\langle i_{DC} \rangle^2} = \frac{\lambda^2 \ell_3^2}{A_{lens} A_{tis}} f_D (2 - f_D) \quad (4)$$

On comparison of Eqs. (3) and (4), we can conclude that when we use a photodetector without focusing, we obtain the same modulation depth as when the photodetector is replaced by a lens of equal size that focuses the light within the physical borders of another detector. Furthermore, we see that the influence of the size of the irradiating tissue spot is the same for both configurations. When no lens is used, a change in A_{tis} will change the modulation depth through the effect on the speckle size, while when using a lens, the modulation depth

will change because the effective size of the photodetector (the image on the photodetector surface of the light-emitting spot on the skin) will change. Eq. (3) and (4), indicate that in LDPI those factors that affect the irradiating tissue area, will determine the response of the system. Serov *et al.* [9] give a more rigorous treatment of the problem, including a definition of the effective speckle size and its relation to the angular distribution of the detected light. From that, it follows that the number of speckles will depend on the size and shape of the laser beam used for scanning the tissue, and the amount of lateral broadening that the light will undergo before escaping the tissue. The latter will depend on the optical properties of the tissue. Hence, the beam shape and size, and the optical properties, might affect perfusion maps through the effect of these quantities on the spatial properties of the dynamic speckle pattern that is created on the photodetector. In this letter, we show experimental evidence that this effect is significant for practical LDPI instrumentation, by studying the amplitudes and Doppler spectra of photocurrents generated by well defined particle suspensions having a range of scattering levels, and using a range of laser beam diameters.

3. Materials and methods

The experimental set up consists of a simple back-scattered configuration in which we illuminate the medium with a perpendicular laser beam, and collect the back-scattered photons using a lens and photoreceiver. A linearly polarized Uniphase 1125P He-Ne laser, of 632.8nm, with output power of 5mW is used as the source. A beam expander made of two positive lenses of focal length 20 and 30mm respectively is used to vary the beam diameter. The beam diameter is measured with a commercial beam profiler. A glass cuvette of 8ml is used as a sample holder. A microscopic glass slide (500 microns) is used to cover the cuvette. A lens ($f=50\text{mm}$) is placed at a distance of 25cm from the sample to collect the back-scattered light, with a photoreceiver on focus. Detection is performed with a New Focus (model 2001) photoreceiver, with an effective detector area of 0.81mm^2 . The AC signal is amplified by 40 dB and then applied to an anti-aliasing low-pass filter (5th order sampled capacitor Butterworth, $f_c=20\text{kHz}$). The filtered signal is then applied to a 12-bit analogue to digital converter where it is sampled at 40kHz. A water suspension of Polystyrene micro spheres (Polysciences Inc) of $\varnothing 0.771\ \mu\text{m}$ ($g=0.9$) of known concentration is used to make the phantoms, which mimic tissue optical properties. The polystyrene suspension is further diluted to make samples with reduced scattering coefficients (μ'_s) of 0.5, 1, 2, 3 and $4\ \text{mm}^{-1}$ following from Mie theory calculations. Ecoline Black dye (Talens) is added to get absorption realistic for tissue ($\mu_a=0.02\text{mm}^{-1}$).

4. Results and discussion

Fig. 2 shows the normalized power spectra for the suspension of $\mu'_s=4.0\text{mm}^{-1}$, for three beam sizes. In fig. 3 the DC²-normalised values of zero order moment M_0 are given (which by definition are the same as the modulation depth values $\langle i_{AC}^2 \rangle / \langle i_{DC} \rangle^2$), while Fig. 4 shows the ratio M_1/M_0 , which actually is the mean Doppler shift.

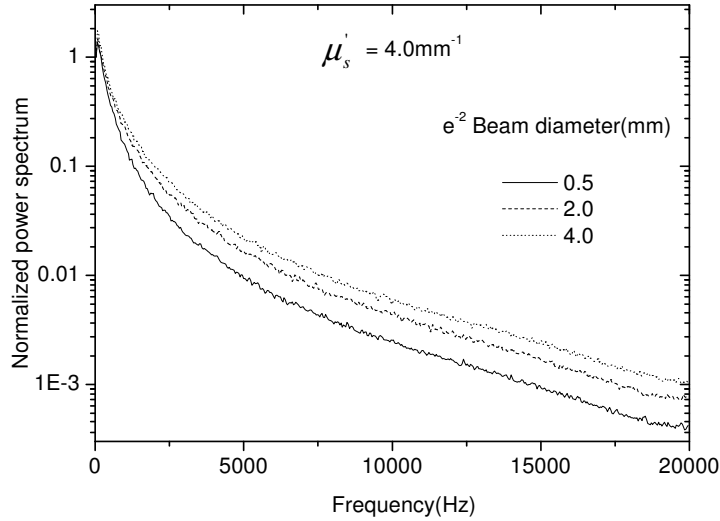


Fig. 2 The normalized power spectra for $\mu'_s=4.0\text{mm}^{-1}$

It is observed that (Fig. 3) the variation in scattering level results in a considerable variation of M_0 . Moreover the variation in M_0 due to variation in scattering level decreases with increasing beam diameter. For a beam of 0.5mm diameter, M_0 shows a variation by a factor of 5, whereas for a 4mm beam the variation is only a factor of approximately 1.5. For a 4mm beam the limiting value of M_0 seems to be reached for the highest level of scattering, while for the narrowest beam M_0 is likely to still increase on a further increase of μ'_s . The observed variations clearly show the speckle related effects of the scattering level and the beam diameter on the LDPI signal. As the scattering level increases, the number of speckles on the effective detector decreases, since the higher scattering level results in a narrow back scattered intensity distribution. This variation is larger for narrow beams than for wide beams, since the relative

change of the width of the intensity variations by variations in the scattering level is larger for narrow beams than for wide beams. For wide beams that result in wide intensity distributions and more speckles on the detector, the speckle number variation by scattering level variations is suppressed.

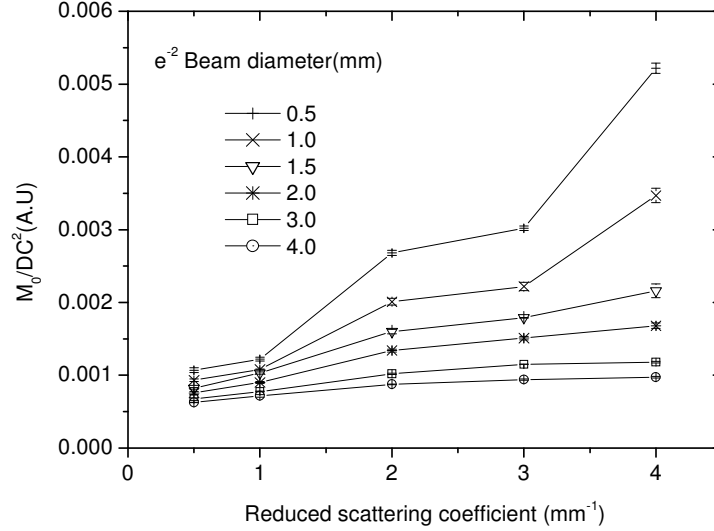


Fig. 3 M_0/DC^2 vs the reduced scattering coefficient for different beam widths.

In Fig. 4 the spectral width (M_1/M_0), which represents the average Doppler frequency of the spectrum, is plotted. The spectral width increases with the beam diameter. This is a remarkable observation, since the Doppler shifts of individual photons will only depend on the cumulative effect of a series of scattering events of these photons by particles, processes which are completely independent on the beam diameter. The effect can be explained by stating that photons with large Doppler shifts have a wider lateral distribution than photons with small Doppler shifts. If this is true, then for a given scattering level the sensitivity of M_1/M_0 to beam size should be largest for the smallest beams, where the lateral distributions are governed by the multiple scattering process rather than by the beam size itself. This can be observed in Fig. 4, in particular for the highest scattering levels where the curves for small beams diverge. In summary we have shown that scattering level of the tissue strongly affects laser Doppler imager signal due to the number of speckles involved in the detection process.

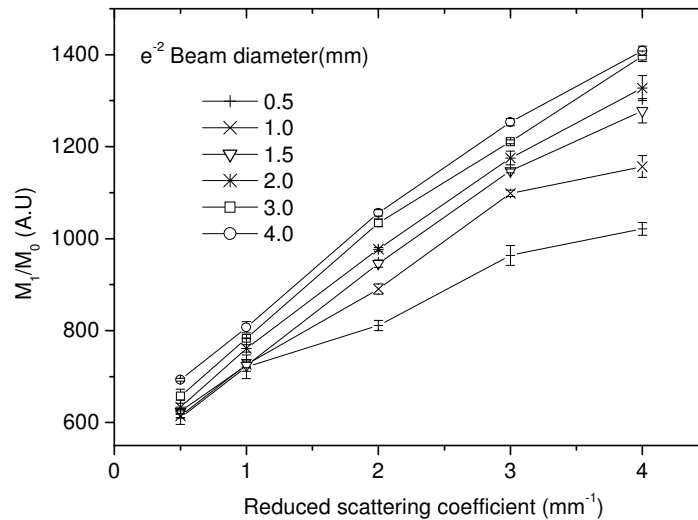


Fig. 4 M_1/M_0 vs the reduced scattering coefficient for different beam widths.

This speckle-related cross talk between the scattering level and LDPI signal can be suppressed using a sufficiently large beam size, but at the expense of signal to noise ratio and spatial resolution. Both the signal modulation depth and the frequency content are affected by this speckle-related influence. This demonstrates that the effect of speckles should be modeled to predict the system response to different tissue optical properties and particle velocities.

Acknowledgements

This research was sponsored by the Dutch Technology Foundation STW under grant TTF.5840. Erwin Hondebrink and Johan C. G. Van Hespén are acknowledged for their technical support.

References

1. R. Bonner and R. Nossal, "Model for laser Doppler measurements of blood flow in tissue," *Appl. Opt.* **20**, 2097-2107 (1981).

2. H. Fujii, K. Nohira, Y. Yamamoto, H. Ikawa, and T. Ohura, "Evaluation of blood flow by laser speckle image sensing: Part 1," *Appl. Opt.* **26**, 5321-5325 (1987).
3. J.D. Briers and S. Webster, "Quasi-real time digital version of single-exposure speckle photography for full-field monitoring of velocity or flow fields," *Opt. Commun.* **116**, 36-42 (1995).
4. J.D Briers, "Laser Doppler and time-varying speckle: a conciliation," *J. Opt. Soc. Am. A* **13**, 345-350 (1996).
5. K. Wårdell, A. Jakobsson, and G. E. Nilsson, "Laser Doppler perfusion imaging by dynamic light scattering," *IEEE Trans. Biomed. Eng.* **40**, 309-316 (1993).
6. Y. Piederrière, J. Cariou, Y. Guern, B. Le Jeune, G. Le Brun, J. Lotrian, "Backscattered speckle size as a function of polarization: influence of particle-size and concentration," *Opt. Express* **13**, 5030-5039 (2005).
7. D.A Boas and A.G. Yodh, "Spatially varying dynamical properties of turbid media probed with diffusing temporal light correlation," *J. Opt. Soc. Am. A* **14**, 192-215 (1997).
8. T. Binzoni, T.S Leung, M.L seghier and D.T. Delpy, "Translational and Brownian motion in laser-Doppler flowmetry of large tissue volumes," *Phys. Med. Biol.* **49**, 5445-5458 (2004).
9. A. Serov, W. Steenbergen, and F. F. M. de Mul, "Prediction of the photodetector signal generated by Doppler-induced speckle fluctuations: theory and some validations," *J. Opt. Soc. Am. A* **18**, 622-630 (2001).
10. T.J.H. Essex and P.O. Byrne, "A laser Doppler scanner for imaging blood flow in skin," *J. Biomed. Eng.* **13**, 189-193 (1991).
11. A.T Forrester, R.A. Gudmudsen, and P.O. Johnson, "Photoelectric mixing of incoherent light," *Phys. Rev.* **99**, 1691-1700 (1955).

Chapter 4

Quantification of spatial intensity correlations and photodetector intensity fluctuations of coherent light reflected from turbid particle suspensions*

We present a model for predicting the spatial intensity correlation function of dynamic speckle patterns formed by light backscattered from turbid suspensions, and an experimental validation of these predictions. The spatial correlation varies remarkably with multiple scattering. The provided computational scheme is a step towards correctly interpreting signals obtained from instruments based on the measurement of dynamic speckle patterns in the far field.

* This chapter has been published as: V. Rajan, B. Varghese, T. G. van Leeuwen, and W. Steenbergen, "Quantification of spatial intensity correlations and photodetector intensity fluctuations of coherent light reflected from turbid particle suspensions," *Phys. Rev. E* **75**, 060901-4 (2007).

1. Introduction

In biomedical imaging a number of measurement techniques are based on the spatial and temporal analysis of coherent intensity fluctuations [1, 2, 3, 4, 5], also known as dynamic speckle patterns. Dynamic speckle patterns are produced by the interference of coherent waves which are emitted by media with internal motion of scattering particles. Such a speckle pattern depends on several parameters like the distance from the medium to the detector, the illumination pattern, the absorption level, and the particle size, shape and concentration. So a system which performs detection of back-scattered photons in the far field, is also influenced by these parameters. The quantification of such variations is thereby necessary for all the instruments based on imaging dynamic coherent intensity fluctuations on a detector. The laser Doppler perfusion imager (LDPI) is such an instrument, which is based on collecting back-scattered photons to construct blood flow maps of an area of tissue. In this instrument, a collimated laser beam illuminates an area of tissue and a detector is used to collect back-scattered photons propagated through free air. It is known that the signal from such a system is influenced by the number of coherence areas, or speckles, on the detector [4, 6]. The diffusion of temporal field correlations through turbid media, which is also of interest in such imaging systems detecting back scattered photons, was reported earlier [5, 7].

The spatial field and intensity correlation of speckles was extensively studied in terms of particle size and concentration [8], distance to the detector [9], scattering angle [10] and angle of rotation of source and sample [11]. Several studies were also reported on the contribution of different correlation ranges [12] and spatial correlation of microwaves [13, 14]. In this manuscript we focus on the prediction of the effect of multiple scattering and absorption on the spatial intensity correlation in the far field. Li and Genack [15] showed that the intensity distribution on the output surface due to point excitation and the intensity correlation function on a distant speckle pattern, are Fourier transform pairs. We use this result as a building block of a general theoretical framework to predict photocurrent fluctuations generated by dynamic speckle patterns from mixed dynamic-static media illuminated by coherent light. Our model is able to deal with fields generated by different fractions of backscattered photons. These fractions can be defined according to the Doppler shift, number of scattering events and penetration depth of photons. Our method utilizes an effective amount of speckles on the far field detector calculated by a weighted integration of the calculated intensity correlations functions. The provided computational scheme is a step towards quantification of speckle effects in instruments based on imaging dynamic coherent intensity fluctuations on a detector.

In the following description, various quantities occur which are indicated and localized in Fig. 1.

2. Theoretical Background

A component of our theoretical approach is a relation established between the photodetector signal and the two-point statistics of the speckle intensity field. First the space-time correlation function $\Gamma_{II}(\Delta r, \tau)$ of the intensity variations is expressed in terms of the space-time correlation function $\Gamma_{EE}(r, \tau)$ of the electric field by the Siegert relation [16]. An expression for the space-time field correlation coefficient is derived from the correlation functions of Doppler-shifted or non-Doppler shifted fields that together compose the total electric field. Eventually, the variance of photocurrent fluctuations can be written in terms of so-called fractional coherence areas of these composing local field complex amplitudes by [17]

$$\langle i_{ac}^2 \rangle \equiv \Gamma_{ii}^{AC}(\tau = 0) = A_{\text{det}} R^2 \langle I \rangle^2 \left[2 \sum_i^M f_0 f_i A_{coh}^{0i} + \sum_{i=1}^M \sum_{j=1}^M f_i f_j A_{coh}^{ij} \right] \quad (1)$$

where A_{det} is the effective detection area, R is the responsivity of the detector, $\langle I \rangle$ is the average intensity of the light within the detection area. Furthermore f_0 is the fraction of non-Doppler shifted photons, while f_1, \dots, f_M represent fractions of Doppler shifted photons that can be defined on the basis of various criteria, such as the Doppler shift, the number of Doppler scattering events, the (optical) path length and the penetration depth into the medium. A_{coh}^{ij} represents the so-called fractional coherence area on the detector formed by all pairs of photon groups i and j . This can be written in terms of the correlation coefficient of the fields,

$$A_{coh}^{ij} = 2\pi \int_0^\infty \gamma_{EE}^i(\Delta x, 0) \gamma_{EE}^{*j}(\Delta x, 0) \Delta x d\Delta x \quad (2)$$

where Δx is the spatial separation on the detection plane, and γ_{EE}^i and γ_{EE}^j are the field correlation coefficients of various photon fractions f_1, \dots, f_M of Doppler shifted photons. For $M=0 \dots I$ these are indicated in Fig. 1.

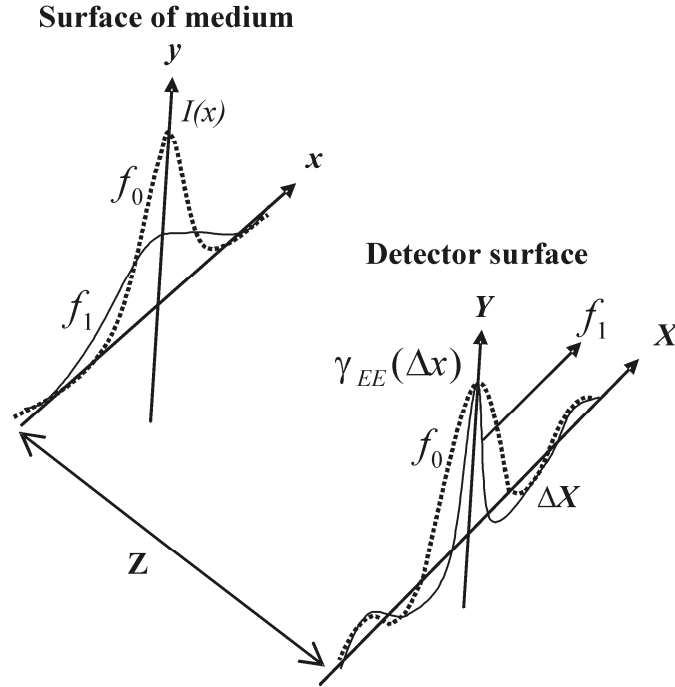


Fig. 1 Illustration of quantities on the surfaces of the medium and the detector; correlation functions for Doppler-shifted and unshifted light fractions f_1 and f_0 on the detector generated by the intensity distributions on the scattering medium surface.

It is assumed that the intensity distribution of each photon fraction is homogenous over the detector and is time independent, and that the speckles are isotropic. The latter implies a circular symmetry of the light emitting spot of the turbid medium. Another assumption which has been made in deriving Equations (1) and (2) is that the effective photodetection area comprises many coherence areas. This condition is required to allow sufficient spatial averaging of the intensity field to obtain space-time correlations. If this condition is not satisfied, Eq. (1) will adopt a slightly more complicated form, and is only valid if the spatiotemporal intensity fluctuations are ergodic. In most cases the effective photodetector will include sufficient coherence areas or speckles for our theory to be applicable.

Equation (1) can be further simplified if apart from a fraction f_0 of non-shifted photons only a single fraction f_1 of Doppler shifted photons is specified, which gives for Eq. (1) with $M=1$

$$\langle i_{ac}^2 \rangle = A_{\text{det}} R^2 \langle I \rangle^2 \left[2f_0 f_1 A_{\text{coh}}^{01} + f_1^2 A_{\text{coh}}^{11} \right] \quad (3)$$

Equation (3) gives the mean square value of photocurrent fluctuations in terms of correlation functions of one group of unshifted photons and one group of Doppler shifted photons. This will occur in mixed static and dynamic media like skin which reflect a combination of photons with nonzero and zero Doppler shift depending on the optical properties and blood volume.

In order to predict the coherence area we need to express the spatial correlation functions γ_{EE}^i on the detector, as appearing in Eq. (2) in terms of the light back-scattered by the medium. Figure 1 illustrates the situation. Here intensity distributions $I(x,y)$ of non-Doppler shifted and Doppler shifted photon fractions f_0 and f_1 are indicated on the surface of the medium, along with their correlation functions $\gamma_{EE}(\Delta X)$ on the detector. Since this can be considered as the problem of far field spatial coherence on a screen illuminated by a spatially incoherent, quasi-monochromatic source, the Zernike-Van Cittert theorem [18] can be applied here, as was shown in Ref.15. This implies that the spatial correlation function of the field on the detector can be determined from the Fourier transform of the intensity distribution on the remote diffusely reflecting medium. Hence if the irradiance distribution on the source is $I(x, y)$, the spatial field correlation on the detector can be written as

$$\gamma_{EE}(\Delta X, \Delta Y) = \frac{\iint_{\text{source}} I(x, y) \exp\left[-i \frac{2\pi}{\lambda Z} (x\Delta X + y\Delta Y)\right] dx dy}{\iint_{\text{source}} I(x, y) dx dy} \quad (4)$$

with $x, y, \Delta X$, and ΔY the positions on the surface of the turbid medium, and spatial separations on the plane of detection, respectively, Z the distance of the medium to the detector plane and λ the wavelength of light in the transparent medium between the turbid medium and the detector. So if the irradiance distribution function of two fractions of the outgoing light on the surface of the medium are known the fractional coherence on the detector can be calculated by substituting the correlation coefficients obtained from Eq. (4) in Eq. (2).

In our approach, we predict the irradiance distribution from a scattering medium with the Monte Carlo simulation technique which allows us to construct irradiance distributions for specific photon fractions. From the photon model we switch to the wave picture of light by application of the Zernike-Van Cittert theorem as expressed by Eq. (4). This switch is made by depicting each photon that is simulated to transit the interface between the turbid medium and the surrounding medium to emit a spherical wave from the surface of the

medium, independent of its k-vector on transition in the Monte Carlo simulation. Hence it is assumed that the k-vectors of all photons leaving the turbid medium are more or less isotropically distributed, so that a photon with a specific k-vector is representative of all photons transiting the interface at that specific position.

In this chapter we validate our approach for the case of completely dynamic particle suspensions. By assuming all photons to be Doppler shifted (hence $f_o=0$ and $f_l=1$), and normalizing with $\langle i_{dc} \rangle = R \langle I \rangle A_{det}$, Eq. (3) can be written as

$$\frac{\langle i_{ac}^2 \rangle}{\langle i_{dc} \rangle^2} = \frac{A_{coh}}{2A_{det}} \quad (5)$$

Equation (5) is valid for a non-polarized speckle pattern. Here a factor of 2 is introduced in the denominator, since a non-polarized speckle pattern is a summation of two independent orthogonally polarized patterns which are formed by multiple scattering. Experimentally the coherence area A_{coh} , or effective speckle size, can be estimated from the modulation depth of the photocurrent intensity fluctuations by using Eq. (5). For validation of our theoretical model we compare the calculated coherence area based on Equations (2) and (4) with the experimental one based on Eq. (5), using the AC and DC photodetector signals as input.

3. Materials and methods

In our experiment we illuminate the medium with a laser beam at normal incidence, and collect the back-scattered photons using a lens of focal length 30 mm, placed at a position of 26 cm from the front surface of the scattering medium, that focuses the light on a photoreceiver. The setup and the signal acquisition have been described in more detail in Rajan *et al.* [6]. A cubic glass cuvette of 8ml is used as a sample holder. Water suspensions of Polystyrene microspheres (Polysciences Inc) with a diameter (\varnothing) of 0.202 μm (anisotropy factor $g=0.3$), 0.771 μm ($g=0.9$) and 1.53 μm ($g=0.93$) are used to make scattering phantoms. Samples with reduced scattering coefficients (μ'_s) of 0.5, 1, 2, 3 and 4 mm^{-1} are made from each particle suspension, based on scattering cross sections following from Mie theory calculations, taking into account the wavelength of the laser light of 632.8 nm, and the refractive index of water. Ecoline Black dye (Talens) is added to get absorption coefficient $\mu_a=0.02\text{mm}^{-1}$.

In the Monte Carlo simulation [19] the scattering phantom is defined as a semi-infinite layer. The optical properties are defined as that of the experimental phantoms. Since the scattering properties and the particle number density of calibrated polystyrene sphere suspensions as used in this study, are

well known it is possible to exactly mimic these properties in simulations. A collimated Gaussian beam with different beam diameters is used as the source and is positioned perpendicular to the interface of the medium. In typical diagnostic tissue imaging systems [3, 4], the photons are detected at a relatively large distance from the sample. In principle, the correlation coefficient can also be calculated on the basis of the angular intensity distribution of photons arriving at the location of the lens. However when this detection configuration would be exactly mimicked in the simulation, almost no simulated photons would be detected. For this reason the simulated detector was positioned just above the medium and all the photons that are emitted by the medium are regarded as detected.

Simulations are performed on the above configuration and particle suspensions. Each simulation includes 60000 detected photons. The resulting back-scattered intensity distributions are used to calculate the spatial coherence of the field by applying Eq. (4), using the distance from the medium to the detector in the experimental set-up. The A_{det} used is the area of the lens (95 mm^2) in front of the photodetector. It was shown earlier [6] that focusing light to within the physical borders of a photodetector will give the same modulation depth as when the lens is replaced with a photodetector of similar size.

4. Results and discussion

Figure 2 shows the coherence area vs. the reduced scattering coefficient for different beam diameters, for the $\text{Ø}0.771 \text{ }\mu\text{m}$ particle suspension. It is observed that the variation in scattering level results in a considerable variation of coherence area. Moreover the variation in coherence area due to variation in scattering level decreases with increasing beam diameter. As the scattering level increases, the number of speckles on the effective detector decreases, since the higher scattering level results in a narrow backscattered intensity distribution. This variation is larger for narrow beams than for wide beams, since the relative change of the width of the intensity distribution by variation in the scattering level is larger for narrow beams than for wide beams. For wide beams the speckle number variation by scattering level variations is suppressed. The same kind of variation is also seen in the plot of the $\text{Ø}1.53 \text{ }\mu\text{m}$ particle suspension (Fig. 3).

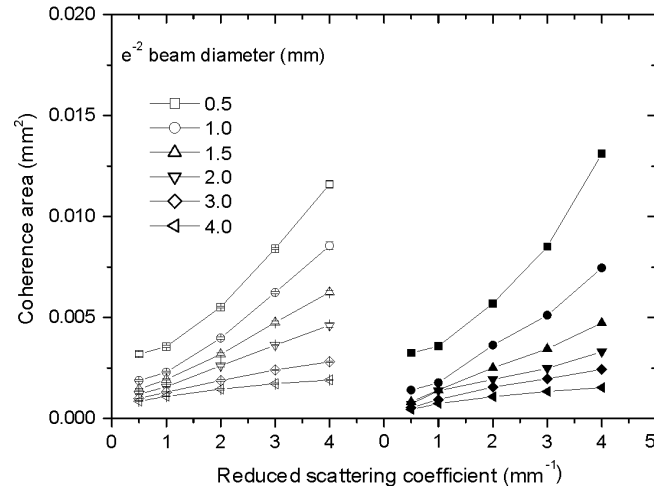


Fig. 2 Coherence area as a function of reduced scattering coefficient and intensity profiles for a particle suspension of $\text{Ø}0.771 \mu\text{m}$ (Scattering anisotropy $g=0.9$) particles. *Left: measurement; Right: simulation.*

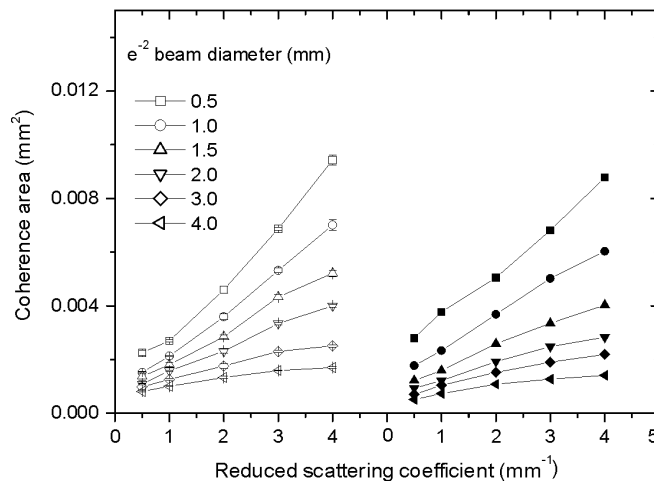


Fig. 3 Coherence area as a function of reduced scattering coefficient and intensity profiles for a particle suspension of $\text{Ø}1.53 \mu\text{m}$ ($g=0.93$). *Left: measurement; Right: simulation.*

Our theoretical calculations match with the experimental results. We correctly predicted the coherence area for a range of scattering anisotropies, scattering levels and beam sizes. It can be said from the results for the anisotropic particles, with anisotropy factors resembling those of biological tissue, that the spatial correlation varies considerably with scattering level and this variation is very low for broad intensity profiles.

Figure 4 shows the coherence area plot for the $\varnothing 0.202 \mu\text{m}$ particle suspension. It can be observed that for this more isotropically scattering particle, the spatial correlation plot for a single beam diameter shows less variation compared to that of anisotropic particles. Furthermore, for this medium the coherence areas are larger than for the media with higher scattering anisotropy. For large particle sizes with $g=0.9$ and 0.93 the coherence area varies by a factor of 4 for 0.5mm beam in the experiment as well as the simulation.

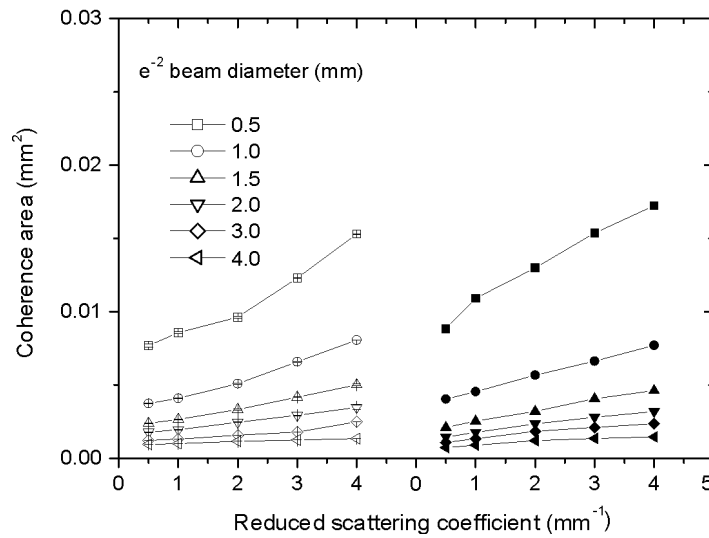


Fig. 4 Coherence area as a function of reduced scattering coefficient and intensity profiles for a particle suspension of $\varnothing 0.202 \mu\text{m}$ ($g=0.32$) . Left: measurement; Right: simulation.

For the $\varnothing 0.202 \mu\text{m}$ particle suspension the coherence area variation for a narrow beam is only a factor of 2. This is because for this medium low order scattering is dominant and is contributing significantly to the intensity distribution on the surface of the medium, hence the relative change of the width of the back-scattered intensity distribution with increasing scattering level is small. Our theoretical calculation agrees well with experimental results even

though we are not considering a polarization factor in applying Eq. (5). For smaller particles a better quantification can be done by taking polarization in to consideration. For this our model can be further extended by considering the contribution from two fractions of back scattered photons in Eq. (2), one is polarized and another one is non-polarized.

In conclusion we have shown that the coherence area detected in reflection mode in the far field of a turbid medium can be predicted with a sequence of models using the photon and wave picture of light. Our theory was able to predict the different behavior for anisotropic as well as isotropic scatterers. It is shown that the spatial correlation varies considerably with diffuse scattering, a variation which can be suppressed by using broader intensity profiles. The theoretical and numerical method will improve the interpretation of results obtained from coherence-based biomedical imaging instruments based on measuring dynamic speckle patterns in the far field. It will for instance allow us to quantify the effect of spatial variations in tissue optical properties on the results obtained with such imaging instruments.

References

1. H. Fujii, K. Nohira, Y. Yamamoto, H. Ikawa, and T. Ohura, "Evaluation of blood flow by laser speckle image sensing: Part 1," *Appl.Opt.* **26**, 5321 (1987).
2. J.D. Briers and S. Webster, "Quasi-real time digital version of single-exposure speckle photography for full-field monitoring of velocity or flow fields," *Opt. Commun.* **116**, 36 (1995).
3. T.J.H. Essex and P.O. Byrne, "A laser Doppler scanner for imaging blood flow in skin," *J.Biomed. Eng.* **13**, 189 (1991).
4. K. Wårdell, A. Jakobsson, and G. E. Nilsson, "Laser Doppler perfusion imaging by dynamic light scattering," *IEEE Trans. Biomed. Eng.* **40**, 309 (1993).
5. D.A. Boas, L. E. Campbell, and A. G. Yodh, "Scattering and Imaging with Diffusing Temporal Field Correlations," *Phys. Rev. Lett.* **75**, 1855 (1995).
6. V. Rajan, B. Varghese, T.G. van Leeuwen, and W. Steenbergen, "Speckles in Laser Doppler Perfusion Imaging," *Opt. Lett.* **31**, 468 (2006).
7. G. Maret and P. E. Wolf, "Multiple light-scattering from disordered media - the effect of Brownian motion of scatterers," *Z. Phys. B* **65**, 409-431 (1987).

8. Y. Piederrière, J. Cariou, Y. Guern, B. Le Jeune, G. Le Brun, J. Lotrian, "Backscattered speckle size as a function of polarization: influence of particle-size and concentration," *Opt. Express* **13**, 5030 (2005).
9. A. Apostol and A. Dogariu, "Spatial Correlation in the Near Field of Random Media," *Phys. Rev. Lett.* **91**, 093901 (2003).
10. B. Hoover, "Optical determination of field angular correlation for transmission through three-dimensional turbid media," *J. Opt.Soc. Am. A*, vol. **16**, 1040 (1999)
11. I. Freund, M. Rosenbluh, and S. Feng, "Memory Effects in Propagation of Optical waves through Disordered Media," *Phys. Rev. Lett.* **61**, 2328 (1988).
12. A. Z. Genack, N. Garcia, and W. Polkosnik, "Long-Range Intensity Correlation in random Media," *Phys. Rev. Lett.* **65**, 2129 (1990).
13. P. Sebbah, B. Hu, A. Z. Genack, R. Pnini, and B. Shapiro, "Spatial-Field Correlation: The Building Block of Mesoscopic Fluctuations," *Phys. Rev. Lett.* **88**, 123901 (2002).
14. A. García-Martín, F. Scheffold, M. Nieto-Vesperinas, and J. J. Sáenz, "Finite-Size Effects on Intensity Correlations in Random Media," *Phys. Rev. Lett.* **88**, 143901 (2002).
15. J. H. Li and A. Z. Genack, "Correlation in laser speckle," *Phys. Rev. E* **49**, 4530 (1994).
16. B. J. Berne and R. Pecora, *Dynamic Light Scattering: With Applications to Chemistry, Biology and Physics* (Wiley, New York, 1976).
17. A. Serov, W. Steenbergen, and F. F. M. de Mul, "Prediction of the photodetector signal generated by Doppler-induced speckle fluctuations: theory and some validations," *J. Opt. Soc. Am. A* **18**, 622 (2001).
18. Born M and Wolf E, *Principles of Optics* (New York Pergamon, 1975).
19. F. F. M. de Mul, M. H. Koelink, M. L. Kok, P. J. Harmsma, J. Greve, R. Graaff, and J. G. Aarnoudse, "Laser Doppler velocimetry and Monte Carlo simulations on models for blood perfusion in tissue," *Appl. Opt.* **34**, 6595 (1995).

Chapter 5

Effect of speckles on the depth sensitivity of laser Doppler perfusion imaging*

A theoretical model is presented and experimentally validated that allows the prediction of the effect of speckles on the depth sensitivity of laser Doppler perfusion imaging. It is shown that the influence of speckles on depth sensitivity is large. In particular the sensitivity to particle motion in superficial layers is strongly beam size dependent: decreasing the beam diameter on the tissue surface increases the sensitivity to superficial motion to a much stronger extent than sensitivity to motion at a larger depth. This can be explained through the effect of beam diameter changes on the fractional coherence areas generated by photons with different penetration depths in the tissue.

* This chapter has been published as: V. Rajan, B. Varghese, T. G. van Leeuwen, and W. Steenbergen, "Effect of speckles on the depth sensitivity of laser Doppler perfusion imaging," *Opt. Express* **15**, 10911-10919 (2007).

1. Introduction

Laser Doppler perfusion imaging (LDPI) [1, 2] is a non-invasive technique to measure blood flow maps on an area of tissue. The photodetector signal generated in a laser Doppler perfusion instrument can be considered to be generated by a large number of dynamic speckles (coherence areas). It has been shown [3] that the scattering level of the tissue strongly affects a laser Doppler imager signal due to the varying number of coherence areas involved in the detection. Variations in absorption as well as the diameter of the illuminating beam will have similar influence on LDPI-readings through the number of coherence areas. Figure 1 shows the speckle pattern generated by a narrow (e^{-2} beam diameter, 0.5mm) and a wide beam (e^{-2} beam diameter, 4mm) illuminating a water suspension of Polystyrene microspheres (Polysciences Inc) of $0.771 \mu\text{m}$ diameter (scattering anisotropy $g=0.9$)

Tissue optical properties also will affect the depth sensitivity of a laser Doppler system. The depth sensitivity here is defined as the sensitivity of the instrument to motion of particles at a certain depth under the illuminated surface of the turbid medium. The decay of the depth sensitivity due to the limited penetration depth of photons is an obvious phenomenon [4]. However, in this paper we demonstrate that, apart from photon penetration depth statistics, the speckle phenomenon has an independent influence on the depth sensitivity. In order to correctly interpret the perfusion signal it is important to know the sensitivity of the instrument to motion at different depths. This is particularly important when we assess the burn depth [5] and perfusion of a grafted skin flap [6]. In this paper we experimentally investigate the depth sensitivity of the laser Doppler perfusion imager. In addition we predict the influence of coherence areas on LDPI depth sensitivity by a theoretical model.

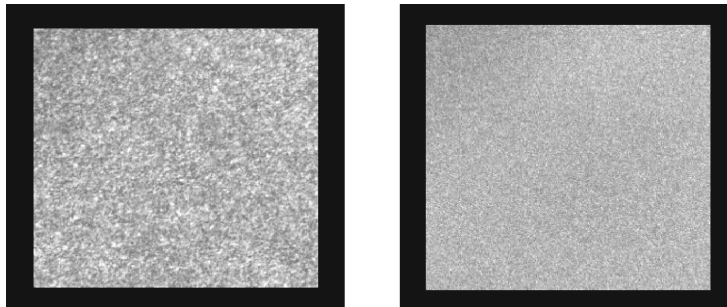


Fig.1 Speckle pattern of light diffusely reflected from a scattering medium which is illuminated with a narrow (to the left) and a broad beam (to the right).

The fundamental output quantities of a laser Doppler instrument are the moments of the power spectra of photodetector intensity fluctuations. M_1 , the first moment is regarded to be proportional to the flux of the moving scatterers (also called the perfusion) and M_0 , the zero order moment is considered to be proportional to the concentration of moving scatterers. These moments of the power spectrum depend on the spectral width and the modulation depth of the photodetector signal. The latter quantity in turn is related to the amount of coherence areas. When all photons are Doppler shifted, the zero order moment, normalized with the DC^2 signal can be written as [7]

$$\frac{M_0}{DC^2} = \frac{\langle i_{ac}^2 \rangle}{\langle i_{dc} \rangle^2} \alpha \frac{1}{N} \quad (1)$$

where $\langle i_{AC}^2 \rangle$ is the mean square of the photocurrent fluctuations, $\langle i_{DC} \rangle$ the mean photocurrent, and N the number of speckles on the detector. So any change in the amount of coherence areas N will influence the laser Doppler perfusion estimate. For a given photodetector size, the amount of speckles (coherence areas) depends on the average coherence area which is roughly dependent on the solid angle at which the photons attack on the detector. Changes in optical properties result in photon trajectories through the medium which make photons to escape from the tissue at different distances from the source. So the solid angle generated by the back scattered photons on the detector changes with optical properties, which changes the average coherence area. This situation is illustrated in Fig. 2 where two solid angles Ω_1 and Ω_2 are shown, which might be associated with narrow and wide illuminating beams, respectively. Figure 1 clearly shows this coherence area variation with illuminating beam diameter.

Earlier we reported [8] on the influence of optical properties on the average coherence area, quantitatively, in an optical configuration used in laser Doppler perfusion imaging. It was observed that with a typical beam diameter of 0.5mm the average coherence area on the detector varies by a factor of 4 when the reduced scattering coefficient varied from 0.5mm^{-1} to 4.0mm^{-1} . This variation drops to a factor of 1.5 when the beam diameter is increased to 4.0mm. This shows the influence of the reduced scattering coefficient on the coherence area which in turn influences the response of the laser Doppler system to the same perfusion level under different optical surroundings.

The coherence area is also influenced by the depth probed by the photons. Photons traveling deep into a scattering medium generate wider intensity patterns in leaving the medium and therefore generate smaller coherence areas (Fig. 2). This reduces the relative contribution of these photons in the total flux signal. Therefore in this optical situation the effect of coherence area is not merely a change in the total system response but also a change in the depth sensitivity of the instrument. In this paper we present and validate a

theoretical approach to quantitatively assess the system's response to motion at different depths.

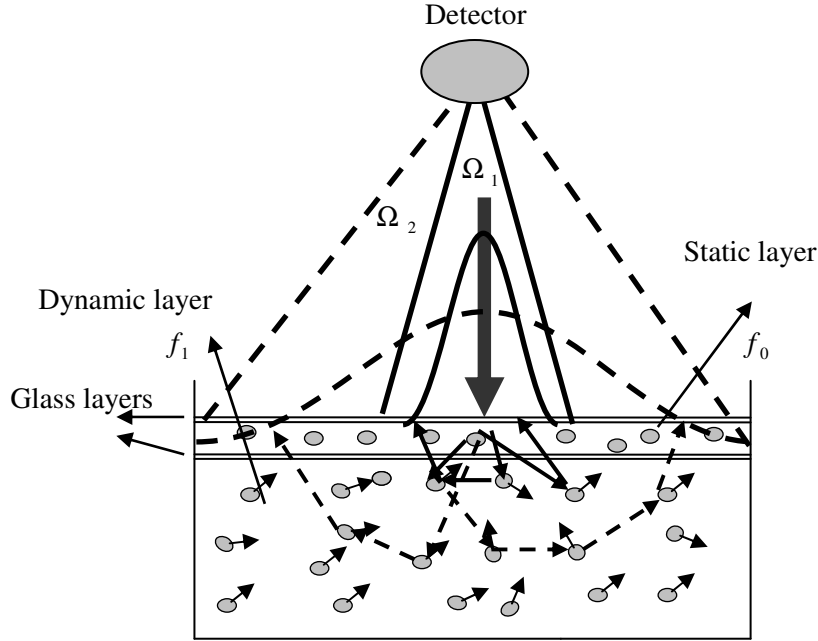


Fig. 2 Schematic of optical scattering phantom with static and dynamic layers. Solid lines represent the back scattered intensity distribution and Dashed line represents the solid angle generated on the detector by photons traveled superficially and deep.

2. Theory

Recently we showed [8] that the spatial correlations of the intensity of far field dynamic speckle patterns generated by mixed static and dynamic turbid media illuminated by coherent light can be predicted. For that we used a theoretical/computational frame work which can model the variance of photocurrent fluctuations on a far-field detector collecting back-scattered photons on the basis of Monte Carlo derived photon statistics, taking in to account the speckle phenomenon.

The photocurrent mean square intensity fluctuations can be expressed in terms of coherence areas formed by different fractions of Doppler shifted photons,

$$\langle i_{ac}^2 \rangle = A_{\text{det}} R^2 \langle I \rangle^2 \left[2f_0 f_1 A_{\text{coh}}^{01} + f_1^2 A_{\text{coh}}^{11} \right] \quad (2)$$

where A_{det} is the effective detection area, R is the responsivity of the detector and $\langle I \rangle$ is the average intensity of the light within the detection area. Furthermore f_0 is the fraction of non-Doppler shifted photons, f_1 is the fraction of Doppler shifted photons ($f_1 = 1 - f_0$) A_{coh}^{01} is the fractional coherence area formed by the interference of Doppler shifted photons with non-Doppler shifted photons, and A_{coh}^{11} is the fractional coherence area formed by only Doppler shifted photons. These fractional coherence areas can be calculated by Fourier-transforming the respective Monte Carlo predicted intensity distributions of these photon fractions according to the Van Cittert Zernike theorem and a simple integration of the resulting spatial field coherence functions $\gamma_{EE}(\Delta x)$ according to

$$A_{\text{coh}}^{ij} = 2\pi \int_0^{\infty} \gamma_{EE}^i(\Delta x) \gamma_{EE}^{*j}(\Delta x) \Delta x d\Delta x \quad (3)$$

with i and j appearing in the same combinations and with the same meaning as in equation (2).

Equations (2) and (3) give the mean square value of photocurrent fluctuations in terms of correlation functions of one group of unshifted photons and one group of Doppler shifted photons. This will occur in, for instance, media like skin which, depending on the optical properties of the tissue matrix, and the blood volume, will reflect photons with nonzero and zero Doppler shift. By normalizing with $\langle i_{dc} \rangle = R \langle I \rangle A_{\text{det}}$ the photodetector signal modulation depth can be written as,

$$\frac{\langle i_{ac}^2 \rangle}{\langle i_{dc} \rangle^2} = \frac{[2f_0 f_1 A_{\text{coh}}^{01} + f_1^2 A_{\text{coh}}^{11}]}{2A_{\text{det}}} \quad (4)$$

With Eqs. (3) and (4) we can predict the signal modulation depth theoretically if we have the intensity distribution on the tissue surface of the Doppler shifted and non-Doppler shifted photons and their fractions f_1 and f_0 . Here a factor of 2 is introduced in the denominator, since a non-polarized speckle pattern is a summation of two independent orthogonally polarized patterns which are formed by multiple scattering. Since the Monte Carlo method [9] can simulate the photon intensity distribution from an optical medium and provide the statistics of the detected photons, it can give input parameters to calculate the fractional coherence areas on the photodetector, and in turn we can predict the signal modulation depth.

3. Materials and methods

Phantoms two layered are made: the top layer which is static, and a bottom layer which is dynamic. A schematic of the scattering phantom is shown in Fig. 2. Both layers are prepared with a reduced scattering coefficient $\mu'_s=2.0\text{mm}^{-1}$, a scattering anisotropy $g=0.9$ and an absorption coefficient of $\mu_a=0.02\text{mm}^{-1}$. The dynamic scattering phantom is made of polystyrene microspheres $\varnothing 0.771 \mu\text{m}$ mixed with water. Ecoline Black ink (Royal Talens) is added to get the desired absorption. The self-diffusion coefficient of the particles in Brownian motion is calculated as, $D_B = K_B T / 3\pi\eta a = 5.56 * 10^{-9} \text{ cm}^2/\text{s}$ (Stokes-Einstein relation). Here K_B is the Boltzmann constant, T is the temperature (293 K), η is the viscosity of the suspending liquid [$\eta = 1.0 \text{ cps}$ for water] and a is the hydrodynamic diameter ($\varnothing 0.77 \mu\text{m}$) of the scattering particles. From this the expected single-scattering correlation time (the inverse of product of the diffusion coefficient of particles and the squared wavenumber of probe light) for the particle suspension used is found to be 0.018 seconds.

The static layer is made of a poly(vinyl alcohol) (PVA) gel with polystyrene particles. In the past, PVA has been used to produce elastic [10] or viscoelastic [11] gels as optical tissue phantoms. The advantage of PVA is its solubility in water, so we can make phantoms of known scattering and absorption properties by adding polystyrene spheres and water-soluble dyes before gelation.

Solid phantoms of PVA gel are made by adding sodium borate (Borax, $\text{Na}_2\text{B}_4\text{O}_7 \cdot 10\text{H}_2\text{O}$) as a cross-linking agent to an aqueous PVA solution. For this at first a PVA (Aldrich chemical company Inc, 99+% hydrolyzed) solution of 4% (by weight) in water is prepared. Another solution of 4% (by weight) of borax in water is prepared. Polystyrene particles and Ecoline black are added to this solution to make the desired scattering and absorption properties. Then this solution is mixed with a mixing ratio Borax/PVA of 20%. PVA gel when mixed with Borax is optically transparent. So the phantom will only show the properties of the particles and ink added. It is tested that the static and dynamic scattering phantoms have the same optical properties by total attenuation measurement. A glass cuvette of 2.5cm^3 is used as a sample holder for dynamic phantoms. The static phantom is placed in between two thin glass slides (150 microns) and the thickness is exactly defined by placing two spacers of known thickness between the glass slides. The thicknesses of static phantoms used are 0.25, 0.5, 1.0, 1.5 and 2.0mm excluding the glass layer. The static phantom is placed on a frame which is attached to a linear translational stage and is placed on top of the dynamic scattering phantom.

The optical set up consists of a simple reflection mode configuration in which we illuminate the medium with laser beam perpendicular to the phantom surface, and collect the back-scattered photons using a lens and photoreceiver.

A linearly polarized Uniphase 1125P He-Ne laser, of 632.8nm, with output power of 5mW is used as the source. A beam expander made of two positive lenses of focal length 20 and 30mm respectively is used to vary the beam diameter. The second lens is moved with respect to the other to obtain a change in beam diameter. It was measured with a commercial beam profiler that the beam diameter (e^{-2}) at the position of the sample surface can be obtained in a range of 0.5 mm to 4.0mm by translating the lens 2 in the direction of the beam. A lens ($f=30$ mm) is placed at a distance of 25cm from the sample to collect the back-scattered light, with a photoreceiver on focus. Detection is performed with a New Focus (model 2001) photoreceiver, with an effective detector area of 0.81mm^2 . The AC signal is amplified by 40 dB and then applied to an anti-aliasing low-pass filter (5th order sampled capacitor Butterworth, $f_c=20$ kHz). The filtered signal is then applied to a 12-bit analogue to digital converter (National instruments, model AT-MIO-16E-10) where it is sampled at 40 kHz.

3.1. Monte Carlo simulation and speckle size computation

In the Monte Carlo simulation the scattering phantom is defined as a two-dimensional system. A collimated Gaussian beam of 632.8 nm with varying beam diameter is used as the source and is positioned perpendicular to the interface of the medium. A multilayer system is defined as used in the experimental set up, with the same optical properties including the glass layers. The thickness of the static layer is varied in steps, as in the experiments. The dynamic layer is defined with particles undergoing random motion, to tag photons having penetrated to this layer. Each simulation consists of 90000 detected photons. The detected photons are then separated to get two fractions: one from the static layer and one from the dynamic layer. This is done by separating Doppler-shifted and non-shifted photons. With the intensity distributions of these two fractions of photons the field correlation coefficients of statically scattered photons and dynamically scattered photons, and consequently the fractional coherence areas A_{coh}^{01} and A_{coh}^{11} can be calculated. By applying these values and fractions of non-Doppler shifted and Doppler shifted photons f_0 and f_1 in Eq. (4) we can calculate the modulation depth of the signal which is equal to M_0/DC^2 .

4. Results and discussion

Figure 3 shows calculated spatial field correlation functions produced by two fractions of photons. To the left is the correlation function of photons that traveled only within a static top layer of 0.5mm thickness and hence are non-Doppler shifted. To the right is the correlation function formed by photons which traveled through the dynamic layer and have undergone a Doppler shift.

The width of the correlation function is a qualitative measure of the average coherence area. It can be observed that the correlation function of the photons coming from the deep layer is narrow compared to that from the static layer. This is because the photons coming from the deeper layer generate a wide intensity distribution on the surface of the medium, which is associated with smaller coherence areas. In contrast, photons from superficial statically scattering layer generate a narrow intensity distribution and large coherence areas as illustrated in Fig. 2. Furthermore, the width of the field correlation function of static photons is much more sensitive to beam diameter than the correlation function of Doppler photons: due to the larger amount of scattering events undergone by the Doppler shifted photons, their lateral distribution is much more governed by the optical properties of the medium than by the beam diameter.

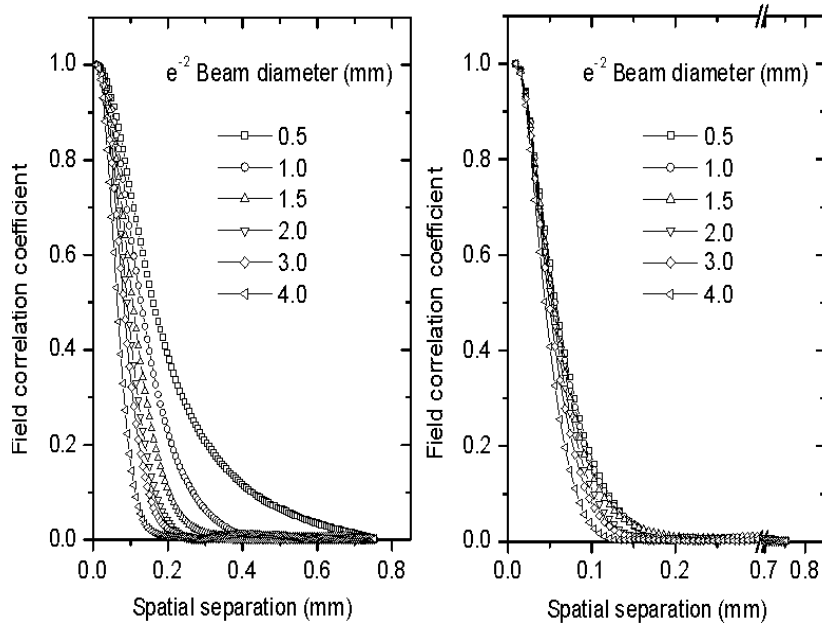


Fig. 3 Field correlation coefficients as a function of beam size for a two layered medium with a static layer of 0.5mm and a dynamic layer of 20mm. Left: field correlation coefficient γ_{EE}^0 of non-Doppler shifted photons γ_{EE}^1 Right: of Doppler shifted photons (note the different horizontal scales).

Figure 4 shows the signal modulation depth for different thicknesses of the static layer, from experiments (*left*) and from theoretical prediction using Eq. (4), (*right*). Here the modulation depth as a function of the static layer thickness defines the depth sensitivity of the instrument, which is the sensitivity

of the instrument to motion vs the depth at which motion occurs. As expected, it is observed that, as the thickness of the static layer increases the modulation depth decreases. However, this trend is suppressed with increasing beam diameter. For the narrowest beam the signal modulation ratio for motion at 0 and 0.5 mm depth, respectively, is 2.9. But for a wide beam (4.0mm) this ratio is reduced to 1.6. This shows that a narrow beam is more sensitive to scattering from superficial layers compared to a wide beam, while the sensitivity to motion at large depth is much less dependent on beam diameter. Measurements performed with a narrow beam will be very sensitive to changes in number of coherence areas with depth. In contrast, a wide beam which itself results in a wide intensity distribution of back scattered light and large number of coherence areas suppresses the depth related changes in the amount of coherence areas. This difference must completely be attributed to the effect of speckles, since the statistics of the photon penetration depth will be independent of beam diameter.

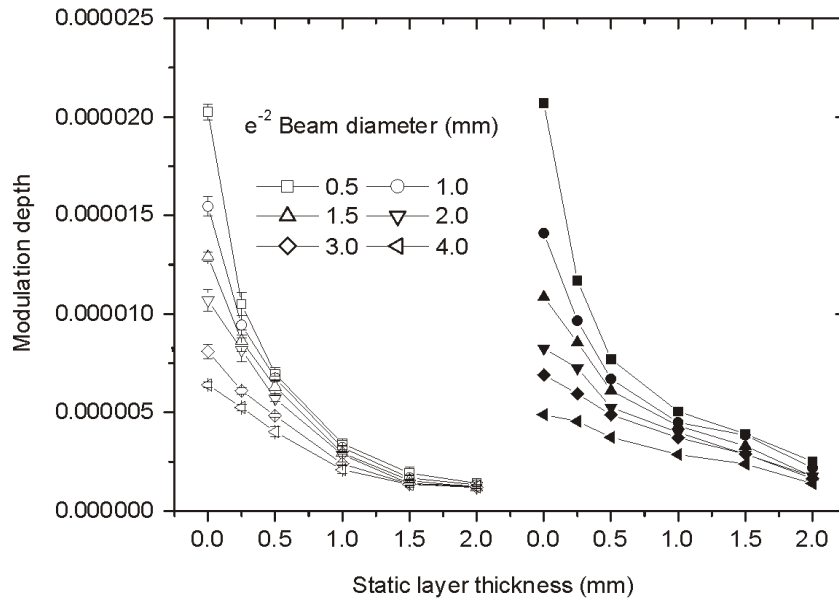


Fig. 4 Plot of modulation depth of a particle suspension for various thicknesses of static top layer. Left: measurement (Error bar represents standard deviation, error is very small); Right: simulation.

The Monte Carlo simulated modulation depth (normalized to zero depth) vs static layer thickness with speckle effects (closed symbols) and without taking speckle effects (shaded symbols, by keeping $A_{coh}^{01} = A_{coh}^{11} = 1$ in Eq. (4)) into account for each beam diameter is shown as Fig. 5. The shaded symbols depict the data of Fig. 4 (right) without speckle effects, thus the modulation depth is only a function of the fraction of Doppler shifted and non-Doppler shifted photons and depends on photon penetration depth statistics alone. Consequently the modulation depth is equal for all beam diameters since the photon penetration depth is independent of beam diameter. Figure 5 shows that with speckle effects the signal modulation ratio for motion at 0 and 2.0 mm depth, respectively, is 8.33 for a beam of 0.5mm diameter. But for 4.0mm beam this ratio is only 3.57. When speckle effects are not taken in to account (Fig. 5(shaded symbols)) the modulation ratio for motion at 0 and 2.0 mm depth is only 3.13 for all beam diameters. This trend clearly shows the effect of speckle phenomenon on the depth sensitivity of the instrument.

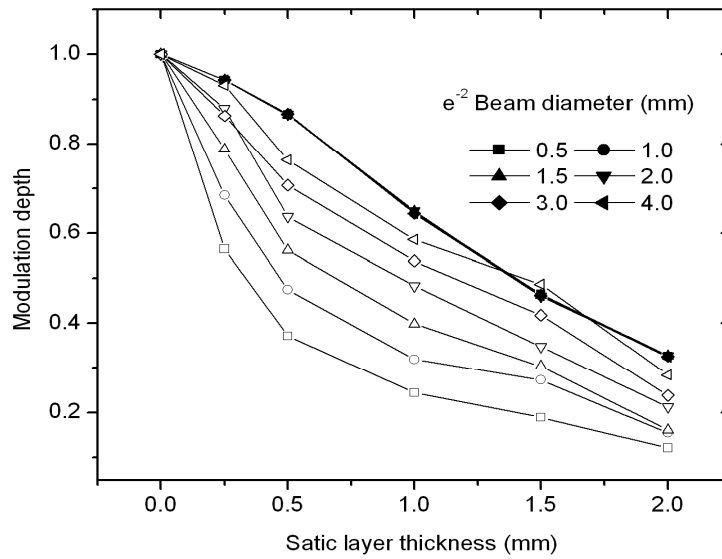


Fig. 5 Modulation depth (normalized to zero depth) vs static layer thickness with speckle effects (closed symbols) and without the speckle effects (shaded symbols, $A_{coh}=1$).

In Fig. 6 experimental modulation depth values are plotted against predicted values. It can be observed that for narrow beams (0.5 and 1.0 mm) and superficial layers (0 to 0.5 mm) the agreement between theoretical prediction and experimental results is within 10%. The variation is significant (up to 40%) for deeper layers because the signal-to-noise ratio in measurements is very low in these cases. Since the Monte Carlo detector is more sensitive and effectively collects very low amount of Doppler shifted light the measured modulation depth tends to saturate faster compared to the predicted results. This can be seen in Fig. 4 where for 1.5 to 2mm thickness the modulation depth is getting leveled off in measured result but not in the prediction.

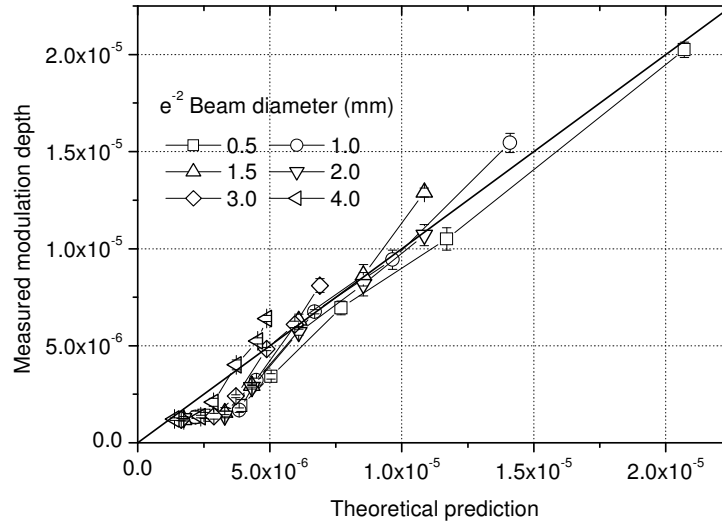


Fig. 6 Theoretical prediction vs measured modulation depth

5. Discussions and conclusion

Our results show that the depth sensitivity of the laser Doppler instrument is strongly influenced by coherence areas. A narrow beam is more sensitive to scattering in superficial layers than a wide beam due to the change of the average coherence area. Our earlier experimental study [3] showed that this beam diameter dependency will depend on the scattering level of the medium. A wide beam can be used to suppress the speckle effects and the sensitivity to scattering levels, but the modulation depth and lateral resolution will be compromised. The strength of the speckle effect on depth sensitivity will also depend on the scattering and absorption level of the tissue. The lower the level

of the scattering and absorption the smaller the effect will be. This is because when scattering or absorption is high photons will travel shorter distances and leave the medium closer to the illuminating beam making a narrow back-scattered intensity profile. So the effective coherence area will be larger and also the modulation depth. In this situation the LDPI flux signal will be very sensitive to the depth related changes in width of the intensity distribution and the resulting changes in the number of coherence areas.

Since our model proved to be correct it can be used to predict this sensitivity variation for different scattering and absorbing media. This is very relevant in LDPI applications where skin optical properties vary significantly in the region of interest and in time. For example during the uptake of certain drugs or in allergy tests [12] where the skin color changes, the optical properties of the skin vary which influences the signal response irrespective of the perfusion variation. Also in the case of a burn depth [5] or wound healing [6] assessment the changes in absorption and scattering by skin color or a grafted skin influences the measured perfusion signal, not only through the photon statistics, but also because of the speckle effects demonstrated here. Our theoretical model offers a valuable tool to predict the depth sensitivity and modulation depth changes in these complex situations.

In conclusion, the depth sensitivity of laser Doppler imagers as a function of tissue optical properties and illuminated beam diameter was assessed, both experimentally and theoretically. Our work shows that in scanning beam laser Doppler perfusion imagers a significant coherence area related cross talk will exist between the perfusion maps and the optical properties of the scanned tissue area, in particular for the contribution of superficial perfusion to the total perfusion map.

References

1. K. Wårdell, A. Jakobsson, and G. E. Nilsson, "Laser Doppler perfusion imaging by dynamic light scattering," *IEEE Trans. Biomed. Eng.* **40**, 309-316 (1993).
2. T. J. H. Essex and P. O. Byrne, "A laser Doppler scanner for imaging blood flow in skin," *J. Biomed. Eng.* **13**, 189-193 (1991).
3. V. Rajan, B. Varghese, T. G. van Leeuwen, and W. Steenbergen, "Speckles in Laser Doppler Perfusion Imaging," *Opt. Lett.* **31**, 468-470 (2006).
4. A. Jakobsson, G. E. Nilsson, "Prediction of sampling depth and photon pathlength in laser Doppler flowmetry," *Med. Biol. Eng. Comput.* **31**, 301-307 (1993)

5. E. J. Droog, W. Steenbergen and F. Sjöberg, "Measurement of depth of burns by laser Doppler perfusion Imaging," *Burns* **27**, 561–568 (2001).
6. W. Eichhorn, T. Auer, E. D. Voy, K. Hoffmann "Laser Doppler imaging of axial and random pattern flaps in the maxillo-facial area. A preliminary report," *J. Craniomaxillofac. Surg.* **22**, 301-306 (1994).
7. A. Serov, W. Steenbergen, and F. F. M. de Mul, "Prediction of the photodetector signal generated by Doppler-induced speckle fluctuations: theory and some validations," *J. Opt. Soc. Am. A* **18**, 622-630 (2001).
8. V. Rajan, B. Varghese, T. G. van Leeuwen, and W. Steenbergen, "Quantification of spatial intensity correlations and photodetector intensity fluctuations of coherent light reflected from turbid particle suspensions," *Phys. Rev. E* **75**, 060901-4 (2007).
9. F. F. M. de Mul, M. H. Koelink, M. L. Kok, P. J. Harmsma, J. Greve, R. Graaff, and J. G. Aarnoudse, "Laser Doppler velocimetry and Monte Carlo simulations on models for blood perfusion in tissue," *Appl. Opt.* **34**, 6595-6611 (1995).
10. A. Kharine, S. Manohar, R. Seeton, R. G. M. Kolkman, R. A. Bolt, W. Steenbergen, F. F. M de Mul "Poly(vinyl alcohol) gels for use as tissue phantoms in photoacoustic mammography," *Phys. Med. Biol.* **48**, 357–70 (2003).
11. J. C. Hebden, B.D Price, A. P. Gibson and G. Royle, "A soft deformable tissue-equivalent phantom for diffuse optical tomography," *Phys. Med. Biol.* **51**, 5581-5590 (2006).
12. A. Fullerton, B. Rode, and J. Serup, "Skin irritation typing and grading based on laser Doppler perfusion imaging," *Skin Res. Technol.* **8**, 23–31 (2002).

Chapter 6

Influence of tissue optical properties on laser Doppler perfusion imaging, accounting for photon penetration depth and the laser speckle phenomenon*

The influence of tissue optical properties on laser Doppler perfusion imaging (LDPI) is not well understood. In this study we address this problem by quantifying the dependence of the signal response to tissue optical properties based on speckles or coherence areas and on photon statistics. We have investigated the effect *in vivo* showing the amplitude of photocurrent fluctuations in normal skin and portwine stain with a range of beam diameters, and its relation to the speckle size variation difference between these two tissues. For the case of a low concentration of moving particles moving within a static turbid medium, a model is described and applied to predict the influence of speckles on the overall and depth sensitivity of LDPI, for a range of scattering levels and absorption levels. The results show that the speckle related effects on overall and depth sensitivity are large and that the depth sensitivity is highly likely to be misinterpreted without taking the speckle phenomenon into account.

* This chapter has been submitted for publications in *Journal of Biomedical Optics* as: V. Rajan, B. Varghese, T. G. van Leeuwen, and W. Steenbergen, "Influence of tissue optical properties on laser Doppler perfusion imaging, accounting for photon penetration depth and the laser speckle phenomenon."

1. Introduction

Coherence domain optical methods used for tissue perfusion imaging [1-5] are based on the analysis of dynamic speckles formed by the light backscattered from the tissue [6]. Laser Doppler perfusion imaging (LDPI) is such a technique which is based on the analysis of spatial and temporal variation of speckles due to the motion of moving blood cells in the microcirculation [3, 4]. Recently we showed that independent of the perfusion the LDPI response is influenced by speckles [7]. The modulation depth of the photodetector signal depends on the speckles and thus beam diameter. We showed that with a typical beam diameter of 0.5mm the average speckle size on the detector varies by a factor of 4 when the reduced scattering level varied from 0.5mm^{-1} to 4.0mm^{-1} . This variation drops to a factor of 1.5 when the beam diameter is increased to 4.0mm, which demonstrates the interplay between the speckle size and perfusion signal on the LDPI response due to the fact that the speckle size is inversely related to the width of the intensity distribution.

The perfusion in a region where the optical properties are either spatially heterogeneous or change in time can be erroneously estimated. For example during a vasodilatory stimulus [8] the tissue optical properties change resulting in intensity distribution variations of the reflected light in course of time. In the case of burn diagnosis [9] the heterogeneous nature of the burn tissue and presence of inflammation can influence the perfusion map, since the scanning beam will go through areas where either absorption or scattering is different. This will result in different widths of back-scattered intensity distributions and different solid angles of illumination on the far field detector (Figure 1). The speckle size and number will vary in time and with the location on the tissue with optical properties, causing variations in the perfusion reading independent of actual perfusion variations. So it is very important that the issue of speckles is quantified in these cases.

We have reported that the spatial correlations of the intensity of far field dynamic speckle patterns generated by mixed static and dynamic turbid media illuminated by coherent light can be predicted [10]. Based on a theoretical /computational frame work the variance of photocurrent fluctuations was modeled for a far-field detector collecting back-scattered photons on the basis of Monte Carlo derived photon statistics, taking in to account the speckle phenomenon. The speckle size variations were estimated for different scattering levels and anisotropies.

In this paper, first we will demonstrate the influence of tissue optical properties on the signal response as mediated by the speckle effect *in vivo* by comparing the signal from normal skin and port wine stained skin for various beam diameters. Next, we use our validated computational method to quantify

the overall sensitivity and depth resolved response of LDPI due to the combined effect of photon penetration depth statistics and the speckle phenomenon. This will be done for a range of tissue optical properties.

2. Theoretical Background

In the laser Doppler perfusion measurement technique information about the amount and flux of the moving scatterers (red blood cells) are extracted from the power spectra of photocurrent intensity fluctuations [11]. The moments of the power spectra give an estimation of perfusion,

$$M_i = \int_0^{\infty} P(\omega) \omega^i d\omega \quad (1)$$

often normalized with DC^2 to cancel out laser power fluctuations. M_1 , the first moment is regarded as a measure of the flux of the moving scatterers (also called the perfusion) and M_0 , the zero order moment is considered to represent the concentration of moving scatterers.

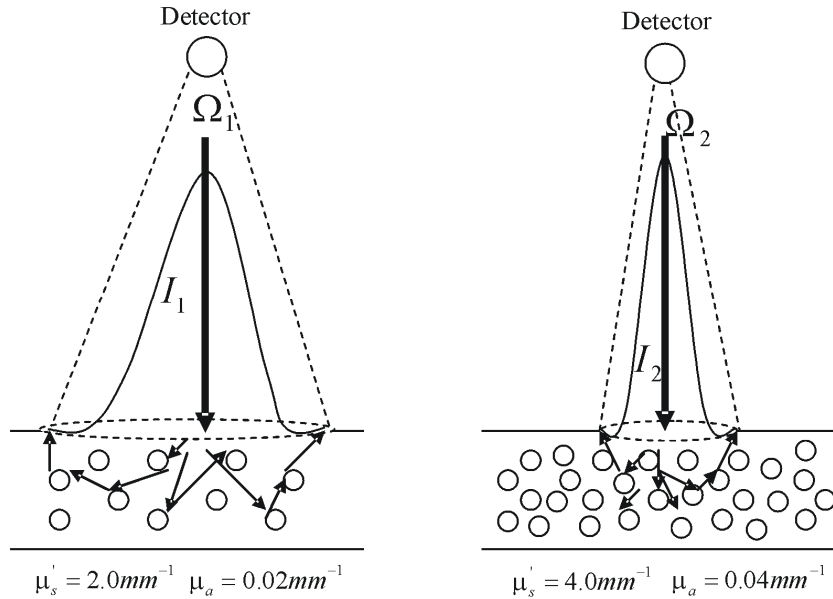


Fig. 1 Illustration of the intensity profile and the solid angle generated by the back-scattered photons for two different optical properties. I_1 and I_2 represent the intensity distributions and, Ω_1 and Ω_2 represent the solid angles.

2.1 The modulation depth of the LDPI signal

In LDPI the moments of the power spectrum of the detector current fluctuations depend on the spectral width and the modulation depth of the signal. The latter quantity in turn is related to the amount of speckles within the photodetector area. The zero order moment normalized with the DC² signal can be written as [11],

$$\tilde{M} \equiv \frac{M_0}{DC^2} \equiv \frac{\langle i_{ac}^2 \rangle}{\langle i_{dc} \rangle^2} = \frac{\left[2 \sum_i^M f_0 f_i A_{coh}^{0i} + \sum_{i=1}^M \sum_{j=1}^M f_i f_j A_{coh}^{ij} \right]}{A_{det}} \quad (2)$$

where $\langle i_{ac}^2 \rangle$ is the mean square of the photocurrent fluctuations, $\langle i_{dc} \rangle$ the mean photocurrent, A_{det} is the effective detection area (in the case of light collection with a lens, the area of the lens is the effective detection area). Furthermore f_0 is the fraction of non-Doppler shifted photons, while $f_1 \dots f_m$ represent fractions of Doppler shifted photons that can be defined on the basis of various criteria, such as the Doppler shift, the number of Doppler scattering events, the (optical) path length and the penetration depth into the medium. A_{coh}^{ij} represents the so-called fractional coherence area on the detector formed by all pairs of photon groups i and j . These fractional coherence areas can be written in terms of respective correlation functions as,

$$A_{coh}^{ij} = 2\pi \int_0^\infty \gamma_{EE}^i(\Delta x) \gamma_{EE}^{*j}(\Delta x) \Delta x d\Delta x \quad (3)$$

Here i and $j = 0, 1$, represent non Doppler shifted light and Doppler shifted light, respectively, and γ_{EE} represents the field correlation function of the waves of Doppler shifted and unshifted light that illuminate the photodetector. The field correlation function for each fraction of light can be written in terms of the intensity distribution using the Zernike-van Cittert theorem,

$$\gamma_{EE}(\Delta X, \Delta Y) = \frac{\iint_{source} I(x, y) \exp\left[-i \frac{2\pi}{\lambda Z} (x\Delta X + y\Delta Y)\right] dx dy}{\iint_{source} I(x, y) dx dy} \quad (4)$$

Where $I(x, y)$ is the intensity distribution on the surface of the medium with $x, y, \Delta X$, and ΔY the positions on the surface of the turbid medium, and spatial separations on the plane of detection, respectively, Z the distance of the medium to the detector plane and λ the wavelength of light in the transparent medium between the turbid medium and the detector. Since the Monte Carlo method [12] can simulate the photon intensity distribution from an optical medium and provide the statistics of fractions of Doppler shifted photons, it can

give input parameters to calculate the fractional coherence areas on the photodetector, and in turn we can predict the signal modulation depth.

2.2 Prediction of the depth sensitivity in laser Doppler perfusion imaging

The depth sensitivity of LDPI can be defined as the sensitivity of the instrument to motion of red blood cells at a certain depth under the tissue surface. Our initial approach is to analyze this quantity for a static medium with a relatively low concentration of moving scatterers. In that case the modulation depth can be predicted for two fractions of photons; one which has interacted only with the static medium and is non-Doppler shifted and one which interacted with the particles moving at a certain depth and is Doppler shifted.

In this case we can write Eq (2) as,

$$\tilde{M} \equiv \frac{M_0}{DC^2} \equiv \frac{\langle i_{ac}^2 \rangle}{\langle i_{dc} \rangle^2} = \frac{[2f_0f_1A_{coh}^{01} + f_1^2A_{coh}^{11}]}{2A_{det}} \quad (5)$$

where f_0 is the fraction of non-Doppler shifted photons and f_1 is the fraction of Doppler shifted photons. A_{coh}^{01} is the coherence area formed by the interference of Doppler shifted photons with non-Doppler shifted photons, and A_{coh}^{11} is the fraction of coherence area formed by only Doppler shifted photons. Here a factor of 2 is introduced in the denominator, since a non-polarized speckle pattern is a summation of two independent orthogonally polarized patterns which are formed by multiple scattering. The first term of the numerator of Eq. (5) represents the heterodyne signal formed by the interference of Doppler shifted light with non Doppler shifted light. The other part represents the homodyne signal which is formed by the interference of only Doppler shifted light.

In tissue which is sparsely perfused the Doppler shifted fraction of photons will be significantly smaller than the non-Doppler shifted photons, and hence $f_1^2 \ll f_0 f_1$. In that case the contribution from the homodyne part of the signal (the second term in the numerator of Eq. (5)) will be negligible and Eq. (5) assumes a more simplified form,

$$\tilde{M} \equiv \frac{M_0}{DC^2} \equiv \frac{\langle i_{ac}^2 \rangle}{\langle i_{dc} \rangle^2} = f_0 f_1 \frac{A_{coh}^{01}}{A_{det}} \quad (6)$$

3. Materials and methods

In this section we describe the methods we followed to give in vivo evidence of the independent effect of speckles on the response of LDPI. Next, we analyze the influence of tissue optical properties on LDPI signal, with incorporation of speckle effects.

We did measurements on two skin sites to analyze the LDPI signal differences and to correlate this with the speckle size predicted on the basis of the measured intensity distribution. A relation between the measured perfusion levels, the optical properties and the speckle phenomenon, is also suggested by a concise Monte Carlo study. Finally, having given proof of the relevance of the speckle effect in vivo, we performed a series of simulations with various optical properties.

3.1 In vivo measurements

The aim of the in vivo measurements was to confirm the effect of speckles on perfusion measurements in real tissue. For this we measured on a and next to a port wine stain in the face of a human subject. Since the port wine stain has an abnormal density of blood vessels the optical properties will be significantly different from the surrounding normal skin.

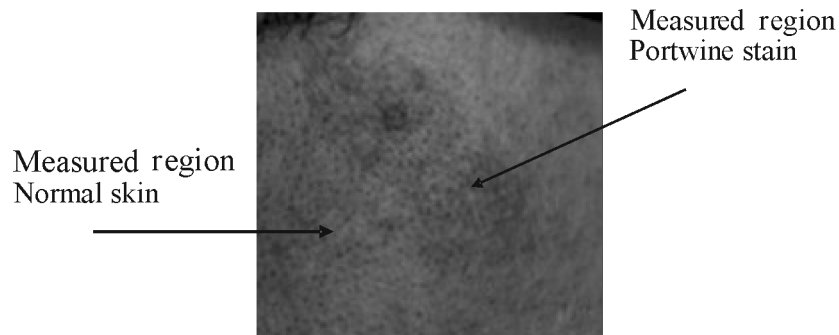


Fig. 2 A photograph of the measured portwine stain on the right cheek of the subject.

The port wine stain we measured was on the right cheek of a healthy subject (Male, 42 year old) and was pale red in color. Figure 2 is a photograph of the measured region of the cheek with portwine stain. A photoacoustic image of the cheek skin was obtained, with a set up available in our group [13], to analyze the thickness and depth of the portwine stain region. The thickness of the portwine stain was measured to be 2mm and the depth of the lesion under

the skin surface was estimated as $300\ \mu\text{m}$. Since the penetration depth of the laser Doppler imager set up is around 1mm (depends on the tissue optical properties) the probed tissue volume was completely inside the boundaries of the highly vascularised region.

3.1.1 Experimental set up for laser Doppler measurements

The experimental set up consisted of a simple back-scattered configuration in which we illuminated the skin with a perpendicular laser beam, and collected the back-scattered light using a lens and photoreceiver. A linearly polarized Uniphase 1125P He-Ne laser, of 632.8nm, with output power of 5mW is used as the source. A beam expander made of two positive lenses of focal length 20 and 30mm respectively was used to vary the beam diameter. The beam diameter was measured with a commercial beam profiler. A lens ($f=30\text{mm}$) of diameter 11mm was placed at a distance of 25cm from the sample to collect the back-scattered light, with a photoreceiver in focus (New Focus, model 2001) with a detector area of 0.81mm^2 . The AC signal was amplified by 40 dB and then applied to an anti-aliasing low-pass filter (5th order sampled capacitor Butterworth, $f_c=20\ \text{kHz}$). The filtered signal was then applied to a 12-bit analogue to digital converter where it was sampled at 40 kHz. The power spectrum of this AC signal was used to calculate the normalized zero order moment M_0/DC^2 . The M_0/DC^2 signal was measured using a range of beam diameters and measurements were compared between normal skin (adjacent to the stain) and the port wine stained skin. In all cases only a one-point measurements were taken, with averaging over three measurements.

3.1.2 Average speckle size measurement

We have shown earlier that the average speckle size produced on a far field detector by light back-scattered from a scattering medium can be calculated using the intensity distribution of back scattered light [10]. In order to measure the back-scattered intensity distribution from the normal skin and port wine stain we used a CMOS camera (C-Cam, Bci4-USB). The correlation function and the speckle size were calculated from this intensity profile with the procedure explained in section 2.1. For simplicity it was assumed that there was only one fraction of photons, since it is not possible to discriminate between fractions of photons according to the depth or Doppler shift in real tissue. This will give the average speckle size (coherence area, see Eq.(3)) related to the measured intensity distribution.

3.2 Monte Carlo simulations

In the Monte Carlo simulation the scattering phantom was defined as two-dimensional layered system containing particles of diameter $\varnothing 0.771\ \mu\text{m}$ (scattering anisotropy $g=0.89$). A collimated Gaussian beam of 632.8 nm with

different beam diameters was used as the source and was positioned perpendicular to the interface of the medium. In Mont Carlo simulation a circular detector was used with a radius of 50mm, which is sufficient enough to collect all the back-scattered photons. Each simulation was carried out with a fixed number of detected photons (90000).

3.2.1 Influence of beam diameter on modulation depth

In order to validate our observations in in vivo measurements we used our model to calculate the modulation depth for two optical situations resembling to normal skin and portwine stain. Since the optical properties of the portwine stain and the adjacent skin we measured on are not known we assumed a higher scattering and very high absorption compared to normal skin [14]. For this one medium was defined with scattering and absorbing levels of $\mu'_s=2.0\text{mm}^{-1}$, $\mu_a=0.02\text{mm}^{-1}$ and another medium with $\mu'_s=4.0\text{mm}^{-1}$, $\mu_a=0.04\text{mm}^{-1}$. A series of simulations were performed by varying the $1/e^2$ beam diameter as 0.5, 1.0, 1.5, 2.0, 3.0 and 4.0mm.

In each simulation the intensity distribution of all detected photons (not discriminating the depth) was used in calculating the average speckle size by Eqs. (3) and (4). Next, using Eq. (5) the overall response of the signal in terms of its modulation depth was calculated assuming $f_0=0$ and $f_i=1$. This will give an overall response of the signal for different tissue optical properties and beam diameters.

3.2.2 Influence of tissue optical properties on the depth sensitivity

For quantifying the influence of tissue optical properties on depth sensitivity we considered motion of a low concentration of scattering particles in a static medium, and we analyzed the signal modulation depth generated by particles confined within a thin layer at a certain depth. This was repeated for a number of depths of the thin dynamic layer in the range 0-2mm, and for different combinations of tissue optical properties as given in table 1. The scattering medium was illuminated with a Gaussian beam of $1/e^2$ beam diameter of 1mm. Since this beam diameter is typical for commercially available laser Doppler imagers the results will be very useful for analyzing the performance of the method. The refractive index of the medium containing the scattering particles and the surrounding medium were defined as 1.33 and 1 respectively. A series of simulations were performed with all combinations of optical properties defined in table 1.

Table 1 Optical properties and depth of moving layer for the Monte Carlo simulation

μ_s' (mm ⁻¹)	1.0	2.0	3.0	4.0			
μ_a (mm ⁻¹)	0.01	0.02	0.04	0.08			
g	0.89						
Depths of dynamic layer (mm)	0	0.25	0.5	0.75	1.0	1.5	2.0

For each simulation the intensity distributions of Doppler shifted and unshifted photons were determined. This discrimination was done by separating the photons with maximum penetration depth exceeding the depth of the assumed moving layer (leading to fraction f_l) from photons with a maximum depth upto the depth of the moving layer (leading to fraction f_0). In designing this procedure the key reasoning was that motion in a thin layer at a certain depth can only be detected by light reaching at least that specific depth. While the relative amount of photons that will be Doppler shifted by motion in thin layers at the various depths is regarded as proportional to the relative amount f_l of photons reaching at least these depths, the absolute amount of photons Doppler shifted by a certain thin moving layer would also depend on the assumed thickness of the moving layer, the concentration of particles moving within this layer and the number of times that an eventually detected photon will cross this layer. The latter quantity is assumed to be only a weak function of the optical properties, and to be only weakly depth dependent. And as long the first two quantities are not specified, f_l as a function of depth is a measure for the relative sensitivity to motion at a certain depth.

In order to find the contribution of the motion at a certain depth to the modulation depth of the signal Eq. (6) is used. The coherence area A_{coh}^{01} is calculated by Eq. (3) using the field correlation functions obtained with intensity distribution of the statically scattered photons and dynamically scattered photons by Eq. (4). Considering the optical situation of tissue which is sparsely seeded with dynamic scatterers (mimicking sparsely perfused tissue) we assume a constant intensity distribution for the fraction f_0 of non-Doppler shifted photons and a depth dependent intensity distribution of the fraction f_l of Doppler shifted photons, in calculating A_{coh}^{01} . This fixed intensity distribution of nonshifted light is taken equal to the intensity distribution of all photons being diffusely reflected from the medium. Furthermore we assumed the fraction f_0 of nonshifted photons to be independent of the depth at which motion is assumed. For sparsely dynamic media this is a realistic assumption, since the real relative variation of f_0 , which is close to one in all cases, is much smaller than the relative variation of f_l which ranges from 0 for motion at large depth, to a

maximum value for motion at zero depth.. The consequence of this approach is that Eq. (6) is reduced to

$$\tilde{M} \equiv \frac{M_0}{DC^2} \equiv \frac{\langle i_{ac}^2 \rangle}{\langle i_{dc} \rangle^2} = \beta f_1 A_{coh}^{01} \quad (7)$$

with β depending on the thickness of the thin moving layers, the concentration of moving scattering particles, and the effective detector area.

3.2.3 Overall sensitivity and mean sampling depth

The overall sensitivity is defined as the modulation depth of the instrument for simultaneous motion at all possible depths. This can be calculated from the modulation depth distribution for motion at various depths. If $\tilde{M}(x)$ is the calculated modulation depth generated by motion at a certain depth x , the overall sensitivity is given by $\int_{x_0}^{\infty} \tilde{M}(x) dx$, with x_0 the zero depth. This simple

summation of sensitivities is allowed as long as the condition $f_1^2 \ll f_0 f_1$ holds even when there is motion at all depths at the same time.

The mean sampling depth is defined as the weighted function of the overall depth sensitivity given by,

$$\text{Mean sampling depth} = \frac{\int_{x_0}^{\infty} x \tilde{M}(x) dx}{\int_{x_0}^{\infty} \tilde{M}(x) dx} \quad (8)$$

The mean sampling depth function gives the average depth probed by the photons for various optical properties. The average sensitivity and mean sampling depth were calculated for all optical properties given in table 1. This was done for plots with Eq. (6) where the speckle phenomenon is considered and without speckle phenomenon by putting $A_{coh}^{01} = 1$ in Eq. (7) in calculating the modulation depth.

4. Results and discussion

4.1.1 In vivo measurements

Figure 3 shows measured values of M_0/DC^2 (modulation depth) with different beam diameters for one position on the portwine stain and one position on the surrounding normal skin. It can be observed that for normal skin and port wine

stained skin the modulation depth is decreasing with increasing beam diameter. This change of decreasing modulation depth with beam diameter is larger for port wine stained skin than for normal skin. On the portwine stained region increasing the beam diameter from 0.5mm to 4.0mm results in a decrease in modulation depth by a factor of 4.8 where as for a normal skin this decrease is signal modulation depth for both skin locations converge. only a factor of 3.3. Another observation is that for increasing beam diameter the signal modulation depth for both skin locations converge.

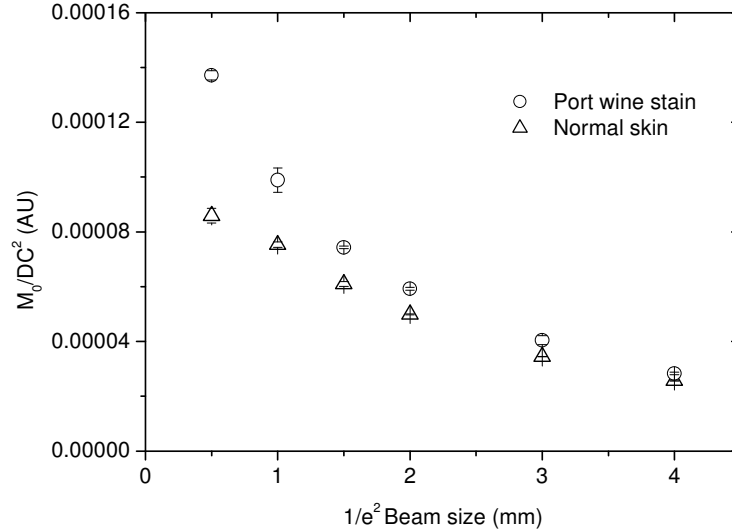


Fig. 3 M_0/DC^2 as a function of beam diameter for normal skin and port wine stain.

4.1.2 Average speckle size measurement

The intensity distributions measured with the CMOS camera for two skin types for a narrow beam and wide beam are plotted in Fig. 4. The raw intensity distribution is Gaussian fitted and normalized. The plot shows a clear difference in intensity width for the narrow beam in two skin types, while for a wide beam there is no significant difference. The speckle areas as calculated on the basis of the measured intensity distributions in the port wine stain and the adjacent normal skin are shown in Fig. 5

For a narrow beam (0.5mm) the speckle size in a normal skin is a factor of 1.9 less compared to that in a port wine stain. The effect of that can be seen in the measured modulation depth M_0/DC^2 where for 0.5 mm there is a factor of 1.6 difference between normal skin and port wine stained skin. For a wide

beam, however, the average speckle size difference is only by a factor of 1.1 which is also reflected in the measured M_0/DC^2 for this beam diameter.

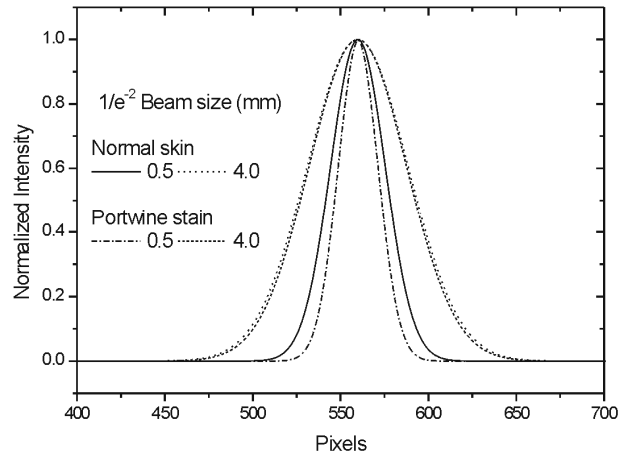


Fig. 4 The back-scattered intensity distribution obtained with CMOS sensor from normal skin and portwine stain. The raw intensity distribution is Gaussian fitted and normalized.

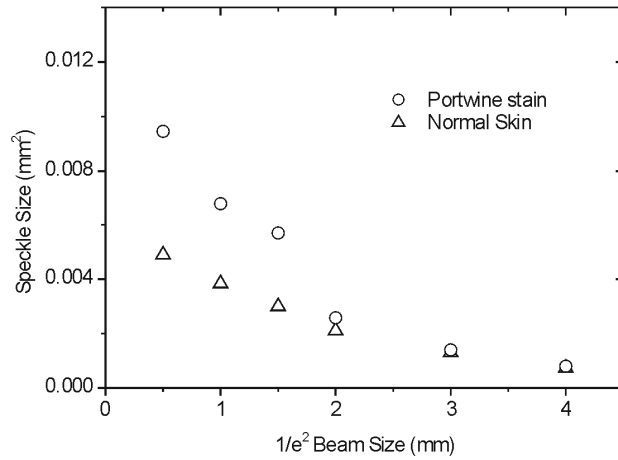


Fig. 5 The average speckle size calculated from the measured intensity distributions, for normal skin and portwine stain.

A port wine stain contains an abnormal density of blood vessels which results in higher absorption and scattering by red blood cells compared to normal skin [14]. This leads to a narrow back scattered intensity distribution and a smaller number of speckles on the detector compared to normal skin. In experiments with a narrow laser beam, the obtained signal amplitudes will be very sensitive to this intensity width variation with tissue type. On the other hand, for a wide beam which itself generates a wide intensity distribution and large number of speckles the speckle number variation with tissue types is suppressed. For beam diameters of 3mm and larger this leads to almost identical speckle areas and signal modulation depths.

4.2.1 Influence of beam diameter and tissue optical properties on modulation depth

Figure 6 shows the modulation depth for different beam diameters calculated with Monte Carlo simulations, for simulated tissues representing normal and port wine stained skin. It can be seen that the modulation depth decreases with beam diameter for the two scattering mediums. However when the reduced scattering level and absorption are increased from $\mu'_s=2.0\text{mm}^{-1}$, $\mu_a=0.02\text{mm}^{-1}$ to $\mu'_s=4.0\text{mm}^{-1}$, $\mu_a=0.04\text{mm}^{-1}$ the decrease in modulation depth with beam diameter increases from a factor of 5 to 8. This supports our observation of bigger influence of speckles in a port wine stain, which has a higher scattering and absorption level compared to normal skin. For a narrow beam this influence is significant whereas for a wide beam this effect is suppressed.

4.2.2 Influence of tissue optical properties on the depth sensitivity

The depth sensitivity, which is defined here as the modulation depth of the photodetector signal generated by particle motion at a certain depth under the surface of the static medium, has been studied computationally. Figure 7 (a) to (d) shows the modulation depth for various scattering levels as a function of the depth at which motion occurs, considering all the combinations of scattering levels, absorption levels and depths given in table 1. It is clear from the graph that the modulation depth drops with motion depth, which is more pronounced for higher scattering levels for a particular absorption level.

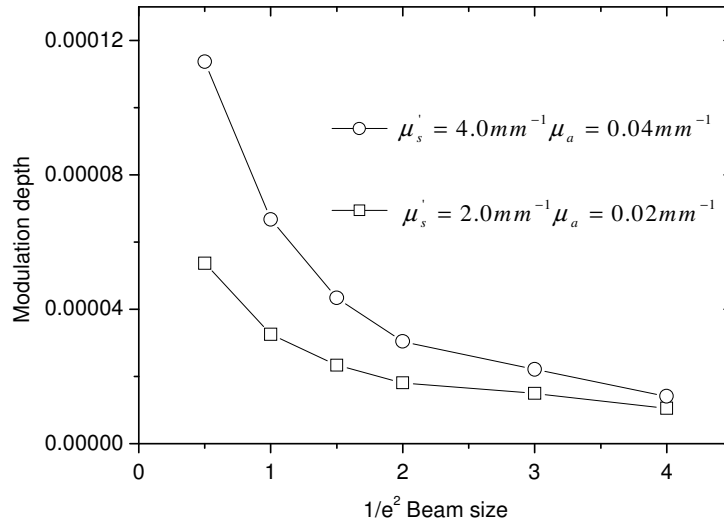


Fig. 6 Modulation depth vs beam diameter for two scattering mediums $\mu'_s=2.0\text{mm}^{-1}$, $\mu_a=0.02\text{mm}^{-1}$ and $\mu'_s=4.0\text{mm}^{-1}$, $\mu_a=0.04\text{mm}^{-1}$.

It can be observed that in Fig. 7 (a) for a scattering level of $\mu'_s=4.0\text{mm}^{-1}$ and $\mu_a=0.01\text{mm}^{-1}$ the sensitivity for motion at largest depth decreases by an order of magnitude (factor 50). The relative suppression of deep photons is reduced for decreasing scattering levels. For a scattering level of $\mu'_s=1.0\text{mm}^{-1}$ this decrease is only by a factor of 8.7. This recovery is stronger for increasing absorption. In Fig. 7 (d) for $\mu_a=0.08\text{mm}^{-1}$ the sensitivity at larger depth for $\mu'_s=4.0\text{mm}^{-1}$ is reduced by 2 orders of magnitude (factor 373) whereas for $\mu'_s=1.0\text{mm}^{-1}$ it is only by a factor of 19. This trend is a combination of speckle effects and the changes in the photon penetration depth with optical properties.

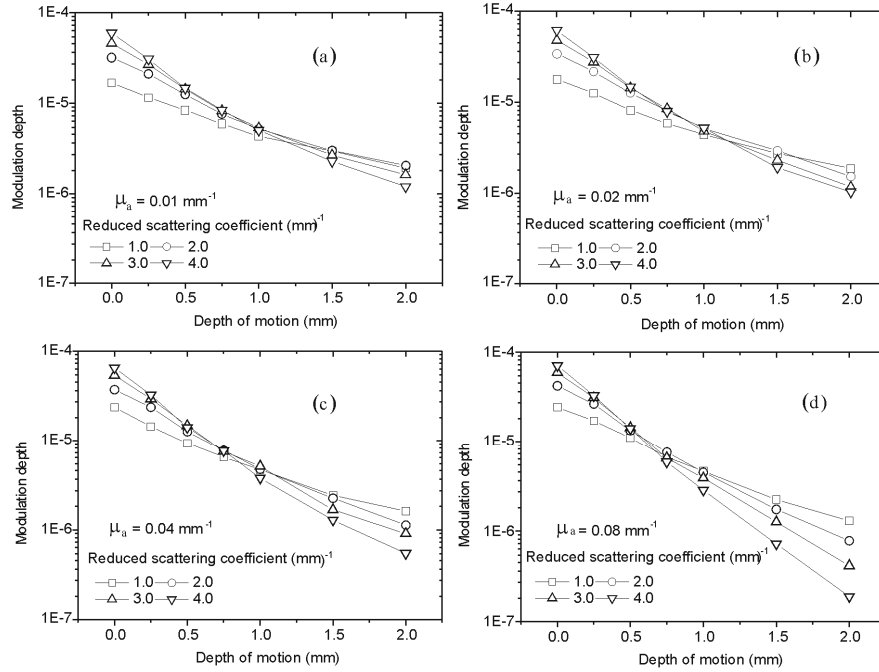


Fig. 7 (a-d) The modulation depth as a function of the assumed depth of motion and scattering and absorption levels.

The modulation depth (normalized to zero depth) vs depth of motion for $\mu_a=0.01\text{mm}^{-1}$ with speckle effects (shaded symbols) and without taking speckle effects (closed symbols, by keeping $A_{coh}^{01} = 1$ in Eq. (7)) into account is shown as Fig. 8. The closed symbols depict the data of Fig. 7 (a) without speckle effects, thus the modulation depth is only a function of the fraction of Doppler shifted photons. Consequently the sensitivity for motion at zero depth is equal for all scattering levels, since all detected photons will cross this level. Figure 8 shows that for a scattering level of $\mu'_s=4.0\text{mm}^{-1}$ ignoring the speckle effects leads to a 10 fold decrease in sensitivity for motion at largest depth while including the speckle phenomenon leads to a 50 fold decrease. For the lowest scattering level ($\mu'_s=1.0\text{mm}^{-1}$) excluding the speckle effect leads to a less pronounced decrease in depth sensitivity (8.7 vs 2.5).

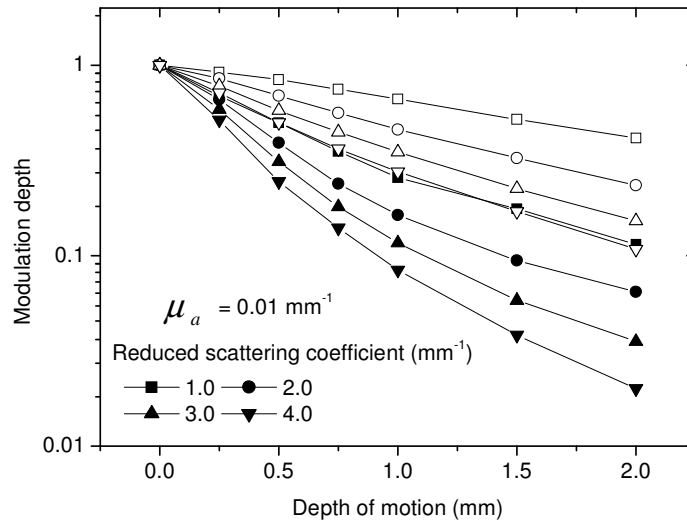


Fig. 8 Modulation depth (normalized to zero depth) vs depth of motion with speckle effects (shaded symbols) and without the speckle effects (closed symbols, $A_{coh}^{01} = 1$) for $\mu_a = 0.01 \text{ mm}^{-1}$.

This trend of speckle effects on the modulation depth with varying scattering and absorption levels can be explained as follows. The deeper the light travels the wider the intensity distribution will be and the smaller the speckles, resulting in an increase in the number of speckles with scattering depth. This increase results in a decreasing modulation depth. In the case of a higher absorption or scattering medium the back-scattered total intensity distribution will be narrow and the number of speckles will be less. So in this case the variation in the intensity width (and number of speckles) with variation in depth of motion of photons will be more sensitive. So the speckle effect will be higher in this case compared to the situation where lower scattering and absorption levels generate a wide distribution of intensity and a large number of speckles.

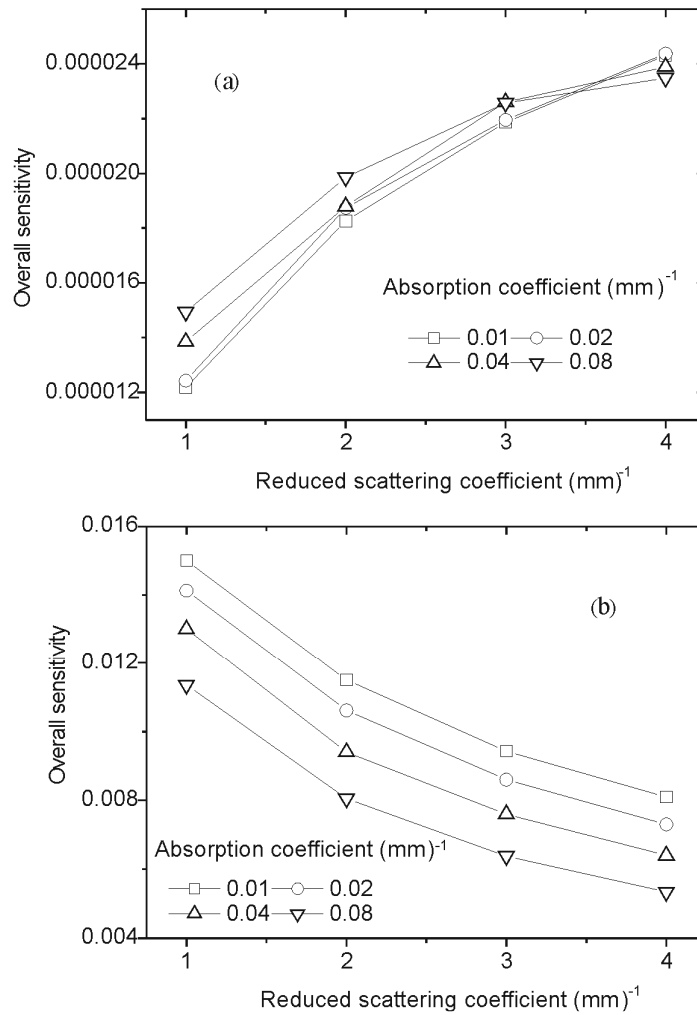


Fig. 9 The overall depth sensitivity for various optical properties (a) with the speckle phenomenon (b) without taking the speckle phenomenon in to consideration ($A_{coh}^{01} = 1$).

4.2.3 Overall sensitivity and sampling depth

The overall sensitivity, which for the sparsely perfused medium is the summation of the sensitivities for motion at all separate depths (see Eq.(8)), is shown in Fig. 9 (a). It shows that the sensitivity increases with increasing scattering and absorption levels. An increase of sensitivity with absorption seems contradictory. However, it can be understood from the speckle

phenomenon. Both an increase in scattering and an increase in absorption result in a more narrow intensity distribution of backscattered light, and therefore lead to larger speckles. At higher scattering levels the absorption has less influence on sensitivity than for lower scattering levels, because photons traveling longer paths will be absorbed before being able to escape the medium, depending on the absorption level. Figure 9 (b) represents the sensitivity when the speckle phenomenon is not taken in to account. Here the overall sensitivity decreases with reduced scattering level and absorption. The penetration depth of the light, and its path length, decreases with increasing scattering and absorption, which reduces the probability that light will interact with moving particles.

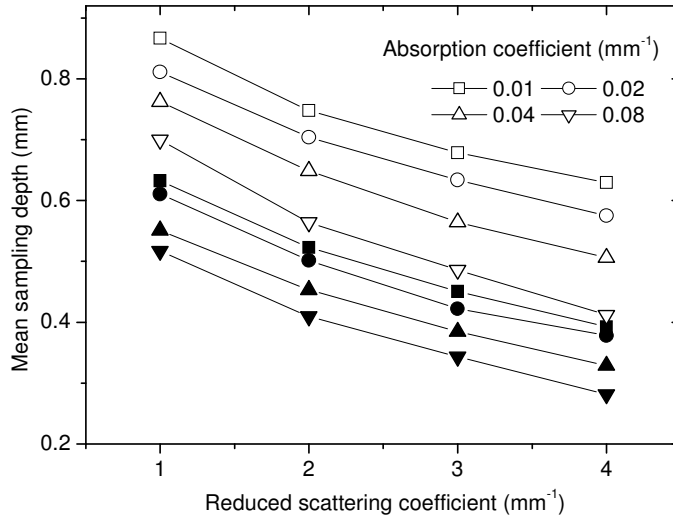


Fig. 10 Mean sampling depth for different scattering levels and absorption levels. Shaded symbols represent the sampling depth with speckle phenomenon taken in to account. Closed symbols where the fractional coherence areas (speckles) kept constant ($A_{coh}^{01} = 1$).

The mean sampling depth (defined by Eq. (8)) is shown in Fig. 10, for the combined effect of speckle and photon penetration depth statistics (shaded symbols), and for the penetration depth statistics alone (closed symbols). The sampling depth decreases with increasing scattering and absorption levels, which is obvious. Accounting for the speckle effect (Fig. 10, shaded symbols) significantly decreases the mean sampling depth. For an absorption coefficient of 0.01mm^{-1} and $\mu_s = 1.0\text{mm}^{-1}$ the mean sampling depth is reduced from 0.87mm

to 0.63mm whereas when the scattering level is increased to $\mu'_s=4.0\text{mm}^{-1}$ the sampling depth drops from 0.41mm to 0.28mm. This trend is also seen with increasing absorption. This shows that the speckle phenomenon is affecting the mean sampling depth, with the relatively strongest effect occurring for the largest scattering coefficient.

4.4 General remarks

In our model we considered a static turbid matrix with moving particles at a sufficiently low concentration to assume heterodyne detection, hence with a fraction of Doppler shifted photons $f_d \ll 1$. For higher perfusion levels associated with a large concentration of moving scatterers, simplifications such as the linear summation of signals generated at various depths cannot be applied anymore, since also interference between Doppler shifted light fractions must be taken into account. Another aspect which has not been taken into account is the number of times that a detected photon will interact with a certain tissue layer. This will be proportional to the number of crossings of the photon with this layer. Since for detection in reflection mode this must always be an even number, the probability of multiple crossings will rapidly decay with the number of crossings.

5. Conclusions and implications

With measurements on two skin locations with largely different absorption and scattering levels, we showed that the signal response (modulation depth of the fluctuating photocurrent) of a laser Doppler perfusion imager using a collimated scanning beam is influenced by tissue optical properties through the speckle phenomenon. We confirmed this with our Monte Carlo based theoretical model. Furthermore we showed that the overall response and the depth sensitivity of the LDPI method are strongly influenced by speckle size changes that occur with changes of tissue optical properties. Due to the speckle phenomenon, the effects of changes in the levels of absorption and scattering on the overall sensitivity can be opposite to those suggested by the photon penetration depth statistics alone, such as illustrated by Fig. 9(a-b). These findings will help in correctly interpreting the results obtained with a laser Doppler perfusion imager, in particular in situations with a large inhomogeneity of the tissue optical properties.

In real tissue the depth sensitivity assessment is difficult because discriminating the fraction of detected photons which traveled to certain depths is not possible. Polarization techniques can be considered but an exact estimation of the depth traveled by photons cannot be calculated. An estimation of only Doppler shifted fraction of photons can be done by using a polarization filter but often will result in filtering out singly scattered Doppler shifted photons which is preserving its polarization, loosing the signal to noise ratio

[15]. The same remarks can be made about low coherence interferometry [16] that enables path length discrimination, but without strong link between the optical path length and the penetration depth of photons. So the depth sensitivity in real tissue was not validated with our model to show the speckle effects. However, the validity of our model as proven experimentally [10] the effects of speckles on the total sensitivity as proven in the port wine stain experiments, and the significance of the predicted effects of speckles on depth sensitivity shown here, are evidence that the depth sensitivity is an effect that will occur in real tissue.

Our observations suggest that at certain applications of the perfusion imager special care has to be taken to arrive at a conclusion regarding a perfusion change. For example in burn depth assessment the optical properties of the damaged skin on top of a perfused tissue will play big role in the instruments sensitivity. Also in interpreting the data obtained with certain drug tests or vasodilatory stimuli were the tissue optical properties can vary rapidly in time and space, care should be taken since both the depth sensitivity and overall response of the instrument can vary independent of perfusion. For instance a large increase of absorption due to strong vasodilation will lead to a relative overestimation of the perfusion estimation. The shown results help in quantifying combined speckle and photon penetration depth related consequences of tissue optical properties for laser Doppler perfusion imaging.

References

1. H. Fujii, K. Nohira, Y. Yamamoto, H. Ikawa, and T. Ohura, "Evaluation of blood flow by laser speckle image sensing: Part 1," *Appl. Opt.* **26**, 5321-5325 (1987).
2. J. D. Briers and S. Webster, "Quasi-real time digital version of single-exposure speckle photography for full-field monitoring of velocity or flow fields," *Opt. Commun.* **116**, 36-42 (1995).
3. T. J. H. Essex and P. O. Byrne, "A laser Doppler scanner for imaging blood flow in skin," *J. Biomed. Eng.* **13**, 189-194 (1991).
4. K. Wårdell, A. Jakobsson, and G. E. Nilsson, "Laser Doppler perfusion imaging by dynamic light scattering," *IEEE Trans. Biomed. Eng.* **40**, 309-316 (1993).
5. D. A. Boas, L. E. Campbell, and A. G. Yodh, "Scattering and Imaging with Diffusing Temporal Field Correlations," *Phys. Rev. Lett.* **75**, 1855-1858 (1995).
6. J. D Briers, "Laser Doppler and time-varying speckle: a conciliation," *J. Opt .Soc. Am. A* **13**, 345-350 (1996).

7. V. Rajan, B. Varghese, T. G. van Leeuwen, and W. Steenbergen, "Speckles in Laser Doppler Perfusion Imaging," *Opt. Lett.* **31**, 468-470 (2006).
8. A. Fullerton, B. Rode, and J. Serup, "Skin irritation typing and grading based on laser Doppler perfusion imaging," *Skin Res. Technol.* **8**, 23-31 (2002).
9. E. J. Droog, W. Steenbergen and F. Sjöberg, "Measurement of depth of burns by laser Doppler perfusion Imaging," *Burns* **27**, 561-568 (2001).
10. V. Rajan, B. Varghese, T.G. van Leeuwen, and W. Steenbergen, "Quantification of spatial intensity correlations and photodetector intensity fluctuations of coherent light reflected from turbid particle suspensions," *Phys. Rev. E* **75**, 060901-4 (2007).
11. R. Bonner and R. Nossal, "Model for laser Doppler measurements of blood flow in tissue," *Appl. Opt.* **20**, 2097-2107 (1981).
12. F. F. M. de Mul, M. H. Koelink, M. L. Kok, P. J. Harmsma, J. Greve, R. Graaff, and J. G. Aarnoudse, "Laser Doppler velocimetry and Monte Carlo simulations on models for blood perfusion in tissue," *Appl. Opt.* **34**, 6595-6611 (1995).
13. R. G. M. Kolkman, E. Hondebrink, W. Steenbergen, T. G. van Leeuwen, F. F. M. de Mul, "Photoacoustic imaging of blood vessels with a double ring sensor featuring a narrow angular aperture," *J. Biomed. Opt.* **9**, 1327-1335 (2004).
14. L. O. Svaasand, L. T. Norvang, E. J. Fiskerstrand, E. K. S. Stopps, M. W. Berns and J. S. Nelson, "Tissue parameters determining the visual appearance of normal skin and port-wine stains," *Lasers in Medical Science*, **10**, 55-65 (1995).
15. M. G. D Karlsson and K. Wårdell, "Polarized laser Doppler perfusion imaging—reduction of movement-induced artifacts," *J. Biomed. Opt.* **10**, 064002 (2005).
16. B. Varghese, V. Rajan, T. G. van Leeuwen and W. Steenbergen, "Path-length-resolved measurements of multiple scattered photons in static and dynamic turbid media using phase-modulated low-coherence interferometry," *J. Biomed. Opt.* **12**, 024020-7 (2007).

Chapter 7

Speckle size and decorrelation time; space-time correlation analysis of coherent light dynamically scattered from turbid media*

We report on the dependence of the decorrelation time on the spatial intensity correlation of speckles. The effects contribute to an explanation of an earlier observation that the average Doppler width of the power spectrum of detector current fluctuations depends on the size of the illuminating laser beam. The space-time correlation of the speckles generated by a particle suspension illuminated by a collimated laser beam is analyzed from serial images taken by a high speed camera. It was found that larger spatial correlation distances, associated with large speckles, exhibit a slower temporal decorrelation.

* This chapter has been submitted for publication in *Optics communications* as: V. Rajan, B. Varghese, T. G. van Leeuwen, and W. Steenbergen, "Speckle size and decorrelation time; space-time correlation analysis of coherent light dynamically scattered from turbid media."

1. Introduction

Temporal correlation analysis has been in use as an essential tool for the characterization of scattering particles [1]. The temporal correlation of speckles can provide information about the motion of biological particles [2-6]. Laser Doppler perfusion imaging (LDPI) is such a technique which is based on the analysis of dynamic speckles to measure tissue perfusion by blood [4, 5]. Earlier, we have shown that the modulation depth of the photocurrent in such an instrument is influenced by the optical properties of the tissue through the number of speckles involved in the detection process [7]. We developed and validated a theoretical model to predict the spatial intensity correlation of speckles generated by mixed static-dynamic turbid media on a far-field detector in a geometry similar to the LDPI instrument, and the consequence for the response of the LDPI method [8, 9]. Aspects of study were the influence of the scattering and absorption properties, and the influence of the beam diameter.

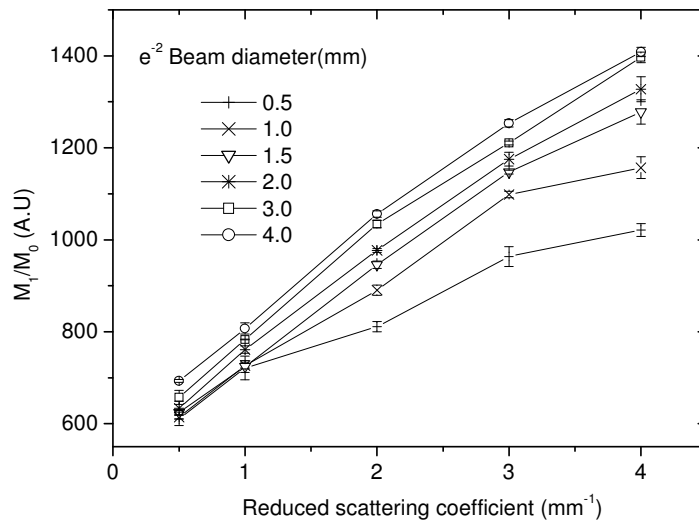


Fig. 1 Average frequency (M_1/M_0) of the power spectrum of intensity fluctuations vs the reduced scattering coefficient for different beam widths [7].

A conspicuous observation was that the Doppler broadening of the power spectra of detector current fluctuations generated by aqueous particle suspensions is influenced by the size of the laser beam (Fig. 1, taken from [7]). When we illuminated a scattering suspension with different beam diameters the

average Doppler shift increased with beam diameter. This was surprising since in the photon picture of light, the average Doppler shift is only a function of the number of scattering events in the medium and the dynamic properties of the moving particles, which do not depend on the beam diameter.

The auto correlation function of photodetector current intensity fluctuations is related to the field correlation functions and the coherence areas (speckle size) of fractions of Doppler shifted photons given by [8],

$$\Gamma_{ii}^{AC}(\Delta r, \tau) = 2\pi A_{\text{det}} R^2 \langle I \rangle^2 \left[\sum_{i=1}^M \sum_{j=1}^M f_i f_j \int_0^{\infty} \gamma_{EE}^i(\Delta r, \tau) \gamma_{EE}^{*j}(\Delta r, \tau) \Delta r d\Delta r \right] \quad (1)$$

where A_{det} is the effective detection area, R is the responsivity of the detector, $\langle I \rangle$ is the average intensity of the light within the detection area, and $\Delta r(\Delta x, \Delta y)$, τ are the spatial and temporal separations respectively. γ_{EE}^{*i} and γ_{EE}^{*j} represent the field correlation coefficient of various photon fractions f_1, \dots, f_M of Doppler shifted photon that can be defined on the basis of various criteria, such as the (optical) path length, Doppler shift, the number of Doppler scattering events and the penetration depth into the medium. Using the correlation coefficient of the fields, the fractional coherence area on the detector formed by a pair of photon groups i and j can be written as

$$A_{coh}^{ij} = 2\pi \int_0^{\infty} \gamma_{EE}^j(\Delta r, \tau) \gamma_{EE}^{*j}(\Delta r, \tau) \Delta r d\Delta r \quad (2)$$

By Eq. (1) and Eq. (2) the autocorrelation function of the photodetector intensity fluctuations and hence the power spectrum is related to the different fractional speckles (coherence areas), which can be defined according to the photon optical path length, on the photodetector.

Photon fractions characterized by a smaller path length, associated with smaller Doppler shifts and therefore longer field correlation times, produce a narrower back scattered intensity distribution and therefore a smaller solid angle of illumination resulting in larger fractional coherence areas on the detector. Whereas photon fractions composed of longer path length photons, associated with larger Doppler shifts and therefore shorter field correlation times, result in a larger solid angle of illumination on the photodetector and smaller fractional coherence areas. Figure 2 illustrates the situation. When a narrow beam is used for illumination which itself generates larger speckles on the photodetector the contribution of smaller speckles or fractional coherence areas A_{coh}^{ij} associated with larger Doppler shifts to the power spectrum is getting suppressed. But for larger beams no such effect is expected because here the broad beam itself results in photons occupying a large solid angle on the detector and in smaller

speckles. Hence for broad beams there is no large distinction in fractional coherence areas between short path length photons and longer path length photons. Therefore, for broad beams large Doppler shift photons are not suppressed in the interference signal. This can all be observed in Fig. 1 where large beams lead to a larger average frequency in the power spectrum, In order to validate the assumption that large speckles feature longer correlation times than small speckles, a space time correlation analysis has been performed.

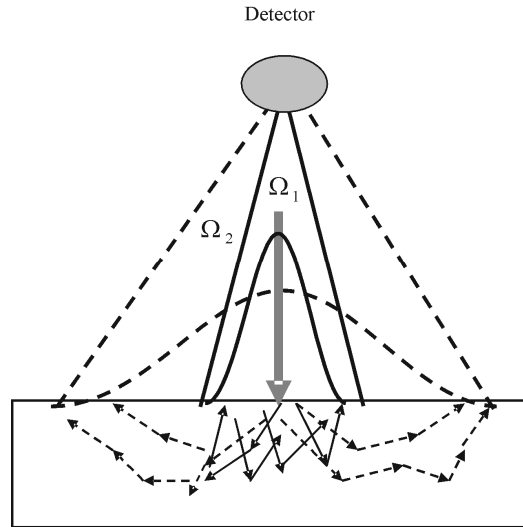


Fig. 2 Back-scattered intensity distributions of photons with shorter and longer paths showing the change in solid angle of illumination which result in speckle size variation.

2. Theoretical background

In this manuscript we analyze the space time behavior of speckles. We used a high speed CMOS camera for acquiring images with sufficient speed to avoid speckle blurring. The temporal correlation of speckles for various laser beam diameters was studied. Also the space-time correlation of speckles was analyzed investigating the temporal decorrelation of small and large speckles, generating correlations for small and large spatial lags, respectively. The larger Doppler shift which hypothetically is associated with smaller speckles should be observable as a shorter decorrelation time for space-time correlation between points at a shorter mutual distance.

In this study we analyze the autocorrelation function of spatiotemporal intensity distributions in dynamic speckle patterns, defined as

$$\Gamma_I(\tau) \equiv \langle I(x, y, t)I(x, y, t + \tau) \rangle \quad (3)$$

where $I(x, y, t)$ is the instantaneous intensity and $\langle \rangle$ represents ensemble average over many realizations or, in the case of ergodic speckle patterns, averaging in space. Here the average value of the intensity $\langle I(x, y, t) \rangle$ was subtracted from all intensity values before calculating the temporal correlation function. Furthermore we study space-time correlations of $I(x, y, t)$, which are defined as,

$$\Gamma_I(\Delta x, \Delta y, \tau) \equiv \langle I(x, y, t)I(x + \Delta x, y + \Delta y, t + \tau) \rangle \quad (4)$$

with x, y spatial coordinates in a 2D image, and $\Delta x, \Delta y$ spatial separations, t represents time and τ is the temporal separation.

If we have N speckle images the space time correlation function of the dynamic speckle pattern can be efficiently obtained by a 3d Fourier transform, squaring the result, and an inverse transform of this three dimensional power spectrum,

$$\Gamma_I(\Delta x, \Delta y, \tau) = \frac{FT^{-1} \left[FT \left[I(x, y, t) - \langle I(x, y, t) \rangle \right]^2 \right]}{N} \quad (5)$$

A similar approach for calculating the spatial correlation from 2D images was reported earlier [10]. We use this to a 3d data set incorporating the time coordinate to the correlation function. For further analysis we consider only spatial separations in x direction, assuming that the speckle distribution is isotropic.

3. Materials and methods

The experimental set up consists of a reflection mode configuration in which we illuminate the medium with a perpendicular laser beam. A linearly polarized He-Ne laser (HRP 350-EC, Thorlabs Inc), of 632.8nm, with output power of 35mW was used as the source. A beam expander made of two positive lenses of focal length 20 and 30mm respectively was used to vary the beam diameter. The beam diameter was measured with a commercial beam profiler. A glass cuvette of 8ml was used as a sample holder. A water suspension of Polystyrene microspheres (Polysciences Inc) of $\varnothing 0.771 \mu\text{m}$ ($g=0.9$) of known concentration was used to make tissue mimicking phantoms. The polystyrene suspension is further diluted to make samples with reduced scattering coefficients (μ'_s) of 2 and 4

mm^{-1} . Ecoline Black dye (Talens) was added to get an absorption coefficient of $\mu_a=0.02\text{mm}^{-1}$.

A fast CMOS camera (FASTCAM-X 1024 PCI, Photron Inc.) without lens was used to record dynamic speckle patterns with a 27000 Hz frame rate. At this acquisition speed the camera can acquire images with 128×128 pixels. Each pixel has a size of $17\times 17\ \mu\text{m}$. The images are digitized with 12 bit precision. The camera was positioned perpendicularly above the scattering medium and the distance between the camera chip and the medium was 22cm. The acquisition speed of 27 kHz is sufficient to track speckle fluctuations caused by Brownian motion of the suspended particles. At 27 kHz speed the exposure time is $37\ \mu\text{s}$. 2000 images were taken which was more than sufficient for getting a complete decorrelation of speckles. The auto correlation function of the intensity distribution of pixels in time was calculated, with an average over 128 pixels. The space time correlation was analyzed using Eq. (5). The space time correlation functions was calculated for x direction by assuming the speckle pattern to be isotropic.

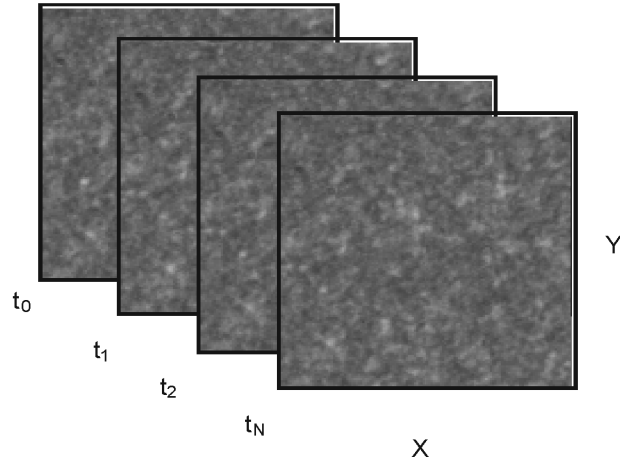


Fig. 3 Consecutive speckle images acquired with a fast CMOS camera at a 27 kHz frame rate, for a beam diameter of 0.5mm.

4. Results and discussion

Figure 3 shows four subsequently acquired images, for a beam diameter of 0.5 mm and a reduced scattering coefficient of 4mm^{-1} . Figure 4 shows the temporal autocorrelation function for a reduced scattering coefficient of 4mm^{-1} for 3 beam diameters. It can be observed that the de-correlation time decreases with the beam diameter. For a 0.5mm beam the $1/e$ decorrelation time is $407\ \mu\text{s}$, whereas when the beam diameter is increased to 4mm the decorrelation time

drops to $296 \mu s$. This observation is a time domain version of our earlier observation that wide beams lead to wider Doppler spectra than narrow beams (see Fig. 1). This trend can also be observed in Fig. 5 where the reduced scattering level of the scattering suspension is 2mm^{-1} .

To check the approximate agreement of the autocorrelation function with the earlier measured power spectra, the autocorrelation function can be further processed to calculate the power spectrum of photocurrent fluctuations by a fast Fourier transformation and correspondingly the moments of the power spectrum and the Doppler width M_1/M_0 can be calculated. This is a simplified approach in which the different weights of small and large speckles, as represented by Eq.(1) and Eq.(2), is not fully taken into account. We performed such an analysis of autocorrelation functions in Fig. 4 ($\mu'_s=4.0 \text{mm}^{-1}$).

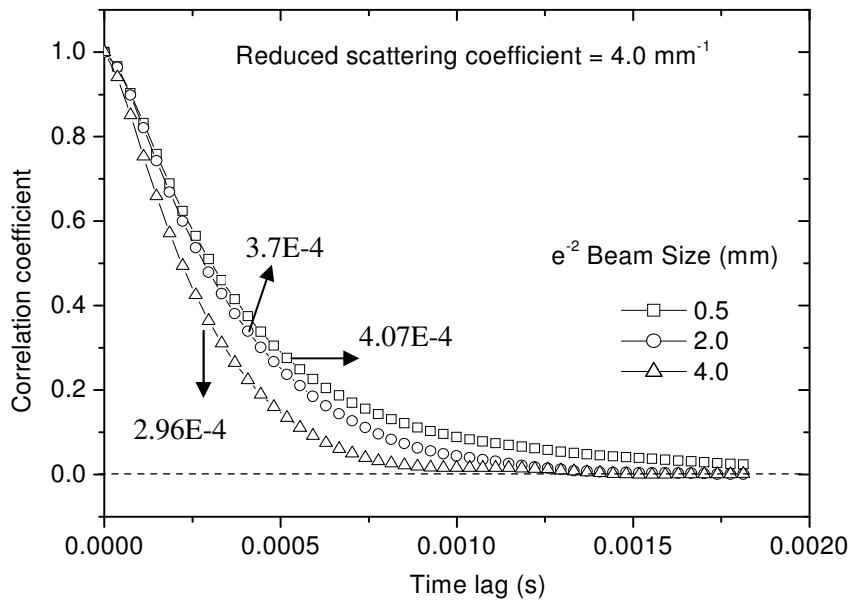


Fig. 4 Temporal correlation functions of speckle images produced by a scattering suspension of $\mu'_s=4.0 \text{mm}^{-1}$, for three beam diameters. The $1/e$ decorrelation time (in seconds) of each correlation plot is indicated with arrow heads.

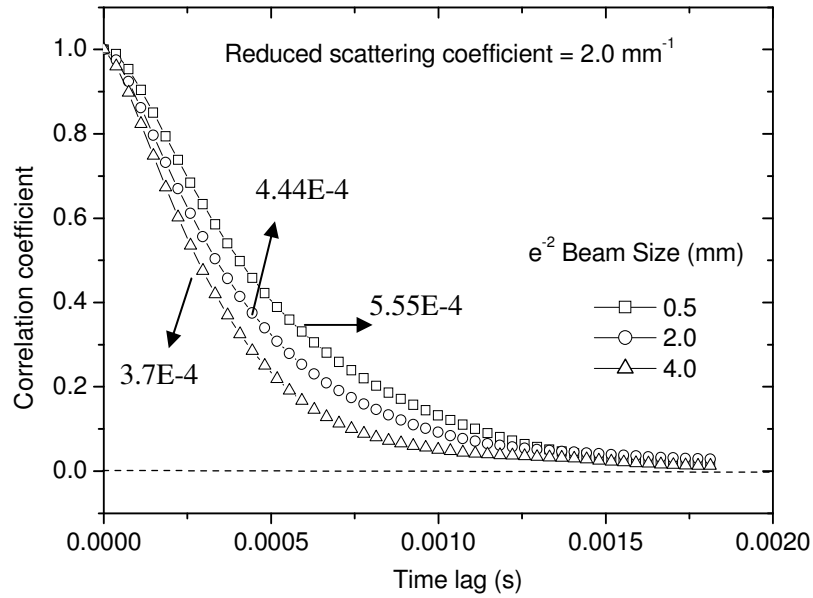


Fig. 5 Temporal correlation functions of speckle images produced by a scattering suspension of $\mu'_s=2.0\text{mm}^{-1}$ for three beam diameters. The $1/e$ decorrelation time (in seconds) of each correlation plot is indicated with arrow heads.

For a beam diameter of 0.5mm the average Doppler width of the power spectrum was calculated to be 1368 Hz, whereas for a beam of diameter 4.0mm the calculated average Doppler shift increased to 1580Hz. This is in agreement with our earlier observation in Fig. 1 for $\mu'_s=4.0\text{mm}^{-1}$ where an increase in beam diameter from 0.5mm to 4.0mm resulted in an increase of average Doppler shift from 1021Hz to 1408Hz. Similar Fourier analysis of the correlation plots shown in Fig. 5 ($\mu'_s=2.0\text{mm}^{-1}$) showed an increase in average Doppler shift from 1159Hz to 1295 Hz for narrow and broad beam respectively which is comparable to the trend observed in Fig. 1 for $\mu'_s=2.0\text{mm}^{-1}$ where the average Doppler shift increased from 963Hz to 1253Hz. The larger average Doppler frequency calculated from the speckle autocorrelation function compared to the average Doppler shift measured with a large photodetector (Fig. 1) can be explained from the fact that in the calculation of the power spectrum of a large detector from the autocorrelation function of the dynamic speckles illuminating, the frequency content of the smallest speckles is relatively overrepresented.

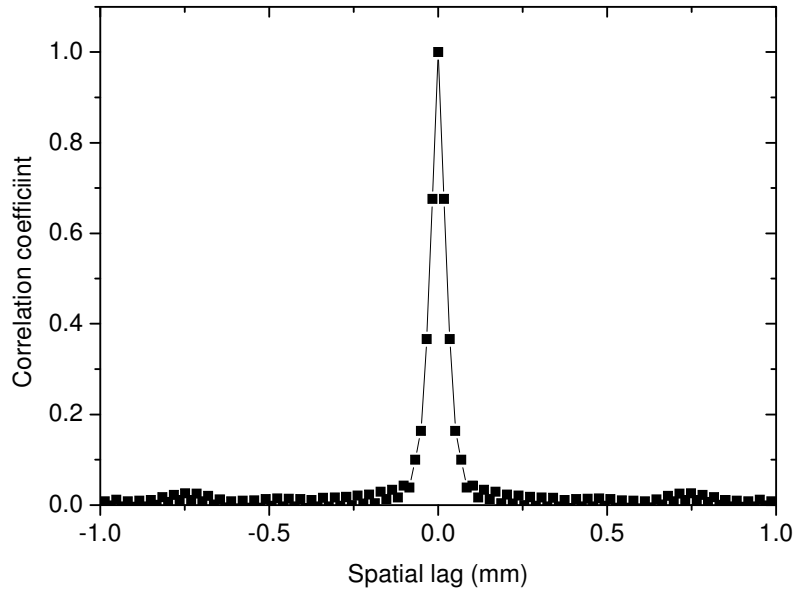


Fig. 6 Spatial correlation functions for a single frame of speckles (time lag $\tau=0$), projection from the space-time correlation of speckles from a scattering suspension of $\mu'_s=4.0\text{mm}^{-1}$ with a narrow beam (0.5mm).

Figure 6 shows the spatial correlation functions of a single frame of speckles, produced by a suspension of $\mu'_s=4.0\text{mm}^{-1}$ with a beam diameter of 0.5mm. This is the space-time correlation function for $\tau=0$. The temporal correlation functions of first three spatial lags are shown as Fig. 7, and a zoomed version of the first half of the peaks can be found in the inset. Each temporal correlation function is normalized to its maximum value, to allow for visual comparison of the decorrelation times. Here the full width half maximum (FWHM) for the correlation function is calculated as a measure of the decorrelation time. Since the correlation distribution is not symmetric the $1/e$ value of the decorrelation time cannot be considered as a measure of the decorrelation time. Figure 7 shows that increasing spatial lag results in an increasing decorrelation time. For spatial lag 0 ($\Delta x=0$) the FWHM of the temporal correlation function is 0.59 ms whereas for $\Delta x=51\mu\text{m}$ the FWHM increases to 1.04 ms. This shows that structures in the speckle patterns that generate large spatial correlations result in a longer temporal correlation. Hence, these structures, which are the large speckles, exist longer. From the Fourier

analysis of the temporal autocorrelation functions in Fig. 4 & 5 it was clear that a longer decorrelation time will result in a smaller average Doppler shift. So the above observation of slower decorrelation of speckle with large spatial correlations indicates a decrease in average Doppler shift of the power spectrum.

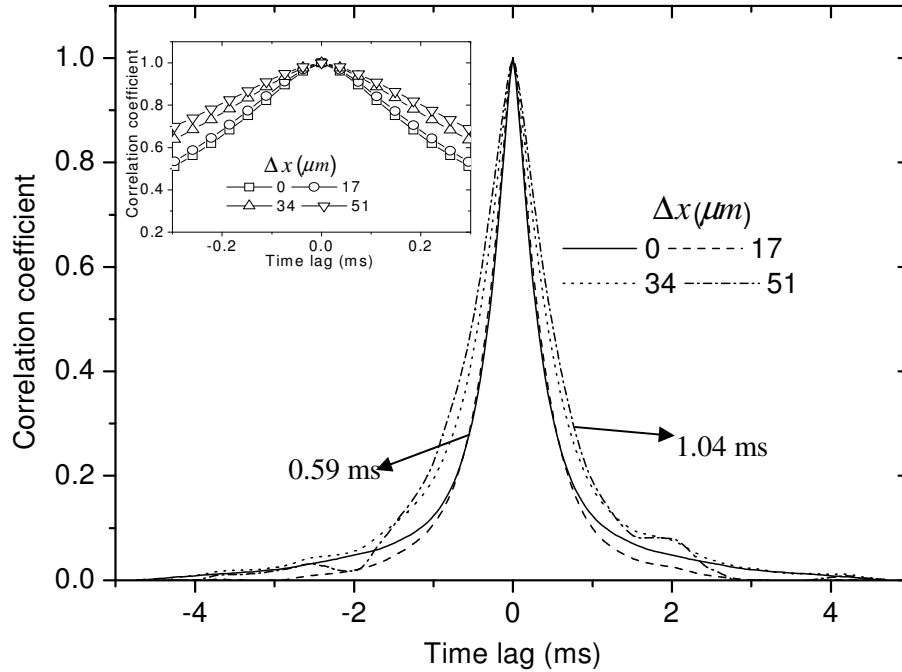


Fig. 7 Temporal correlation functions for different spatial lags (Δx), projections of space-time correlation of speckles from a scattering suspension of $\mu_s=4.0\text{mm}^{-1}$ with a narrow beam (0.5mm). A zoomed version of the first half of the peaks can be found in the inset.

For $\Delta x \gg 51\mu\text{m}$ in Fig. 7 the noise was dominant and we observed an almost complete decorrelation of speckles, hence the decorrelation time could not be estimated for larger spatial separations. A space time correlation analysis of much smaller speckles produced by broader beams (2.0 and 4.0mm), similar to the one for 0.5mm beam as described above, will add to the results explained based on Fig. 7 about the dependence of the decorrelation time on the spatial intensity correlation. But with our data it was not possible to compare the decorrelation time (for various Δx) of larger speckles produced by broad beams (2.0 and 4.0mm) with those of the narrowest beam since we observed a very fast temporal decorrelation of speckles produced by broad beams within small

spatial separations ($\Delta x < 34 \mu\text{m}$). Probably in this case each pixel already contained more than one speckle.

5. Conclusions

In conclusion we have shown that the average speckle size or spatial correlation influences the temporal behavior of speckles. We observed that larger spatial correlation distances, associated with large speckles, exhibit a slower temporal decorrelation. This confirms our hypothesis regarding this behavior of speckles. When a narrow beam is used for illumination the contribution of photons which traveled a longer pathlength, associated with larger Doppler shifts, is present in smaller speckles which are therefore relatively more suppressed in the power spectrum. This resulted in a larger average Doppler width of the spectra for a broad beam compared to a narrow beam. Our observations suggest that in real tissue, when tissue optical properties influence the spatial correlation, the Doppler content of the power spectra can also be altered due to the speckle effect, affecting the perfusion signal. The influence of the spatiotemporal behavior of the speckles has to be further investigated to quantify the results obtained with the space-time correlation techniques and to relate them to power spectra measured with a single photodetector.

Acknowledgements

This research was sponsored by the Dutch Technology Foundation STW under grant TTF.5840. Instrumental support was provided by Perimed AB. We acknowledge Mathijs Draijer and Erwin Hondebrink for assistance with the high speed camera set up, and Aliaksandr Bratchenia for the assistance with Matlab software.

References

1. B. J. Berne and R. Pecora, *Dynamic Light Scattering with applications to Chemistry, Biology and Physics* (John Wiley & Sons, Inc., New York, 1976).
2. H. Fujii, K. Nohira, Y. Yamamoto, H. Ikawa, and T. Ohura, "Evaluation of blood flow by laser speckle image sensing: Part 1," *Appl. Opt.* **26**, 5321 (1987).
3. J.D. Briers and S. Webster, "Quasi-real time digital version of single-exposure speckle photography for full-field monitoring of velocity or flow fields," *Opt. Commun.* **116**, 36 (1995).

4. T. J. H. Essex and P. O. Byrne, "A laser Doppler scanner for imaging blood flow in skin," *J. Biomed. Eng.* **13**, 189 (1991).
5. K. Wårdell, A. Jakobsson, and G. E. Nilsson, "Laser Doppler perfusion imaging by dynamic light scattering," *IEEE Trans. Biomed. Eng.* **40**, 309 (1993).
6. D. A. Boas, L. E. Campbell, and A. G. Yodh, "Scattering and Imaging with Diffusing Temporal Field Correlations," *Phys. Rev. Lett.* **75**, 1855 (1995).
7. V. Rajan, B. Varghese, T. G. van Leeuwen, and W. Steenbergen, "Speckles in Laser Doppler Perfusion Imaging," *Opt. Lett.* **31**, 468 (2006).
8. A. Serov, W. Steenbergen, and F. F. M. de Mul, "Prediction of the photodetector signal generated by Doppler-induced speckle fluctuations: theory and some validations," *J. Opt. Soc. Am. A* **18**, 622-630 (2001).
9. V. Rajan, B. Varghese, T. G. van Leeuwen, and W. Steenbergen, "Quantification of spatial intensity correlations and photodetector intensity fluctuations of coherent light reflected from turbid particle suspensions," *Phys. Rev. E* **75**, 060901-4 (2007).
10. Y. Piederrière, J. Cariou, Y. Guern, B. Le Jeune, G. Le Brun, J. Lotrian, "Backscattered speckle size as a function of polarization: influence of particle-size and- concentration," *Opt. Express* **13**, 5030-5039 (2005).

Chapter 8

The relationship between local scalp skin temperature and cutaneous perfusion during scalp cooling*

Cooling the scalp during administration of chemotherapy can prevent hair loss. It reduces both skin blood flow and hair follicle temperature, thus affecting drug supply and drug effect in the hair follicle. The extent to which these mechanisms contribute to the hair preservative effect of scalp cooling remains unknown. The purpose of this study was to establish a relationship between local scalp skin temperature and cutaneous blood flow during scalp cooling. We measured skin temperature and cutaneous perfusion during a cooling and re-warming experiment. Experiments on a single subject showed that the measurements were reproducible and that the response was identical for the two positions that were measured. Inter-subject variability was investigated on nine subjects. We found that for the first 10°C of cooling, perfusion of the scalp skin decreases to below 40%. Perfusion can be further reduced to below 30% by a few degrees more cooling, but a plateau is reached after that. We found that a generally accepted relation in thermal physiology between temperature and perfusion (i.e. Q_{10} relation) does not describe the data well, but we found an alternative relation that describes the average behavior significantly better.

* This chapter has been published as: F. E. M. Janssen[#], V. Rajan[#], W. Steenbergen, G. M. J. van Leeuwen, and A. A. van Steenhoven, “The relationship between local scalp skin temperature and cutaneous perfusion during scalp cooling,” *Physiol. Meas.* **28**, 829-839 (2007). # equally contributed authorship

1. Introduction

Chemotherapy as a cancer treatment often leads to partial or complete hair loss, one of the most feared side effects of cancer therapy [1]. Cooling the scalp during chemotherapy treatment can reduce or even prevent this hair loss [2]. Two possible mechanisms explain how scalp cooling might contribute to hair preservation [3]. First, a reduced blood flow to the cutaneous tissue during cooling could lead to a reduced drug supply to the hair follicle. Second, a reduction in cutaneous cell metabolism as a response to the hypothermia could simply make hair follicles less susceptible to drug damage. Currently, the dependence of both these mechanisms on temperature is unknown and hence the cooling protocol may not be optimal. Also there is insufficient data available on the relationship between the local skin temperature and local cutaneous blood perfusion, and existing data for the scalp skin during scalp cooling [4] is brief and lacks accuracy. Bülow *et al* [4] used a Xenon washout technique on 10 subjects to identify pre-cooling, cooling and post-cooling perfusion. During cooling, perfusion reduced to about 20% of the pre-cooling level. Unfortunately, standard deviations for pre-cooling and cooling perfusion were very high, leading to a high uncertainty in this minimum perfusion value. Also, no information is given about the relationship between minimum perfusion and scalp skin temperature. Such information is essential for quantitative modeling of human heat transfer and for a better understanding of human thermoregulatory processes.

The initial response of skin blood flow to skin cooling is cutaneous vasoconstriction. According to Thompson *et al* [5], two different mechanisms are responsible for this vasoconstriction. The first mechanism is a response to whole-body skin cooling and is called reflex-mediated response. The second mechanism is a response to local skin cooling and is called locally mediated response. These two mechanisms of skin blood flow control are not mutually exclusive; often these mechanisms operate together during exposure to cold to maximize vasoconstriction. The exact mechanisms of the vasoconstrictor system are not yet well defined, but it is certain that the temperature of the blood vessels themselves plays an important role [6].

During scalp cooling, only the outermost part of the head experiences changes in temperature [7]. The size of the affected region is approximately 2cm, and is too small to have any significant effect on core temperature. Therefore, we investigated whether a local relationship between temperature and perfusion exists during scalp cooling.

The cold provocation induced changes in blood perfusion have been a subject of research for the diagnosis of Raynaud's phenomenon [8, 9, 10]. These studies were mainly focused on the microcirculatory perfusion at

different heat and cold provocations without looking at a periodic change of perfusion with temperature. Maniewski *et al* [11] and Friedman *et al* [12] followed perfusion by gradually decreasing temperature. They analyzed the perfusion level changes with temperature between healthy subjects and patients with Reynaud's phenomenon but not attempted to relate the perfusion with temperature. Since these studies were performed based on protocols which were relevant for the diagnosis for Reynaud's phenomenon and the measurements were performed by either cooling of the whole body or a hand the results cannot be interpreted for scalp cooling protocol for chemotherapy treatment.

The purpose of this study was to find the dependence of cutaneous blood flow on local scalp skin temperature during scalp cooling, in a setting that is relevant for clinical practice. For this, the scalp was cooled using a commercially available scalp cooling device, and temperature and perfusion were measured using thermocouples and laser Doppler perfusion probes, respectively. It was hypothesized that (i) a relationship exists between local skin temperature and cutaneous blood flow during scalp cooling and (ii) that this relationship is independent of the subject regarded.

2. Materials and methods

2.1 Subjects

Experiments were performed on nine subjects (7 male, 2 female; age 24-43) after informed consent. Subjects were not screened for any cardiovascular or neurological disorder. For each subject a single experiment was performed using the mid-front of the hairline (referred to as position 1). On one subject (male, age 26) inter-position and inter-experiment variability were investigated using both the mid-front of the hairline and a top-right position in the hairline (referred to as position 2). Figure 1 illustrates the location of position 1 and position 2 on the head. For each probe position, three experiments were performed with an interval between experiments of 24 hours.

2.2 Blood Flow Measurements

Cutaneous blood flow was measured with the Laser Doppler Flowmetry (LDF) technique. This is a noninvasive technique to monitor the blood microcirculatory flux, with a typical measurement depth of 1 mm for cutaneous measurements. The actual measurement depth varies with tissue optical properties, and the averaged depth for typical tissue optical properties was found based in vitro measurements and Monte Carlo simulation of photon transport in tissue [13, 14]. LDF is based on the induced Doppler shift of light scattered from moving blood cells. The relative amount of Doppler shifted photons, and their mean Doppler shift, are directly related to the concentration

and root mean square velocity of red blood cells in the exposed area of tissue [15].

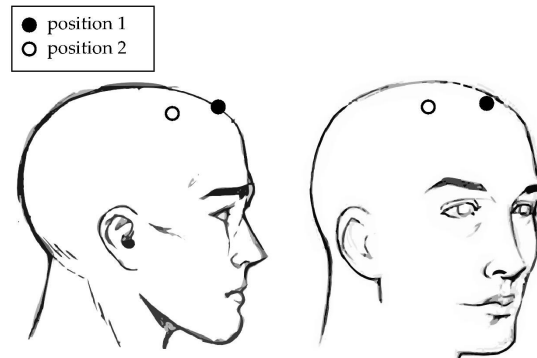


Fig. 1 A cartoon of the positions of the probe on scalp skin, as used in measurements. Position 1 represents the mid-front of the hairline and position 2 a top-right spot on the hairline.

The measurements were performed using a commercial laser Doppler perfusion monitor (PF5000, Perimed AB, Sweden) with two channels. The instrument has a semiconductor laser diode of 780nm and a Doppler bandwidth of 20Hz-13kHz. Two probes were used in the experiment: (i) A small straight probe (Probe 407, Perimed AB) was used to measure the perfusion of the cooled location and (ii) a standard probe (Probe 408, Perimed AB) measured perfusion at the reference site. Each probe has illumination and detection fibers at 250 micrometers mutual distance, with a core diameter of 125 μm and a numerical aperture of 0.37. The laser Doppler instrument was allowed to warm up for 20 minutes before the start of the base measurements. The device in combination with the two probes was calibrated using a motility standard (PF 1000, Perimed AB). Both probes were attached to the measurement site with a probe holder and sticker. Perfusion measurements were taken at a sampling rate of 32Hz. The time constant of the output signals was set at 0.2 s, which means low-pass filtering with a 3 dB cutoff frequency of 1.25Hz.

2.3 Temperature Measurements

Four calibrated J type thermocouples were used in the experiments. One thermocouple was fixed with medical quality glue next to the perfusion probe on the scalp; another thermocouple was fixed to the outside of the cold cap. One thermocouple measured the skin temperature at the reference site. The last thermocouple was used to measure ambient temperature. Thermocouple measurements were taken at a sampling rate of 0.2Hz.

Skin temperature measurements were performed in a high temperature gradient setting. From previous theoretical work, we know that this gradient between the scalp skin and the cold cap can be as high as $1000\text{ }^{\circ}\text{C m}^{-1}$ [7]. To ensure that the registered temperature is a good measure for the skin temperature, each thermocouple end was modified with a specially developed aluminium disc of radius 2mm and thickness 0.5mm. This made the attachment to the scalp skin easier and, in combination with the medical quality glue, ensured that the thermal resistance between the thermocouple and the scalp skin was lower than the thermal resistance between the thermocouple and the cold cap.

2.4 Experimental protocol

All measurements were conducted with the subject sitting upright in an environment with an ambient temperature of approximately 20°C . The subject was allowed to rest for 30 minutes before measurements to obtain a stable perfusion level. The scalp of the subject was cooled using a commercial scalp cooling system (Paxman coolers Ltd UK). It consists of a reservoir of coolant connected to a cap made from silicon tubing. At the beginning of the experiments, this reservoir was at room temperature. During two minutes before the start of a cooling experiment, temperature and perfusion of the scalp skin were measured to establish basal temperature and perfusion. These basal values were used to define the temperature difference and relative perfusion, such that measurements could be compared to each other.

The cooling experiment consisted of three stages. In the first stage the pump of the scalp cooling system is switched on without cooling the reservoir. This induced both pressure changes and small temperature changes in the cap. This stage lasted 5 minutes, and allowed us to discriminate between changes due to the difference in pressure exerted by the cap, and changes due to temperature. In the second stage, the cooling of the device was switched on for 90 minutes. This resulted in a rate of scalp cooling that was slower than in clinical use (where the cap and reservoir are pre-cooled). In the final phase, the cooler of the system was switched off to enable the scalp to re-warm. Once again, the pump of the system remained pumping to avoid pressure changes on the skin. With this phase, it was possible to see if there are hysteresis effects in the relation between temperature and perfusion. The re-warming phase lasted 60 minutes. Skin temperature and perfusion were continuously monitored during the experiment.

2.5 Biological Zero measurements

There is a residual signal in laser Doppler perfusion measurements from the tissue called Biological Zero (BZ), which is present even when there is no flow [16]. It is suggested that this BZ signal should be subtracted from the normal perfusion value to get a better understanding of the perfusion, especially in the

case of very low perfusion measurements [17, 18, 19]. In addition, this BZ signal depends on the temperature of the tissue regarded [19]. A previous study showed that during scalp cooling, perfusion drops to a stable low value that was higher than zero [4]. Therefore we expect that the BZ problem is relevant in our experiment. In general the BZ signal can be measured in vivo by an arterial occlusion with an inflated cuff. Unfortunately it is not possible to measure the BZ on the scalp because an occlusion is not possible. There is no other method for determining BZ on locations which are not accessible for occlusion. Hence the best possible way to find the influence of BZ on the minimum perfusion on scalp is to find BZ on a location of the body which can be occluded and use that data as the BZ of scalp skin.

We measured the BZ at a position on the fore-hand or palm which showed an LDF rest flux level comparable to that in the scalp. It was reported earlier that there is a difference in BZ signal on different body locations with different rest flux [20], but we expect that with the same rest flux level there would not be a significant difference in BZ between the scalp skin and the fore hand. It is also important to investigate the influence of temperature on the BZ signal. We measured the BZ at normal body temperature and at the lowest temperature we reached during scalp cooling (15°C) on 9 healthy subjects (partly the same subjects participated for scalp perfusion measurements). The LDF probe was the same used in scalp perfusion measurements. The temperature was measured using a standard thermocouple. Normal perfusion (rest flux) and biological zero are measured at normal body temperature and at 15°C. In order to cool down the skin at the measured spot to 15°C a water bath with ice was used in which the hand was immersed.

2.6 Data Analysis

A moving average filter with a period of 5 seconds was used to filter out artifacts in the perfusion signal. This time period was chosen to match the sampling period of the thermocouple measurements. Using the base temperature (T_0) and base perfusion (W_0) determined in the first five minutes of each experiment, temperature difference (ΔT) and relative perfusion (φ) were determined:

$$\Delta T = T_0 - T \quad (1a)$$

$$\varphi = W / W_0 \quad (1b)$$

The reductions in metabolism and subsequent reductions in perfusion due to falling temperatures are modelled according to a well known Q_{10} relation of thermal physiology. Due to a reduction in tissue temperature there is a corresponding reduction in cell metabolism [21], and as a consequence the demand for nutrients (e.g. oxygen) will diminish. Subsequently it is no longer

necessary to sustain current level of blood flow and the body reacts by lowering tissue perfusion [22]. The reduction in metabolism and subsequent reduction in blood flow is by a factor Q_{10} for every 10°C decrease in temperature. Relative perfusion may thus be written as:

$$\varphi = Q_{10}^{(-\Delta T / 10^{\circ}\text{C})} \quad (2)$$

With factor $Q_{10} = 2$ [22] up to 3 [21]. It has alternatively been found that perfusion during scalp cooling decreases to a minimum value of about 20% [4]. Therefore, we investigated the goodness of fit of a minimum perfusion equation:

$$\varphi = \varphi_{\min} + (1 - \varphi_{\min}) \exp(-\Delta T / \Theta) \quad (3)$$

where φ_{\min} is the minimum relative perfusion value, and Θ is a constant that determines the rate at which perfusion drops. Fits to the Q_{10} equation (2) and minimum perfusion equation (3) were established using a nonlinear least-squares fitting routine (nlinfit.m) generally available in MATLAB (version 6.5.0, Release 13, The Mathworks, Inc.).

2. Results

3.1 Relation between scalp skin temperature and perfusion

A typical time trace for temperature and perfusion is shown in Fig. 2. Skin temperature drops from 34°C to 16°C in 90 minutes (cooling rate: $0.2^{\circ}\text{C min}^{-1}$). Cutaneous blood flow drops from 30 PU (perfusion units) to 8 PU. After the cooling stage, temperature returns to 30°C and perfusion to 20 PU. There are no significant reductions in either temperature or perfusion at the reference site.

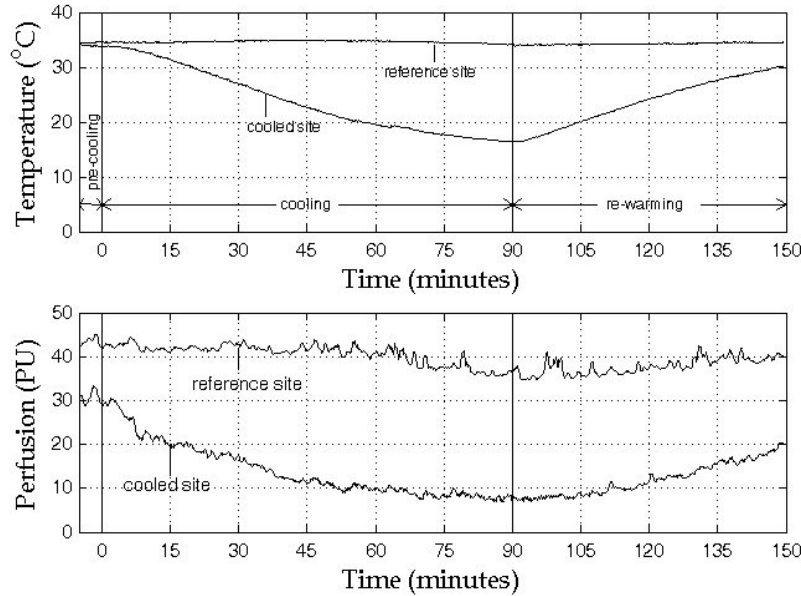


Fig. 2 Typical time trace for temperature (top) and perfusion (bottom) of both the reference site and the cooling site.

Figure 3 shows the average relative perfusion (ϕ) at the two positions (three experiments each) versus the temperature difference (ΔT). Inter-experiment variability (three experiments) is acceptable with an average standard deviation over the complete cooling range of 0.08 (–). Scalp temperature and perfusion were reduced more at position 2 ($\Delta T_{max} = 22^\circ\text{C}$; $\phi_{min} = 0.21$) than at position 1 ($\Delta T_{max} = 12^\circ\text{C}$; $\phi_{min} = 0.29$). A two tailed t-test was performed to check whether significant differences exist between the two positions. Except for two cooling temperatures ($\Delta T = 1.0^\circ\text{C}$ and $\Delta T = 1.5^\circ\text{C}$) relative perfusion did not differ significantly between the two positions ($p < 0.05$). The results of these experiments indicate that both inter-position and inter-experiment variability are low. The achieved skin temperature drop for the nine subjects ranged from 7°C to 22°C (Fig. 4). Lowest relative perfusion for the nine subjects ranged from 21% to 44%. According to a two tailed t-test, there are no hysteresis effects that come into play during the transition between the cooling and the re-warming stage ($p < 0.05$).

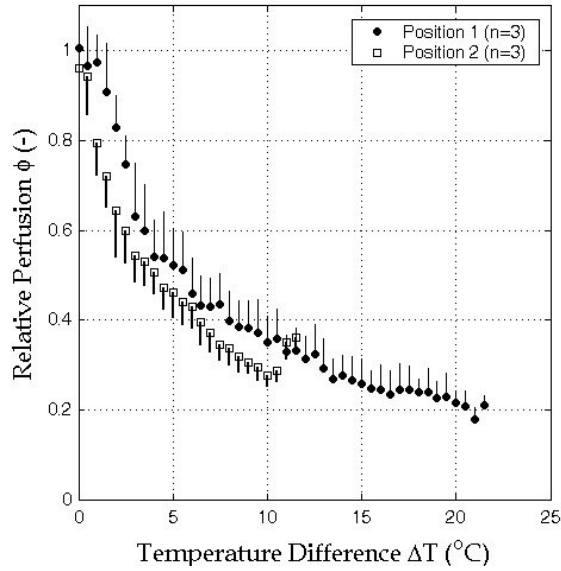


Fig. 3 Average temperature difference and relative perfusion of position 1 (front of the head) and position 2 (top-right of the head) for one subject. Values represent averaged values of three combined experiments. Error bars denote standard deviation. * Position 1 significantly different from position 2 ($P < 0.05$).

We used the data of each individual response to fit the parameters of equations 2–3 using a nonlinear fitting routine. This resulted in $Q_{10} = 3.5 \pm 1.5$ (mean \pm standard deviation) for equation 2 and $\phi_{\min} = 0.27 \pm 0.08$ for equation 3. The range in parameters was $2.1 < Q_{10} < 5.9$ for equation 2 and $0.16 < \phi_{\min} < 0.41$. An averaged response of the nine individuals has been calculated (Fig. 5) to establish a relationship between the temperature difference and relative perfusion. In this calculation, both the cooling and the re-warming stages were used. Relative perfusion starts at a value of 89% at $\Delta T = 0.25^\circ\text{C}$ and with further cooling ($\Delta T = 21^\circ\text{C}$) a minimum perfusion value of 29% is reached. Accumulated data of all nine subjects were used to fit the parameters of equations 2–3 using a nonlinear fitting routine. This resulted in $Q_{10} = 2.5$ ($R^2 = 0.68$) with a 95% confidence interval (CI_{95}) of 2.33–2.79 for equation 2 and $\phi_{\min} = 0.29$ ($0.28 < CI_{95} < 0.30$) and $\Theta = 4^\circ\text{C}$ ($3.85 < CI_{95} < 4.38$) ($R^2 = 0.8$) for equation 3 (Fig. 5). The fitted Q_{10} value is in the range of values cited in literature.

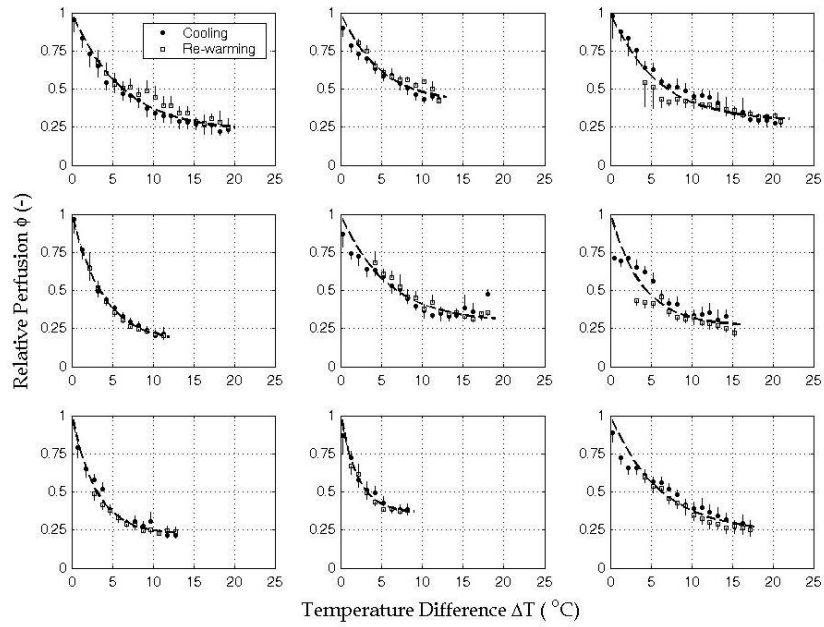


Fig. 4 Average temperature difference and relative perfusion of each individual subject for both the cooling (●) and re-warming (■) stage. Error bars represent standard deviation. The dashed line represents the best fit for the minimum perfusion function.

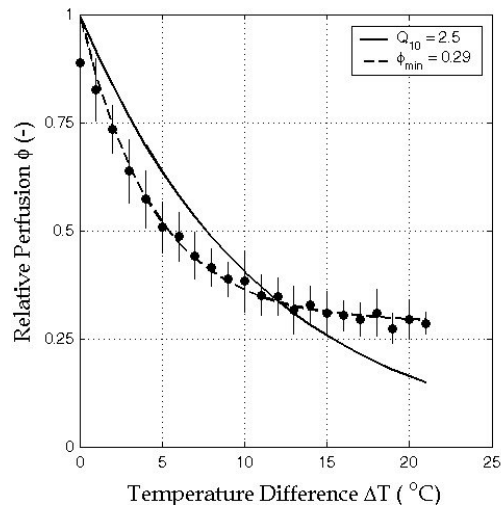


Fig. 5 Average temperature difference and relative perfusion and best fits for Q_{10} and minimum perfusion (θ_{\min}). Error bars represent standard error.

A good fit is impossible due to the observed behavior in our experiments that perfusion levels off at a value of about 25% instead of continuing towards zero. Hence the fit function underestimates relative perfusion for strong cooling ($\Delta T > 12^\circ\text{C}$) while overestimating perfusion for low and mild cooling. The minimum perfusion function gives a much better fit to the data over the entire cooling range. The value of rate constant $\Theta = 4^\circ\text{C}$, signifies that 95% of the drop in perfusion is reached when the temperature difference equals $\Delta T = 12^\circ\text{C}$.

3.2 Influence of Biological Zero (BZ)

The rest flux at body temperature for 9 subjects in perfusion units (PU) –with the range given in brackets– was 29.1PU (24.7–34.4) and the mean BZ was 5.29PU (2.65–7.42). At 15°C the mean perfusion was 10.5PU (7.06–14.79) and the mean BZ was 4.50PU (2.58–5.39). In comparing the PU obtained from different persons one should be aware of the fact that perfusion can vary intra- and interindividually. The variation of optical properties will affect the mean sampling depth and can influence the rest flux [23]. Ideally speaking individual Biological Zero levels measured on the same location should be used in the analysis of perfusion data. However, since in this case no local BZ levels could be measured, a BZ correction has to be based on an average value. Since we choose measurement locations having comparable rest flux in all individuals we expect that the influence of optical properties on our measurements is not significant.

The results show that the difference in BZ between normal skin temperature and 15°C is not significant. This confirms the earlier report on the BZ variation in the temperature range we used [20]. The measured mean biological zero (4.5PU) was significantly less compared to the average minimum perfusion value (11.2PU) we found in our measurements. We investigated the influence of BZ on our results by subtracting the BZ and fitting our model function from the average perfusion in Fig. 5. For this we used the average BZ measured on the hand at the minimum temperature we acquired during scalp cooling, $\text{BZ} = 4.5$. With this correction for the BZ, a fit of the parameters in equation 2–3 to the accumulated data of all nine subjects resulted in $Q_{10} = 3.6$ and $\varphi_{\min} = 0.18$ (Fig. 6). This shows that the minimum perfusion value still exists even after correcting for BZ.

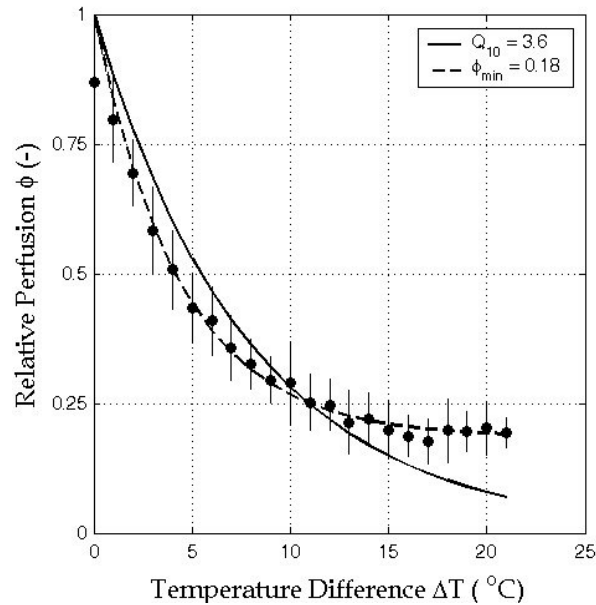


Fig. 6 Average relative temperature difference and relative perfusion and best fits for Q_{10} and minimum perfusion (ϕ_{\min}) corrected for Biological Zero. Error bars represent standard error

4. Discussion and conclusion

We have investigated the relationship between temperature and perfusion on the human scalp skin with thermocouples and Laser Doppler Perfusion probes. The single-subject repetitive experiments showed that the measurements are reproducible, and that no differences exist between the two different positions regarded. We were not able to cool the position on the right-hand side as much as the central position, which can be attributed to better contact between the skin and the cap at the central position for this head/cap combination. Computations have shown a high sensitivity of skin temperature to the gap thickness between the skin and the cap [7]. The experiments on the nine subjects showed that cooling the scalp reduced perfusion down to 20–40%. Re-warming resulted in an increase in perfusion. In a previous study [4], blood flow remained significantly lower than the pre-cooling level during the re-warming phase. However, in our study there were no significant differences between the cooling phase and the re-warming phase, which suggests that this kind of hysteresis effects do not play a role in this experiment. We experienced that we were not able to cool each person to the same degree. This is probably caused

by anatomical differences such as head shape and thickness of the insulating fat layer, two factors that showed to have a high influence on scalp skin temperature during scalp cooling [7]. In contrast, the same study showed that physiological variations in scalp skin perfusion were far less influential. The data was used to establish a relationship between scalp skin temperature and cutaneous perfusion. Perfusion does not exponentially go to zero, instead an exponential decrease with $\Theta = 4^{\circ}\text{C}$ to a relative perfusion level of 0.29 described the data well. Since the minimum perfusion we measured at lower temperatures is significantly higher than the measured Biological Zero at this temperature at another location with a comparable rest flux value, the biological zero variations would not affect our findings of a relation between temperature and scalp skin perfusion.

The minimum perfusion we cite in our measurements (also after correcting for BZ) shows that cooling beyond $\Delta T \approx 3\Theta = 12^{\circ}\text{C}$ does not significantly reduce the supply of the drug to the skin any further. The latter finding is a surprising outcome suggesting that below a certain critical temperature, lower skin temperatures do not significantly reduce the supply of the drug to the skin any further. The consequence of this is that lowering skin temperature beneath this critical temperature might only be useful for reducing local tissue metabolism. This is something that has to be taken into account in the protocol for scalp cooling during administration of chemotherapy. Currently, we are investigating the effect of temperature on doxorubicin uptake and metabolism using *in vitro* experiments.

Acknowledgements

The Eindhoven University of Technology was sponsored by SOBU, an administrative cooperation between Tilburg University and the Eindhoven University of Technology. The University of Twente was supported by the Netherlands Technology Foundation STW (grant 5840). The authors are grateful to Perimed AB and Paxman Ltd for providing instrumentation.

References

1. T. F. Cash, "The psychology of hair loss and its implications for patient care," *Clin. Dermatol.* **19** 161–166 (2001).
2. C. Protière, K. Evans, J. Camerlo, M. P. d'Ingrado, G. Macquart-Moulin, P. Viens, D. Maraninchi and D. Genre, "Efficacy and tolerance of a scalp-cooling system for prevention of hair loss and the experience of breast cancer patients treated by adjuvant chemotherapy," *Support. Care Cancer* **10**, 529–537 (2002).

3. E. G. Grevelman and W. P. M. Breed, "Prevention of chemotherapy-induced hair loss by scalp cooling," *Ann. Oncol.* **16**, 352–358 (2005).
4. J. Bülow, L. Friberg, O. Gaardsting and M. Hansen, "Frontal subcutaneous blood flow, and epi- and subcutaneous temperatures during scalp cooling in normal man," *Scand. J. Clin. Lab. Invest.* **45**, 505–508 (1985).
5. C. S. Thompson, L. A. Holowatz and W. L. Kenney, "Attenuated noradrenergic sensitivity during local cooling in aged human skin," *J Physiol (Lond)* **564**, 313–319 (2005).
6. P. E. Pèrgola, D. L. Kellog, J. M. Johnson, W. A. Kosiba and D. E. Solomon, "Role of sympathetic nerves in the vascular effects of local temperature in human forearm skin," *Am. J. Phys.* **265**, H785–H792 (1993).
7. F. E. M. Janssen, G. M. J. Van Leeuwen and A. A. Van Steenhoven, "Modelling of temperature and perfusion during scalp cooling," *Phys. Med. Biol.* **50**, 4065–4073 (2005).
8. C. S. Lau, F. Khan, R. Brown, P. McCallum and J. J. Belch, "Digital blood flow response to body warming, cooling, and rewarming in patients with Raynaud's phenomenon," *Angiology* **46**, 1-10 (1995).
9. D. Popivanov, A. Mineva, P. Bendayan, P. Leger, H. Boccalon, K. O. Moller, "Dynamic characteristics of laser-Doppler flux in normal individuals and patients with Raynaud's phenomenon before and after treatment with nifedipine under different thermal conditions," *Technol Health Care* **7**, 193-203 (1999).
10. T. Kanetaka, T. Komiyama, A. Onozuka, T. Miyata and H. Shigematsu, "Laser Doppler skin perfusion pressure in the assessment of Raynaud's phenomenon," *Eur J Vasc Endovasc Surg.* **27**, 414-416 (2004).
11. R. Maniewski, P. Leger, P. Lewandowski, A. Lieber, P. Bendayan, H. Boccalon, L. Bajorski, K. O. Moller, "Spectral analysis of laser-Doppler perfusion signal measured during thermal test," *Technol. Health Care.* **7**, 163-169 (1999).
12. E. A. Friedman, P. A. Harris, A. J. Wood, C. M. Stein and D. Kurnik, "The effects of tadalafil on cold-induced vasoconstriction in patients with Raynaud's phenomenon," *Clin Pharmacol Ther.* **81**, 503-509 (2007).
13. A. P. Shepherd, and P. Å . Öberg, (ed.), *Laser-Doppler Blood Flowmetry* (Boston: Kluwer Academic Publishers, 1990).
14. A. Jakobsson and G. Nilsson, "Prediction of sampling depth and photon pathlength in laser Doppler flowmetry," *Med.Biol. Eng. Comput.* **31**, 301-307 (1993).
15. R. F. Bonner and R. Nossal, "Model for laser Doppler measurements of blood flow in tissue," *Appl. Opt.* **20**, 2097–2107 (1981).

16. L. Caspary, A. Creutzig, K. Alexander, "Biological zero in laser Doppler fluximetry," *Int J Microcirc Clin Exp* **7**, 367–371 (1988).
17. B. Fagrell, "Perimed's LDV flowmeter," In: Shepherd A P and Öberg P Å (ed.) 1990 Laser-Doppler Blood Flowmetry. Boston: Kluwer Academic Publishers.
18. G. E. Nilsson, "Peripheral vascular diseases," In: Shepherd AP and Öberg P Å (ed.), Laser-Doppler Blood Flowmetry (Boston: Kluwer Academic Publishers, 1990).
19. D. P. Kernick, J. E. Tooke and A. C. Shore, "The biological zero signal in laser doppler fluximetry –origins and practical implications," *Pflügers Arch – Eur J Physiol.* **437**, 624–631 (1999).
20. N. C Abbot and J Swanson-Beck, "Biological zero in laser Doppler measurements in normal, ischaemic and inflamed human skin," *Int. J. Microcirc. Clin. Exp.* **2**, 89–98 (1993).
21. B. H. Dennis, R. C. Eberhart, G. S. Dulikravich and S. W. Radons, "Finite-element simulation of cooling of realistic 3D human head and neck," *J. Biomech. Eng.* **125**, 832–840 (2003).
22. D. Fiala, K. J. Lomas and M. Stohre, "A computer model of human thermoregulation for a wide range of environmental conditions: the passive system," *J. Appl. Phys.* **87**, 1957–1972 (1999).
23. M. Larsson, W. Steenbergen and T. Strömberg, "Influence of optical properties and fibre separation on laser Doppler flowmetry," *J. Biomed. Opt.* **7**, 236-243 (2001).

Chapter 9

Summary and outlook

1. Summary of the Thesis

Laser Doppler Flowmetry (LDF) is a noninvasive diagnostic method to measure blood flow in tissue [1]. The technique is based on measuring the Doppler shift induced by moving red blood cells to the illuminating coherent light. A laser Doppler instrument often gives output signals related to the flux, velocity and concentration of the moving blood cells. These parameters are extracted from the power spectrum of the intensity fluctuations produced by a photodetector. There are two types of perfusion instruments in practice, the laser Doppler perfusion monitor (LDPM) and the laser Doppler perfusion imager (LDPI). A review of the working principle of these technique and their methodological developments so far is given as **chapter 2**.

The advantage of LDPI over LDPM is that it is non contact in nature. So it can be used in clinical environments where contact with the tissue may be undesirable. Also it gives a perfusion map of a tissue area, which gives average perfusion in a heterogeneous tissue in a single measurement.

The response of the LDPI instrument is influenced by tissue optical properties through two mechanisms: 1) the direct effects of tissue optical properties of the statistics of the detected photons, for instance the path length traveled by the light, determining the extent of multiple Doppler scattering, and 2) the effect of the optical properties on the spatio-temporal properties of the dynamic speckle pattern that generates the perfusion signal.

In this thesis we addressed the influence of tissue optical properties on laser Doppler perfusion imaging taking in to account the speckle phenomenon. In **chapter 3** it is experimentally proved that the scattering level of the tissue strongly affects the laser Doppler imager signal due to the number of speckles involved in the detection process. This speckle-related cross talk between the

scattering level and LDPI signal can be suppressed using a sufficiently large beam diameter, but at the expense of signal to noise ratio and spatial resolution. Both the signal modulation depth and the frequency content are affected by this speckle-related influence. It was observed that with a typical beam diameter of 0.5mm the signal modulation depth varies by a factor of 5 when the reduced scattering level varied from 0.5mm^{-1} to 4.0mm^{-1} . This variation drops to a factor of 1.5 when the beam diameter is increased to 4.0mm. An increase in beam diameter resulted in a decrease in modulation depth of the signal. It was also observed that the weighted first order moment M_1/M_0 (which is the average frequency), of the power spectra of detector current fluctuations is influenced by the diameter of the laser beam. The average Doppler shift increased with the beam diameter. For $\mu_s=4.0\text{mm}^{-1}$ an increase in beam diameter from 0.5mm to 4.0mm resulted in an increase of average Doppler shift from 1021Hz to 1408Hz and for $\mu_s=2.0\text{mm}^{-1}$ this increase was from 963Hz to 1253Hz. This demonstrated that the effect of speckles should be modeled to predict the system response to different tissue optical properties and particle velocities.

A method to predict the coherence area (speckle size) detected in reflection mode in the far field of a turbid medium with a sequence of models using the photon and wave picture of light is described in **chapter 4**. The theoretical model was experimentally validated on particle suspension of various scattering properties. Our theory was able to predict the different behavior for anisotropic as well as isotropic scatterers. For large particle sizes with $g=0.9$ and 0.93 the coherence area varies by a factor of 4 for 0.5mm beam in the experiment as well as the simulation. For the $\varnothing 0.202\ \mu\text{m}$ ($g=0.3$) particle suspension the coherence area variation for a narrow beam is only by a factor of 2. This is because for this medium low order scattering is dominant and is contributing significantly to the intensity distribution on the surface of the medium, hence the relative change of the width of the back-scattered intensity distribution with increasing scattering level is small.

It is shown that the spatial intensity correlation function of dynamic speckle patterns formed by light backscattered from turbid suspensions varies considerably with diffuse scattering, a variation which can be suppressed by using broader intensity profiles. The theoretical and numerical method will improve the interpretation of results obtained from coherence-based biomedical imaging instruments based on measuring dynamic speckle patterns in the far field. It will for instance allow us to quantify the effect of spatial variations in tissue optical properties on the results obtained with such imaging instruments.

The theoretical model described in chapter 4 was further extended to combined static-dynamic media in **chapter 5**. Using this model we predicted the changes in the modulation depth of the photocurrent fluctuations in a free beam laser Doppler experiment for motion at different depths within static tissue like media, taking into account the speckle phenomenon.

We introduced the concept of fractional coherence areas which are related to fractions of photons. These fractions can be arbitrarily chosen, and allow to determine the relative contribution of meaningful photon fractions to the total signal autocorrelation, such as photons which have interacted with a specific compartment at a certain depth within the medium.

The results show that the depth sensitivity of the laser Doppler instrument is strongly influenced by speckles. For the narrowest beam the signal modulation ratio for motion at 0 and 0.5 mm depth, is 2.9. But for a wide beam (4.0mm) this ratio is reduced to 1.6. This shows that a narrow beam is more sensitive to scattering from superficial layers compared to a wide beam, while the sensitivity to motion at large depth is much less dependent on beam diameter. The strength of the speckle effect on depth sensitivity will also depend on the scattering and absorption level of the tissue. The lower the level of the scattering and absorption the smaller the effect will be. This is because when scattering or absorption is high photons will travel shorter distances and leave the medium closer to the illuminating beam making a narrow back-scattered intensity profile. So the effective speckle size will be larger and also the modulation depth. In this situation the LDPI flux signal will be very sensitive to the depth related changes in the width of the intensity distribution and the resulting changes in the number of speckles.

Our results of *in vivo* measurements as described in **chapter 6** on normal skin and a port wine stain confirmed the influence on the laser Doppler imager signal of the speckle dependency on tissue optical properties. We validated our observations in *in vivo* measurements using our theoretical model by calculating the modulation depth for two optical situations resembling to normal skin and port wine stain. For that we used a Monte Carlo program to simulate the light transport in the two tissue types and the modulation depth was calculated using the simulated back-scattered intensity distributions for various beam diameters. Further investigation with Monte Carlo simulations of a range of scattering and absorption levels in combination with motion at various depths showed that speckle effects play an important role on the depth sensitivity of the instrument and these effects are big in higher scattering and absorption media. It was also an important observation that the mean sampling depth and the overall depth sensitivity were significantly affected by the speckle phenomenon. These effects were bigger for higher scattering and absorption levels. Taking the speckle phenomenon into account, the overall sensitivity increased with increasing scattering and absorption levels. When the speckle phenomenon would have been ignored, the overall sensitivity would have been found to decrease with reduced scattering and absorption coefficients. It was observed that the mean sampling depth decreases with increasing scattering and absorption, which is an obvious behaviour. Speckle effect significantly decreases the mean sampling depth. For an absorption coefficient of 0.01mm^{-1} and $\mu'_s=1.0\text{mm}^{-1}$ the mean sampling depth of 0.87mm, without speckle

phenomenon, was reduced to 0.63mm when speckle effects are included. When the scattering level was increased to $\mu'_s=4.0\text{mm}^{-1}$ this sampling depth drop due to the speckle phenomenon was from 0.41mm to 0.28mm. This trend was also seen with increasing absorption. These observations demonstrate the essential role of speckles in the response of laser Doppler perfusion imaging devices. The developed model will help in correctly interpreting the results obtained with an imager in situations where large tissue inhomogeneities are found.

The space-time correlation of the speckles generated by particle suspensions illuminated by a collimated laser beam is analyzed in **chapter 7** from serial images taken by a high speed camera. From the 3d data set obtained from the serial images in space and time the space-time correlation function of the dynamic speckle pattern can be efficiently obtained by a 3d Fourier transform, squaring the result, and an inverse transform of this three dimensional power spectrum. It was observed that the larger spatial correlation distances, associated with large speckles, show a slower temporal decorrelation. This confirms our hypothesis regarding the influence of average speckle size, mediated by the photon path length, on the Doppler content of the power spectra as observed in chapter 3. When a relatively broader beam is used for illuminating a scattering suspension the average Doppler width of the power spectrum of detector current fluctuations increases compared to the situation where a narrow beam is used. When a narrow beam is used for illumination which on average produces larger speckles on the detector, photons which traveled a relatively longer pathlength, associated with larger Doppler shifts, produce the small speckles within the speckle pattern. Because they are smaller, their contribution is relatively more suppressed in the Doppler content of the power spectrum compared to the large speckles which represent short path length photons. Our observations in chapter 3 and 7 show that for the perfusion signal (M_1) the effect of speckles on the average Doppler shifts (M_1/M_0) and the modulation depths (M_0) work against each other, with the influence of speckles on M_0 having the largest effect on the total perfusion signal.

In **chapter 8** we investigated the relationship between temperature and perfusion on the human scalp with thermocouples and laser Doppler perfusion probes. The purpose of this study was to establish a relationship between local scalp skin temperature and cutaneous blood flow during scalp cooling in a setting which is relevant to clinical practice of scalp cooling in chemotherapy treatment to prevent hair loss. Measurements on 9 healthy subjects showed that there is a relationship exists between temperature and scalp skin perfusion. We found that for the first 10°C of cooling of the scalp, perfusion of the scalp decreased to below 40% of the rest flux. Perfusion could be further reduced to below 30% by a few degrees more cooling, but a plateau is reached after that. We defined a minimum perfusion function which could describe the data. The minimum perfusion level found suggests that cooling beyond $\Delta T \approx 12^\circ\text{C}$ does not significantly reduce the supply of a cytostatic drug to the skin any further.

The consequence of this is that lowering skin temperature beneath this critical temperature might only be useful for reducing the local tissue metabolism. This is something that has to be taken into account in the protocol for scalp cooling during administration of chemotherapy [2].

2. Outlook

The laser Doppler perfusion measurement technique (monitoring and imaging) has undergone large progress since its introduction. The improvements in laser technology and fiber optics, and in signal processing, have made LDF into a reliable and user friendly technology. The introduction of the imaging technique opened up clinical research applications where a non contact measurement is a necessity and where perfusion information within an area of tissue is required. The limitations of the technique were thoroughly addressed by the researchers enabling a lot of improvements. But few of the limitations given in chapter 2 still demand a revisit. The problem of multiple Doppler shifts remains unresolved. The multiple Doppler shifts lead to a non linear flow response of the LDF techniques when the concentration blood is very high. A modification of the classical Bonner and Nossal model[3], which is derived to interpret perfusion of sparsely perfused tissue (negligible multiple scattering), is required to interpret the multiple Doppler shifts and related flow response.

The velocity resolved perfusion measurements proposed by a few authors need much more research to be applied to real tissue. Aspects of further study should be the influence of the heterogeneity of the optical properties, multiple Doppler shifts and distribution of different velocity components in the power spectra. Also the problem of tissue optical properties should be addressed in case of scanning laser Doppler perfusion imagers. A method has to be integrated to the laser Doppler perfusion imager which can monitor either the optical properties variation in tissue *in vivo* or the speckle size changes due to optical properties to correct the perfusion image for each pixel. The spatially resolved diffuse reflectance method, SRDR, [4] can be used as tool for non-invasively monitoring the tissue optical properties. But this method is only valid for $\mu_a \ll \mu_s$ and is not yet proved as a quantitative technique to measure skin optical properties. The quantification of the influence of tissue optical properties through the speckle phenomenon, the method proposed in this thesis is a simple approach which can be implemented to the existing imagers.

2. 1 Understanding the speckle phenomenon for better perfusion imaging

The research described in this thesis on the influence of tissue optical properties in LDPI through speckle phenomenon suggests that at certain applications of the perfusion imager special care has to be taken by the physician to arrive at a conclusion regarding a perfusion change [5, 6]. For example in a burn depth assessment the optical properties of the damaged skin on top of a perfused tissue will play a major role in the instruments sensitivity. Also in interpreting the data obtained with a certain drug uptake test or with vasodilatory stimuli where the tissue optical properties can vary rapidly care should be taken since both the depth sensitivity and overall response of the instrument can vary independent of perfusion.

The theoretical/experimental model presented for predicting the spatial intensity correlation function of dynamic speckle patterns formed by light backscattered from mediums like tissue will help in quantifying a major problem faced by a scanning laser Doppler perfusion imagers and it suggests a way to predict this limitation under various optical situations. Our model and findings will help in getting a priori knowledge about what to interpret and how conscious one should be in assessing a laser Doppler perfusion image.

2. 2 Method to account for the influence of tissue optical properties

The method described in chapter 6 for calculating the average speckle size on the photodetector from the back-scattered intensity distribution on the tissue surface captured with a CMOS/CCD camera can be used as a tool for correcting the LDPI signal for variation in tissue optical properties. This method can be implemented in the current scanning LDPI instruments which has an inbuilt camera. If the camera is programmed to capture the back-scattered intensity spots in real time while the laser beam is scanning the tissue area the instrument sensitivity can be calculated in real time which can account for the perfusion variation with tissue optical properties.

In the method proposed above all photons detected are considered to be Doppler shifted and no distinction is made between the back scattered intensity distribution of Doppler shifted and non-Doppler shifted light. The consequence of this will be an underestimation of the average speckle size and hence of the modulation depth which is originally composed by the interference of one fraction of Doppler shifted light and one fraction of non-Doppler shifted light. In normal tissue which is sparsely perfused the contribution of the non-Doppler shifted photons is large.

2. 3 Depth selectivity in perfusion imaging

Polarization techniques can be considered as a tool to discriminate fractions of photons assuming that photons which traveled deeper and encountered with moving red blood cells and multiply scattered will lose their polarization. By this assumption an estimation of only Doppler shifted fraction of photons can be done by using a polarization filter but often will result in filtering out singly scattered Doppler shifted photons which is preserving its polarization, losing the signal to noise ratio [7]. Hence polarization techniques can offer some depth selectivity between superficially scattered and deeply scattered photons.

The observation in chapter 5 showed that a narrow beam is most sensitive to superficial motion whereas use of a wide beam reduces the variation of depth sensitivity due to tissue dependent speckle phenomenon. The different dependence of the depth sensitivity on the beam diameter can be exploited to make a discrimination of superficial and deep flow by varying the beam diameter in a scanning imager. But the lateral resolution will be affected by using a wide beam. Also a quantification of this approach will be hampered by the unknown tissue optical properties and the penetration depth of photons.

2. 4 New approaches in perfusion imaging

2.4.1 Full field LDPI

The emerging full field laser Doppler imaging technique [8, 9] has a lot of potential to overcome the disadvantages of the slow scanning speed of conventional scanning imagers. Here the influence of optical properties on the number of coherence areas will be absent because of the use of a full field beam. In the full field technique the total area of interest is illuminated by a broad beam, and the back-scattered speckles are detected by a lens on an imaging array. Hence, both the solid angle of the light on the detector, and the effective detection area (see chapter 3), are basically constant, since they are now determined by the angular aperture of the imaging system and the pixel size, respectively.

2.4.2 Laser speckle contrast analysis and laser speckle perfusion imaging

Another approach for perfusion imaging is a full field real time technique based on laser speckle contrast analysis (LASCA) [10] for capillary blood flow monitoring. It uses an imaging array which captures an image of the speckle produced by the scattering medium or tissue, with a relatively long exposure time of several milliseconds. Because of the motion of the speckles there will be a contrast variation on the image. This contrast variation is analyzed as a ratio of the standard deviation of the intensity fluctuations to the average intensity on a small area of pixels (5×5 or 7×7). This analysis is then extrapolated over the entire image to make contrast map which indicates flow.

The advantage of LASCA over the laser Doppler imaging techniques commercially available is that there is no scanning part and can be used for real time measurements. Compared to the full field laser Doppler techniques it requires a slower camera and is less expensive. But the spatial resolution of the image is limited by the need to average over a sub-array of pixels. Also, it is not clear how LASCA can provide a linear measurement of blood flow, since it lacks a general physical model that relates contrast as a flow parameter to perfusion. The full field LDPI produces power spectra with full Doppler content and give a linear measurement of blood flow as in other laser Doppler techniques, which is supported by the model of Bonner and Nossal [3].

A modified approach of LASCA was suggested by Forrester et al [11] called laser speckle imaging (LSI) and later named laser speckle perfusion imaging (LSPI) [12]. In this a CCD camera is used to make a series of speckle images from a sample with finite integration time. And the decorrelation of the speckle pattern is related to blood flow. Since the image processing algorithm does not use a group of adjacent pixels like LASCA the full resolution of the image is preserved. Also the temporal analysis of a series of images for various flow rates showed a linear response range comparable with standard LDPI. The method produces perfusion plots within a few seconds whereas an LDPI full scan takes a few minutes. In a comparative study of LSI with LDPI, Forrester et al [11] showed that the LSI is better capable of measuring fast blood flow changes than a scanning mode LDPI technique. However, basically the LSI technique is similar to LASCA, and shares with this technique the disadvantage of not being objectively supported by a physical model.

2.5 Future of perfusion imaging

On the long term, the future of laser perfusion imaging is probably in full field LDPI and speckle contrast techniques (LASCA and LSPI) which both have the advantage of speed. Full field LDPI requires a high speed camera, which is very expensive, so its future depends on the price development of CMOS imaging array technology. Also the quality of the perfusion images obtained with the full field LDPI technique in terms of spatial resolution and signal to noise ratio (SNR) is less compared to scanning LDPI. The diffusion of light in tissue suppresses the resolution of full field LDPI image because of the spreading of the backscattered light in tissue. Also the difference in gain of different pixel arrays in a CMOS camera results in a variation in response of the pixels for the same signal. A third reason is that the detector size in full field LDPI is equal to the pixel size, which is typically in the order of $10 \times 10 \mu\text{m}^2$ instead of a few mm^2 as in scanning beam LDPI devices.

Application of LASCA will depend on its possibility to quantify blood flow, since there is no objective model for flow in LASCA. General introduction of LASCA would be promoted by a physical model that relates LASCA response to the blood flow. The scanning laser Doppler perfusion

imager regardless of its slow speed and speckle related dependence of tissue optical properties will remain for some time as an established tool for microcirculatory blood flow imaging.

References

1. A. P. Shepherd and P. Å Öberg, (Eds) Laser Doppler blood flowmetry, (Kluwer Academic Publishers, Boston, 1990).
2. F. E. M. Janssen, V. Rajan, W. Steenbergen, G. M. J. van Leeuwen, and A. A. van Steenhoven, "The relationship between local scalp skin temperature and cutaneous perfusion during scalp cooling," *Physiol. Meas.* **28**, 829-839 (2007).
3. R. Bonner and R. Nossal, "Model for laser Doppler measurements of blood flow in tissue," *Appl. Opt.* **20**, 2097-2107 (1981).
4. M.S. Patterson, E. Schwartz and B. C. Wilson, "Quantitative reflectance spectrophotometry for thenon-invasive measurement of photosensitizer concentration in tissue during photodynamic therapy," *Proc. SPIE* **1065**, 115-122 (1989)
5. V. Rajan, B. Varghese, T. G. van Leeuwen, and W. Steenbergen, "Speckles in Laser Doppler Perfusion Imaging," *Opt. Lett.* **31**, 468-470 (2006).
6. V. Rajan, B. Varghese, T. G. van Leeuwen, and W. Steenbergen, "Quantification of spatial intensity correlations and photodetector intensity fluctuations of coherent light reflected from turbid particle suspensions," *Phys. Rev. E* **75**, 060901-4 (2007).
7. M. G. D Karlsson and K. Wårdell, "Polarized laser Doppler perfusion imaging—reduction of movement-induced artifacts," *J. Biomed. Opt.* **10**, 064002 (2005).
8. A. Serov, W. Steenbergen, and F. F. M. de Mul, "Laser Doppler perfusion imaging with a complimentary metal oxide semiconductor image sensor," *Opt. Lett.* **25**, 300-302 (2002).
9. A. Serov, B. Steinacher and T. Lasser, "Full-field laser Doppler perfusion imaging and monitoring with an intelligent CMOS camera," *Opt. Express* **13**, 3681-3689 (2005).
10. J. D Briers, G. Richards and X. W He, "Capillary blood flow monitoring using laser speckle contrast analysis," (LASCA) *J. Biomed. Opt.* **4**, 164-175 (1999).
11. K. R. Forrester, C. Stewart, J. Tulip, C. Leonard, and R. C. Bray, "Comparison of laser speckle and laser Doppler perfusion imaging: measurement in human skin and rabbit articular tissue," *Med. & Bio.Eng. & com.* **40**, 687-697 (2002).

12. K. R. Forrester, J. Tulip, C. Leonard, C. Stewart, and R. C. Bray, "A laser speckle imaging technique for measuring tissue perfusion," *IEEE Trans. Biomed. Eng.* **51**, 2074-2084 (2004).

Samenvatting

Laser Doppler Flowmetry (LDF) is een niet invasieve diagnosetechniek om de doorbloeding van weefsel te meten. De techniek is gebaseerd op het meten van de Dopplerverschuiving van coherent licht veroorzaakt door bewegende rode bloedcellen. Een laser Doppler instrument geeft vaak signalen die gerelateerd zijn aan de flux, snelheid en concentratie van bewegende rode bloedcellen. Deze parameters zijn bepaald aan de hand van het vermogenspectrum van de intensiteitfluctuaties van de fotodetector. Er zijn twee soorten apparaten om de doorbloeding mee te meten, de laser Doppler doorbloedingsmonitor (LDPM) en de laser Doppler doorbloedings *imager* (LDPI). Een overzicht van het werkingsprincipe van deze technieken en hun methodistische ontwikkeling tot nu toe is beschreven in **hoofdstuk 2**.

Het voordeel van LDPI boven LDPM is dat er geen contact met het weefsel is. Het kan dus gebruikt worden in een klinische omgeving waarin contact met het weefsel ongewenst is. Ook geeft het een doorbloedingplaatje van een weefseloppervlak, en het geeft gemiddelde doorbloeding in een heterogeen weefsel in een enkele meting. De respons van het LDPI instrument wordt op twee manieren beïnvloed door weefseloptische eigenschappen: 1) de directe effecten van weefseloptische eigenschappen op de statistiek van gedetecteerde fotonen, bijvoorbeeld de afgelegde weglengte door het licht, bepalen de mate van meervoudige Doppler verstrooiing, en 2) het effect van de optische eigenschappen op de eigenschappen in plaats en tijd van het dynamische *speckle* patroon dat het doorbloedings signaal genereert.

In dit proefschrift beschrijven wij de invloed van weefsel optische eigenschappen op laser Doppler doorbloeding *imaging* waarbij rekening wordt gehouden met het *speckle* fenomeen. In **hoofdstuk 3** is experimenteel aangetoond dat het verstrooiingsniveau van het weefsel het laser Doppler *imager* signaal sterk beïnvloed door het aantal *speckles* dat betrokken is bij het detectie proces. Deze *speckle*-gerelateerde overspraak tussen het verstrooiingsniveau en het LDPI signaal kan onderdrukt worden door gebruik te maken van een voldoende grote bundeldiameter, ten koste van de signaal-ruis-verhouding en ruimtelijke resolutie. Zowel de signaalmodulatiediepte als de frequentie-inhoud worden veranderd door deze *speckle* gerelateerde invloed. Het is aangetoond dat bij een bundeldiameter van 0.5mm de signaalmodulatiediepte een factor 5 varieert als de gereduceerde verstrooiingscoëfficiënt varieert van 0.5mm^{-1} tot 4.0mm^{-1} . Deze variatie

reduceert tot een factor 1.5 als de bundeldiameter wordt verhoogd tot 4.0 mm. Een toename in bundeldiameter resulteert in een afname van de modulatie diepte van het signaal. Ook is aangetoond dat het gewogen eerste moment M_1/M_0 (dat gelijk is aan de gemiddelde frequentie) van het vermogensspectrum van de detector wordt beïnvloed door de diameter van de laserbundel. De gemiddelde Dopplerverschuiving neemt toe met de bundeldiameter. Voor een gereduceerde verstrooiingscoëfficiënt van 4.0mm^{-1} resulteert een toename in bundeldiameter van 0.5mm tot 4.0mm in een toename van de gemiddelde Doppler verschuiving van 1021 Hz tot 1408 Hz en voor $\mu'_s=2.0\text{mm}^{-1}$ neemt deze toe van 963 Hz tot 1253 Hz. Dit toont aan dat het effect van *speckles* gemodelleerd moet worden om te kunnen voorspellen hoe het systeem reageert op verschillende optische eigenschappen en deeltjessnelheden.

Een methode om het coherentieoppervlakte (*speckle* grootte) te voorspellen in reflectie-*mode* in het verre veld in een troebel medium, met een aaneenschakeling van modellen welke gebruik maken van het foton- en golf karakter van licht is beschreven in **hoofdstuk 4**. Het theoretische model was experimenteel gevalideerd op deeltjessuspensies met verschillende verstrooiingseigenschappen. Onze theorie was in staat het gedrag voor zowel anisotrope als isotrope verstrooiers te voorspellen. Voor grote deeltjes met verstrooiingsanisotropie $g=0.9$ en 0.93 varieerde de coherentieoppervlakte zowel in simulaties als in metingen met een factor 4 voor een laserbundel van 0.5mm. Voor de $\text{Ø}0.202 \mu\text{m}$ ($g=0.3$) deeltjessuspensie varieerde de coherentieoppervlakte slechts met een factor 2 voor een smalle laserbundel. Dit komt omdat voor dit medium de lagere orde verstrooiing dominant is en dus sterk bijdraagt aan de intensiteitverdeling aan het oppervlak van het medium. Hierdoor is de relatieve verandering van de breedte van het terugverstrooide licht met toenemend verstrooiingsniveau klein.

Het is aangetoond dat de ruimtelijke intensiteitscorrelatiefunctie van dynamische *speckle* patronen, gevormd door teruggekaatst licht van troebele suspensies, sterk varieert met diffuse verstrooiing, een variatie die onderdrukt kan worden door gebruik te maken van een breder intensiteitsprofiel. De theoretische en numerieke methode zal de interpretatie verbeteren van resultaten verkregen met *coherence-based* biomedische afbeeldinginstrumenten gebaseerd op metingen van dynamische *speckle* patronen in het verre veld. Het zal ons bijvoorbeeld in staat stellen om het effect van ruimtelijke variaties in weefsel optische eigenschappen op dergelijke afbeeldingsmethoden te kwantificeren.

Het theoretische model beschreven in hoofdstuk 4 zal verder worden uitgebreid tot gecombineerde statisch-dynamische media in **hoofdstuk 5**. Door gebruik te maken van dit model en het *speckle* fenomeen mee te nemen hebben wij in een experiment, waarbij de laser niet in contact was met de huid, de verandering in modulatie diepte van de fotostroom-fluctuaties berekend voor beweging op verschillende dieptes in op weefsel lijkende materialen. Wij hebben het concept van fractionele coherentie-oppervlaktes geïntroduceerd die

gerelateerd zijn aan bepaalde fracties van fotonen. Deze fracties kunnen willekeurig gekozen worden en geven de mogelijkheid om de relatieve bijdrage van een relevante fractie van fotonen tot het totale signaal te bepalen, zoals fotonen die een interactie hebben ondergaan in een specifiek subvolume in het medium.

De resultaten laten zien dat de dieptegevoeligheid van laser Doppler instrumenten sterk wordt beïnvloed door *speckles*. Bij de smalste bundeldiameter is de signaalmodulatieverhouding voor beweging op respectievelijk 0 en 0.5 mm gelijk aan 2.9. Voor een brede bundel (4.0 mm) is deze verhouding afgenomen tot 1.6. Dit toont aan dat de smalle bundel gevoeliger is voor verstrooiing van oppervlakkige lagen in vergelijking met een brede bundel, dit terwijl de gevoeligheid voor beweging op grotere diepte veel minder afhankelijk is van de bundeldiameter. De invloed van het *speckle* effect op de dieptegevoeligheid zal dan ook afhangen van het verstrooiing- en absorptieniveau van het weefsel. Hoe lager het niveau van verstrooiing en absorptie hoe kleiner het effect zal zijn. Dit komt vanwege het feit dat bij hoge absorptie of verstrooiing fotonen slechts een kleine afstand afleggen en het medium dus dichterbij de belichtingsbundel zullen verlaten, wat resulteert in een smal intensiteitsprofiel. Hierdoor zal de gemiddelde specklegrootte toenemen en daardoor de modulatie diepte. In deze situatie zal het LDPI flux signaal erg gevoelig zijn voor diepte gerelateerde veranderingen in de breedte van de intensiteitsverdeling en de daar uit voortkomende verandering in aantal *speckles*.

Onze *in vivo* resultaten op normale huid en wijnvlekken zoals beschreven in **hoofdstuk 6** bevestigen de invloed op het laser Doppler *imager* signaal van speckle afhankelijkheid van weefsel eigenschappen. Wij hebben onze bevindingen in *in-vivo* metingen gevalideerd door in ons theoretisch model de modulatie diepte voor twee situaties uit te rekenen, voor normale huid en voor wijnvlekken. Daarbij hebben wij gebruik gemaakt van een Monte Carlo programma om het lichttransport in de twee weefseltypes te simuleren. De modulatie diepte was berekend door gebruik te maken van de gesimuleerde terugverstrooide intensiteitsverdeling voor verschillende bundeldiameters. Nader onderzoek met Monte Carlo simulaties voor verschillende verstrooiings- en absorptie niveaus in combinatie met beweging op verschillende dieptes liet zien dat het *speckle* effect van grote invloed is op de dieptegevoeligheid van het instrument en dat deze effecten groter zijn in media met een hogere verstrooiing en absorptie. Een andere belangrijke waarneming was dat de gemiddelde diepte en de gemiddelde dieptegevoeligheid sterk werden beïnvloed door het *speckle* fenomeen. Deze effecten waren groter voor hogere verstrooiing en absorptie. Rekening houdend met het *speckle* fenomeen neemt de totale gevoeligheid toe met toenemende verstrooiing en absorptie. Zonder rekening te houden met het *speckle* effect neemt de totale gevoeligheid af met toenemende verstrooiing en absorptie. De gemiddelde indringdiepte neemt af met toenemende verstrooiing

en absorptie, wat opmerkelijk is. Het *speckle* effect heeft namelijk een afname in indringdiepte tot gevolg. Bij een absorptie coëfficiënt van 0.01mm^{-1} en een gereduceerde verstrooiingscoëfficiënt van 1.0mm^{-1} zal de gemiddelde indringdiepte van 0.87mm zonder *speckle* fenomeen, afnemen tot 0.63mm indien het *speckle* fenomeen wel wordt meegenomen. Wanneer de gereduceerde verstrooiingscoëfficiënt toeneemt tot 4.0mm^{-1} zal de gemiddelde indringdiepte afnemen van 0.41mm naar 0.28mm indien het *speckle* effect wordt meegenomen. Dezelfde trend is waar te nemen indien de absorptie toeneemt. Deze veranderingen laten duidelijk zien welke belangrijke rol *speckles* spelen in LDPI apparatuur. Het ontwikkelde model zal helpen om de resultaten correct te kunnen interpreteren indien er metingen zijn gedaan in situaties met grote weefsel-inhomogeniteiten.

De plaats-tijd-correlatie van *speckles* gegenereerd door een deeltjessuspensie belicht met een gecollimeerde laser bundel, is geanalyseerd in **hoofdstuk 7** door gebruik te maken van plaatjes van een hogesnelheidscamera. Van deze 3D data-set in plaats en tijd kan de plaats-tijd-correlatie bepaald worden door een 3D Fourier analyse uit te voeren op deze data set, het resultaat te kwadrateren en een inverse Fouriertransformatie te nemen van dit 3-dimensionale vermogensspectrum. Voor grote plaats correlatie afstanden, wat overeenkomt met grote speckles, is een langzame decorrelatie in tijd te zien. Dit bevestigt de hypothese zoals beschreven in hoofdstuk 3 over de invloed van *speckle*-grootte en fotonweglengte op de Doppler component in het vermogensspectrum. Wanneer een relatief brede bundel wordt gebruikt om een verstrooiende suspensie te belichten, zal de breedte van het Doppler vermogensspectrum toenemen vergeleken met de situatie waarbij een smalle bundel wordt gebruikt. Wanneer een smalle bundel wordt gebruikt, die over het algemeen grote *speckles* produceert, zullen er fotonen zijn die een relatief lange weg afleggen, wat overeenkomt met een grotere Doppler verschuiving, en kleine speckles veroorzaken. Omdat ze klein zijn, wordt hun aandeel in het vermogensspectrum onderdrukt in vergelijking met de grote speckles. De bevindingen in hoofdstuk 3 en 7 laten zien dat voor het doorbloedingsignaal (M_1) het effect van speckles op de gemiddelde Doppler verschuiving (M_1/M_0) and de modulatie diepte (M_0) tegengesteld werken, maar dat de invloed van speckles op M_0 het grootste is.

In **hoofdstuk 8** hebben wij het verband onderzocht tussen temperatuur en doorbloeding van de menselijke hoofdhuid met thermokoppels en laser Doppler doorbloedingsopnemers. Doel van dit onderzoek was het vaststellen van een verband tussen lokale temperatuur van de hoofdhuid en huiddoorbloeding tijdens koeling van de huid in een omgeving die relevant is voor de klinische praktijk, waarin hoofdhuidkoeling wordt toegepast tijdens chemotherapie om haaruitval tegen te gaan. Metingen op 9 gezonde proefpersonen wezen uit dat er een relatie is tussen temperatuur en doorbloeding van de hoofdhuid. Wij vonden dat voor de eerste 10°C koeling de

doorbloeding van de hoofdhuid afnam tot onder 40% van de waarde in rust. De doorbloeding zou nog verder onderdrukt kunnen worden tot onder 30% door nog enkele graden extra te koelen, maar verder koelen heeft geen invloed op de doorbloeding. Wij hebben een functie gedefinieerd die in staat was de data te beschrijven. De minimale waarde van de doorbloeding geeft een indicatie dat meer dan 12°C koelen geen aanwijsbare verlaging van de aanvoer van celgroei remmende medicijnen naar de huid oplevert. Het gevolg hiervan is dat verlagen van de temperatuur beneden deze kritische waarde enkel zinvol zou kunnen zijn voor het lokale weefselmetabolisme. Dit is iets waar rekening mee moet worden gehouden bij het uitvoeren van hoofdhuidkoeling tijdens een chemokuur.

Acknowledgements

This thesis is the result of four years of work whereby I have been accompanied and supported by many people. When I look back till October, 2003 the day I started my PhD here in University of Twente I can see a lot of faces who made these years an exciting and pleasant experience. Here, I would like to thank all of them.

First of all I would like to thank Wiendelt Steenbergem my supervisor for showing faith in me and considering me for this PhD position. It is with great pleasure I acknowledge here, his invaluable suggestions, dedicated persistence and affectionate advice during the various stages of my present work. You were always there with a smiling face to discuss about my work.

I wish to express my sincere gratitude to my promoter Ton van Leeuwen for his constant encouragement during the progress of my work. Thank you for being a friendly and flexible professor.

I regard it as my pleasant duty to express my sincere thanks to the chair of BPE, Vinod Subramaniam for his valuable support during last 3 years of my research in the group.

I acknowledge prof. dr. A. A. van Steenhoven, prof. dr M.J.C. van Gemert, Prof. Dr. Alfred Driessen and Prof. Dr. C. H. Slump for being the committee members of my defense.

I express my profound and hearty thanks to my colleague Babu Varghese. We had a wonderful time together doing research. Thank you for being with me.

I am thankful to Francis Janssen of Biomedical Engineering group of Technical University of Eindhoven, for a successful team work in materialising the chapter 8 of my thesis.

Rik Buschman and Cecile deVos of Twente Institute of Neuro modulation are acknowledged for the clinical collaboration and for giving me an insight in to the clinical research.

Special thanks to Roy and Srirang for your suggestions and help at various stages of my work. I consider you both as the encyclopaedias of BMO group.

It is my great pleasure to acknowledge Yohan, Erwin and Robert for the technical support.

I am grateful to my colleagues Matthijs, Alex and Constantin for providing me a nice time during office hours. Mathijs, special thanks for writing the Dutch summary of my thesis.

Frans for the general support and tolerating my Dutch. At the final stage of my work I could see that you started trying my regional language 'Malayalam'.

Special thanks are also to cheerful Sylvia for making all the administrative work very smooth. I hope that you could learn lot of Dutch immigration rules because of me.

My room mates Remco and Sjoerd are acknowledged for creating a friendly working atmosphere.

I am thankful to Tony for his moral support, brotherly affection and for being a great housemate.

I would like to acknowledge the Kerala family in Netherlands Tony, Babu, Indu, Vipin, Shaji, Mercy, Maria, Sandeep, Suby, Denny, Rani, Bejoy, Gincy, Shahina and, Kamala and Berny peters, Seshan and Jayanthi, and Arbind and Selina for keeping the South Indian culture alive making me feel at home.

I also like to acknowledge my desi colleagues Kiran, Vishnu, Chandra and Raja for sharing a nice time at office.

I am highly indebted to all my teachers, friends and classmates who have been encouraging me throughout my research career.

Above all, I would like to thank my dearest family members in India, especially my parents V. K Rajan and Valsala Rajan, brother Gopikrishnan, Smitha and Gowtham for supporting me with their love and affection without which this work would not have materialised. I cordially devote this dissertation to them.

Vinayakrishnan Rajan

Publications

V. Rajan, B. Varghese, T. G. van Leeuwen, and W. Steenbergen, "Speckles in laser Doppler perfusion imaging," *Optics Letters*, 31, 468-470 (2006).

V. Rajan, B. Varghese, T. G. van Leeuwen, and W. Steenbergen, "Quantification of spatial intensity correlations and photodetector intensity fluctuations of coherent light reflected from turbid particle suspensions," *Physical Review E*, 75, 060901-4 (2007).

V. Rajan, B. Varghese, T. G. van Leeuwen, and W. Steenbergen, "Effect of speckles on the depth sensitivity of laser Doppler perfusion imaging," *Optics Express* 15, 10911-10919 (2007).

V. Rajan, B. Varghese, T. G. van Leeuwen, and W. Steenbergen, "Review of methodological developments in laser Doppler flowmetry," In press, *Lasers in Medical Science* (2007).

F. E. M. Janssen[#], V. Rajan[#], W. Steenbergen, G. M. J. van Leeuwen, and A. A. van Steenhoven, "The relationship between local scalp skin temperature and cutaneous perfusion during scalp cooling," *Physiological Measurements* 28, 829-839 (2007). [#] equally contributed authorship

C. de Vos, V. Rajan, W. Steenbergen, H. van der Aa, R. Buschman, "Spinal Cord Stimulation for treatment of chronic pain caused by Diabetic Neuropathy," In press, *Journal of Diabetes and its Complications* (2007).

V. Rajan, B. Varghese, T. G. van Leeuwen, and W. Steenbergen, "Influence of tissue optical properties on laser Doppler perfusion imaging, accounting for photon penetration depth and the laser speckle phenomenon," *Journal of Biomedical Optics* (In review).

V. Rajan, B. Varghese, T. G. van Leeuwen, and W. Steenbergen, "Speckle size and decorrelation time; space-time correlation analysis of coherent light dynamically scattered from turbid media," *Optics communications* (In review).

B. Varghese, V. Rajan, T. G. van Leeuwen and W. Steenbergen, "Path length resolved measurements of multiple scattered photons in static and dynamic turbid media using phase modulated low coherence Interferometry," *Journal of Biomedical Optics*, 12 (2), 024020 (2007).

B. Varghese, V. Rajan, T. G. van Leeuwen and W. Steenbergen, "Quantification of Optical Doppler broadening and optical path lengths of multiply scattered light with phase modulated low coherence interferometry," *Optics Express*, 15 (15), 9157-9165 (2007).

B. Varghese, V. Rajan, T. G. van Leeuwen and W. Steenbergen, "High angle phase modulated low coherence interferometry for path length resolved Doppler measurements of multiply scattered light," *Optics Communications*, (In press).

B. Varghese, V. Rajan, T. G. van Leeuwen and W. Steenbergen, "Evaluation of a multimode fiber optic low coherence interferometer for path length resolved Doppler measurements of diffuse light," *Review of Scientific Instruments* (In press).

B. Varghese, V. Rajan, T. G. van Leeuwen and W. Steenbergen, "Discrimination between Doppler-shifted and non-shifted light in coherence domain path length resolved measurements of multiply scattered light," *Optics Express* (In review).

B. Varghese, V. Rajan, T. G. van Leeuwen and W. Steenbergen, "Path length resolved optical Doppler perfusion monitoring," *Journal of Biomedical Letters* (In review).

B. Varghese, V. Rajan, T. G. van Leeuwen and W. Steenbergen, "In vivo optical path lengths and path length resolved Doppler shifts of multiply scattered light," *Microcirculation* (In review).

B. Varghese, V. Rajan, T. G. van Leeuwen and W. Steenbergen, "Influence of static scattering matrices on coherence domain path length resolved Doppler measurements of multiply scattered light," *Optics Letters* (to be submitted).

Nibu A George, Vinayakrishnan R, "Photoacoustic evaluation of the thermal diffusivity of coconut shell," *Journal of Physics: Condensed Matter* 14, 4509–4513 (2002).

Nibu A George, Vinayakrishnan R, "Thermal wave propagation in multilayer samples: a laser induced photoacoustic investigation," *Lasers in Engineering* 11, 283-292 (2002).

Conference proceedings/Presentations

V. Rajan, B. Varghese, T. G. van Leeuwen, and W. Steenbergen, "Depth sensitivity of laser Doppler perfusion imager: quantification based on experiments and Monte Carlo simulations on static and dynamic scattering phantoms," *Optical Diagnostics and Sensing VII*. Edited by Coté, Gerard L.; Priezzhev, Alexander V. Proceedings of the SPIE, Volume 6445, pp. 644506, (2007) *Oral paper presentation*

B. Varghese, V. Rajan, T. G. van Leeuwen and W. Steenbergen, "Quantification of Doppler broadening in path length resolved diffusive light scattering using phase modulated low-coherence interferometry," *Biomedical Applications of Light Scattering*. Edited by Wax, Adam; Backman, Vadim. Proceedings of the SPIE, Volume 6446, pp. 644603, (2007) *Oral paper presentation*

V. Rajan, B. Varghese, T. G. van Leeuwen, and W. Steenbergen, " Role of speckles in laser Doppler perfusion imaging: an investigation on particle suspensions," *Biophotonics and New Therapy Frontiers*. Edited by Grzymala, Romualda. Proceedings of the SPIE, Volume 6191, pp. 281-288, (2006). *Oral paper presentation*

B. Varghese, V. Rajan, T. G. van Leeuwen and W. Steenbergen, "Path length resolved Doppler measurements of multiple scattered photons in turbid media for various absorptions using phase modulated low-coherence interferometry," *Biophotonics and New Therapy Frontiers*. Edited by Grzymala, Romualda. Proceedings of the SPIE, Volume 6191, pp. 322-329, (2006) *Oral paper presentation*

V. Rajan, W. Steenbergen, T.G. van Leeuwen, "Speckles in laser Doppler perfusion imaging: Experimental quantification on particle suspensions," *Biophotonics '05, 2nd International Graduate summer school*, Ven, Sweden (2005). *Poster presentation*.

V. Rajan, C. de Vos , H. P. J Buschman , H. E. Van der Aa, W. Steenbergen, T. G. van Leeuwen, "Laser Doppler assessment of the influence of spinal cord stimulation on micro-vascular blood flow in diabetic patients with chronic neuropathic pain," *Dutch Annual Conference on Biomedical Engineering, IBME*, Papandal, the Netherlands (2004). *Oral paper presentation*

Curriculum Vitae

Vinayakrishnan Rajan was born in Anthinad, Kerala, India on October 8, 1979. He obtained Bachelor of Science (B.Sc) degree in 2000 from St: Albert's College, Mahatma Gandhi University, India. In 2002 he completed his Master of Science (M.Sc) degree in Physics with a specialization in laser physics from Pondicherry Central University, India. As part of the M. Sc course he carried out a research project titled "A laser induced photoacoustic investigation of certain natural and synthetic samples" at international school of photonics, Cochin University of Science and Technology, India.

From October 2003 until October 2007 he performed research towards his Ph.D thesis at the Biophysical Engineering Group (BPE) of the University of Twente, The Netherlands under the supervision of Prof. Dr. Ton G. van Leeuwen and Dr. Wiendelt Steenbergen. He was involved in the research and development of laser Doppler perfusion monitoring and imaging techniques for the optical probing of structure and microcirculatory function in living tissue. During this research he worked to improve the laser Doppler perfusion imaging technique by carefully mapping the properties of the diffused laser light using the optical 'speckle theory'. The results of this are presented in this thesis. In October 2007, he joined Daniel den Hoed Cancer Center, Erasmus MC, Rotterdam as a Scientific Researcher in the unit of Medical Physics, department of Radiation Oncology.